The Dissertation Committee for Behdad Mofarraj Kouchaki Certifies that this is the approved version of the following Dissertation:

FIELD STUDY OF THERMALLY-INDUCED SOIL-STRUCTURE INTERACTIONS IN SEMI-INTEGRAL BRIDGE STRUCTURES

Committee:

Jorge G. Zornberg, Supervisor

Robert B. Gilbert

Todd A. Helwig

Shin-Tower Wang

FIELD STUDY OF THERMALLY-INDUCED SOIL-STRUCTURE INTERACTIONS IN SEMI-INTEGRAL BRIDGE STRUCTURES

by

Behdad Mofarraj Kouchaki

Dissertation

Presented to the Faculty of the Graduate School of

The University of Texas at Austin

in Partial Fulfillment

of the Requirements

for the Degree of

Doctor of Philosophy

The University of Texas at Austin

December 2022

Dedication

To my parents, for giving me the wings to fly and for bearing the burdens of this long-distance relationship. To my family, for their unending support, and to my partner, for always being there for me.

Acknowledgements

First and foremost, I would like to acknowledge my advisor, Dr. Jorge Zornberg for believing in me and inviting me to his research group. Under the supervision of Dr. Zornberg, I was able to participate in many fascinating studies regarding novel bridge systems and reinforced earth structures, many of which were not outlined in this dissertation. Under Dr. Zornberg, I gradually learned how to become an independent researcher, a collaborator and a professional engineer.

This dissertation also benefitted greatly from the thoughtful and constructive feedback of the dissertation committee members. Dr. Helwig provided his invaluable insight from decades of experience with researching the thermal behavior of highway bridges and Dr. Gilbert always challenged me in the evaluation of the outcomes of my research through brief but highly insightful interactions. Lastly, Dr. Wang greatly supported my efforts in this study from the early stages, by inviting me to their industry workshops at Ensoft, Inc., advising me on the development of the instrumentation and monitoring system and contributing significantly to the refinement of my analyses.

Next, I would like to thank the wonderful faculty members of the Department of Civil, Architectural and Environmental Engineering (CAEE) at the University of Texas at Austin. I owe much of my engineering knowledge to Dr. Bob Gilbert, Dr. Zornberg, Dr. El Mohtar, Dr. Kumar and Dr. Murcia.

I would also like to acknowledge Texas Department of Transportation (TxDOT) for sponsoring the work presented in this dissertation through the Center for Transportation Research (CTR) at the University of Texas at Austin. We received great support from the

TxDOT research panel for their support in the instrumentation and monitoring of the two of the first semi-integral bridges in the state of Texas. I am specially thankful to Mr. Samuel Groves for the support provided during the instrumentation of China Creek Bridge. Mr. Groves went above and beyond to enable the successful implementation of the China Creek instrumentation system.

I would also like to thank many of my colleagues and peers at UT Austin for providing feedback on my research and occasionally going the extra mile to contribute to this research. I am especially thankful to the support provided by my friends Subramanian Sankaranarayanan (Subu), Calvin Blake, Etienne Gonzalez, Dawie Marx and Jakob Walter for their contributions to the field activities and for being good company in tough times. I would also like to extend my gratitude to the CAEE staff members Phil Tomlinson and Lamont Prosser for lending me their technical know-how in preparation for my many field and laboratory activities.

I am also thankful to the many wonderful friendships I've enjoyed during my time in Austin. Good friends are hard to find but I believe I found my fair share of them while living in Austin. I would like to thank Vinci Chan, Matthew Rodriguez, Chihun Sung, Subu, Dawie Marx, Federico Castro, Nathan Threlkeld, Ahmed Hussien, Meibai Li, Jodie Crocker, Amr Morsy, Benchen Zhang, Pierre Estrada and many others for brightening my days in Austin.

Lastly, I would like to express my gratitude to Dr. John A. White, former chancellor of the University of Arkansas, for encouraging me during the last year of my Master's studies to continue my path towards a PhD. Participating in his leadership course and the personal conversations we had, was a life-changing experience for me.

Abstract

FIELD STUDY OF THERMALLY-INDUCED SOIL-STRUCTURE INTERACTIONS IN SEMI-INTEGRAL BRIDGE STRUCTURES

Behdad Mofarraj Kouchaki, Ph.D.

The University of Texas at Austin, 2022

Supervisor: Jorge G. Zornberg

Semi-integral bridges are considered a promising alternative to conventional bridge designs because they eliminate the need for deck expansion joints. The elimination of expansion joints has been shown to significantly reduce bridge maintenance cost, which can lead to significant savings over the service life of the bridge. These potential savings have led to the increasing utilization of jointless bridge construction with many transportation agencies. However, the elimination of expansion joints is known to lead to secondary problems such as soil-structure interaction between the bridge structure and the abutment backfill due to daily thermal expansion/contraction of the bridge which is not well understood. In this dissertation, the data collected from monitoring of two pilot semi-integral bridges in Texas, USA are presented and evaluated. In this study, the effect of daily and seasonal temperature changes on the displacement of various bridge components, changes in abutment earth pressure, foundation interaction, ratcheting, backfill settlement, etc. have been successfully captured. Among the findings are increased backfill lateral earth pressure due to ratcheting, continuous settlement of the backfill, loss of vertical

support for the approach slabs, asymmetric expansion/contraction of the bridge and slight displacement of the bridge superstructure towards one end of the bridge. In addition, it was found that the thermal expansion/contraction of the bridge deck results in cyclic latera loading of the abutment caps and the bridge foundations, despite a lack of rigid connection between the foundations and the superstructure. The cyclic loading of the foundations was also found to cause accumulation of plastic strains in the foundation soil. The causes of the undesired behaviors are identified through successful monitoring of the two semi-integral bridge structures and recommendations are made to minimize the occurrence of such issues in future semi-integral bridge constructions.

Table of Contents

List of Tables 13

List of Figures 14

Chapter 1: Introduction 25

1.1. Background 25

1.2. Organization of Dissertation 32

Chapter 2: Monitoring of Temperature-induced Lateral Earth Pressures in Semi-integral Bridges 37

Abstract 37

2.1. Introduction 37

2.2. Project Description 43

2.3. Subsurface Geotechnical Characterization 45

2.4. Field Instrumentation Program 47

2.5. Phase 1 Instrumentation Results 49

2.6. Phase 2 Instrumentation Results 57

2.7. Conclusions 67

2.8. Acknowledgements 69

2.9. References 69

Chapter 3: Development of an Instrumentation System for Monitoring Long-term Thermally-induced Interactions in Semi-integral Bridges 72

Abstract 72

3.1. Introduction 72

3.2. Description of China Creek Semi-integral Bridge 80

3.3. Geotechnical Characterization of China Creek Semi-integral Bridge 83

3.4. Semi-integral Bridge Monitoring Plan 83

3.5. Typical Outcomes of the Bridge Deck Instrumentation 86

3.6. Typical Outcomes of the Abutment Area Instrumentation 90

3.7. Typical Outcomes of the Substructure Instrumentation Plan 94

3.8. Typical Outcomes from Temperature Measurements 101

3.9. Conclusions 105

3.10. Acknowledgements 107

3.11. References 107

Chapter 4: Field Investigation of Soil-Structure Interaction in Semi-integral Bridge Abutments 111

Abstract 111

4.1. Introduction 112

4.2. Bridge Description 114

4.3. Instrumentation Description 116

4.4. Thermal expansion and contraction of the bridge 118

4.5. Lateral Earth Pressures on Abutment Walls 130

4.6. Abutment Backfill Settlements 138

4.7. Conclusions 141

4.8. Acknowledgements 145

4.9. References 145

Chapter 5: Long-Term Field Monitoring of Lateral Loads in Semi-Integral Bridge Foundations 148
ABSTRACT 148
5.1. INTRODUCTION 148
5.2. DESCRIPTION OF CHINA CREEK BRIDGE 150
5.3. GEOTECHNICAL CHARACTERIZATION OF THE FOUNDATION SOIL 152
5.4. INSTRUMENTATION OVERVIEW 153
5.5. INSTRUMENTATION DATA 155
5.6. ANALYSIS OF THE DRILLED SHAFT BEHAVIOR 162
5.7. CONCLUSIONS 171
5.8. ACKNOWLEDGEMENTS 174
5.9. REFERENCES 174
Chapter 6: Conclusions 177
6.1. SUMMARY 177
6.2. FUTURE WORK 180
Appendix A: Instrumentation of Mack Creek Bridge 182
A.1. INTRODUCTION 182
A.2. ASSEMBLY AND IN-HOUSE TESTING 182
A.3. DATA COLLECTION, PROCESSING AND VISUALIZATION PROGRAM 186
A.4. PYTHON LIBRARIES 188
A.5. FILE MANAGEMENT 188
A.6. VISUALIZATION 190

A.7. FIELD INSTALLATION 192
A.8. REFERENCES 196
Appendix B: Construction and Instrumentation of China Creek Bridge 197
B.1. INTRODUCTION 197
B.2. SURVEY OF THE ORIGINAL BRIDGE STRUCTURE 197
B. 3. CONSTRUCTION OF THE CHINA CREEK BRIDGE 200
Vita 254

List of Tables

Table 2.1: Predicted lateral earth pressures at the location of the EPCs.....53

Table 3.1: Summary of studies on the field performance of integral and semi-integral bridges. (Continues).....74

Table 3.2: Sensors used on China Creek semi-integral Bridge.....85

List of Figures

Figure 1. 1: A sketch of a conventional bridge details with deck expansion joints 25

Figure 1. 2: Seepage of surface runoff through the bridge expansion joint between two adjacent spans in China Creek Bridge, Wichita County, TX 26

Figure 1. 3: General sketch of jointless bridge abutments (a) semi-integral bridge abutment (b) integral bridge abutment.....28

Figure 2.1: Schematic illustrating the phenomenon of "soil ratcheting" within the backfill behind the abutment in a semi-integral bridge: (a) Initial position (neutral) (b) Deck contraction (backfill movement in the active direction) (c) Deck expansion back to initial position (backfill movement in the passive direction) (d) Additional deck expansion (backfill movement in the passive direction) 41

Figure 2.2: Schematic view of the Mack Creek semi-integral bridge: (a) Transverse cross-section (half width); and (b) Longitudinal cross-section with the location of sensors. (Note: EPC stands for earth pressure cell).....44

Figure 2.3: Mohr-Coulomb shear strength envelope for the abutment backfill material, as defined from large-scale CD triaxial tests.....46

Figure 2.4: Mohr-Coulomb interface shear strength envelope between concrete and abutment backfill, defined using large-scale direct shear tests.....47

Figure 2.5: Data collected during the first phase of instrumentation: (a) south abutment EPC data; (b) north abutment EPC data; and (c) ambient air temperature 50

Figure 2.6: Daily ambient air temperature change vs daily lateral earth pressure changes at the south abutment wall (November and July 2018) 54

Figure 2.7: Evaluation of the relationship between ambient air temperature and ratcheting: (a) south abutment average earth pressure increase vs the average ambient air temperature (b) south abutment average earth pressure vs average ambient air temperature.....56

Figure 2.8: Data collected during the second phase of instrumentation: (a) Deck length changes; (b) Ambient air temperatures; and (c) Deck surface temperatures. 58

Figure 2.9: Daily changes in deck length as a function of daily ambient air temperature changes (for August and December 2020) 60

Figure 2.10: Recorded ambient air temperature, deck concrete surface temperature and solar irradiance at the bridge: (a) August 2020, and (b) December 2020 61

Figure 2.11: Crackmeter measurements in the two bridge abutments, quantifying the relative displacement between abutment walls and caps 64

Figure 2.12: Sum of abutment cap displacements. Positive values indicate increasing distance between abutment caps (relative to their position in February 2020). 65

Figure 3.1: Schematic of China Creek Semi-integral Bridge: (a) Transverse cross-section (half-deck); and (b) Longitudinal cross-section showing the location of installed sensors. (EPC: Earth Pressure Cell) 82

Figure 3.2: Deck strain gauge installation locations. 87

Figure 3.3: Typical time history of data collected in the bridge deck: (a) Deck length changes measured by laser distance sensor, longitudinal deck-embedded strain gauges and perpendicular low modulus (LM) strain gauge (Note: Vertical axis range is truncated and does not display full range of laser sensor measurements); and (b) Changes in deck curvature near the location of the laser distance sensor. 89

Figure 3.4: Field monitoring results of backfill settlements: (a) West abutment settlements as recorded by the settlement sensor; and (b) west abutment GPR survey profile showing a 50 mm gap between backfill and approach slab at location of settlement sensor. 92

Figure 3.5: Typical time history of movements in the abutment walls: (a) Changes in width of the abutment cap joint as measured by a crackmeter; and (b) abutment wall rotation as measured by a tiltmeter (Note: Positive values indicate tilting towards the backfill) 93

Figure 3.6: West abutment drilled shaft profiles: (a) foundation profile; (b) deflection profile; (c) curvature profile; and (d) moment profile (shape array data captured at 7:30 pm on December 5, 2020). 95

Figure 3.7: Schematic of a deflected segment of the drilled shaft. 96

Figure 3.8: Instrumented west drilled shaft's maximum moment and abutment cap displacement data (Note: Positive displacements correspond to drilled shafts bending toward the center of the bridge). 98

Figure 3.9: Effect of daily temperature variation on expansion/contraction of the bridge: (a) Abutment wall displacement calculated by adding results from the drilled shaft shape arrays to those obtained from the abutment cap crackmeters; and (b) Comparison between the changes in deck length calculated using data from shape arrays, abutment cap crackmeters, and abutment wall tiltmeters versus the data from the deck strain gauges.....100

Figure 3.10: Comparison of different temperature records collected at the China Creek Bridge site.....104

Figure 4.1: Schematic of semi-integral China Creek Bridge and location of installed sensors. 115

Figure 4.2: Instrumentation and backfilling of China Creek Bridge's west abutment. Top right picture shows a close-up view of the steel plate attached to the top of settlement sensors after completion of backfill placement.....117

Figure 4.3: Ambient air temperature time-history data collected from the China Creek Bridge site.....119

Figure 4.4: Time-history of changes in the bridge length measured using strain gauges mounted on girders compared to foundation shape array and abutment cap crack meter measurements. 120

Figure 4.5: Coefficient of Thermal Expansion (CTE) calculation based on deck strain gauges.....122

Figure 4.6: Time history of east and west abutment wall displacement relative to their original positions at completion of construction. 123

Figure 4.7: Diagram showing neutral thermal expansion point and effective expansion length for each abutment wall.....125

Figure 4.8: Time history of the distance of the neutral thermal expansion point from east abutment wall, normalized to total length of bridge.....126

Figure 4.9: Time history of the change in position of bridge midpoint relative to time of construction (positive values indicate that midpoint has moved eastward).....128

Figure 4.10: Semi-integral bridge abutment resistance model: (a) Diagram showing elements that resist thermal expansion/contraction of a semi-integral bridge; and (b) hypothetical force-displacement diagram of resisting elements (positive 'x' signifies abutment wall displacement toward backfill).....129

Figure 4.11: Time history of lateral earth pressures recorded in (a) east abutment; and (b) west abutment.....131

Figure 4.12: Time history plot of ratio between the thermal expansion of deck slab right above the girder's top flange relative to the bottom of girder (girder top-to-bottom thermal expansion ratio).....134

Figure 4.13: Time history plot of lateral thrust force acting on abutment walls estimated from EPC readings.....135

Figure 4.14: Measured stress – strain behavior for abutment backfills at abutment wall mid-depth: (a) east abutment; and (b) west abutment. (Note: positive strain values indicate backfill compression.).....137

Figure 4.15: Time history of settlement data collected from four backfill settlement sensors. Settlement data presented is calculated relative to start of monitoring (10/22/2020).....139

Figure 4.16: East backfill settlement and wall displacement during a 10-day period in October 2021.....140

Figure 5.1: Schematic of semi-integral China Creek Bridge, including some of the installed sensors.....151

Figure 5.2: Installation of shape arrays in the drilled shaft foundations: (a) Installation of drilled shaft rebar cage fitted with shape array casing; and (b) installation of shape array inside casing after abutment caps were formed. 154

Figure 5.3: Time-history of ambient air temperature data collected by on-site weather station. 156

Figure 5.4: Time-history of changes in deck length (deck thermal expansion/contraction). 157

Figure 5.5: Time-history of change in width of expansion joints between abutment caps and abutment walls measured via crackmeters. 158

Figure 5.6: Time-history of abutment cap displacement data measured using drilled shaft shape arrays. 159

Figure 5.7: Schematics of changes to abutment area in response to thermal expansion/contraction of bridge: (a) initial position; (b) bridge expansion; and (c) bridge contraction. 161

Figure 5.8: Profiles for the west abutment drilled shaft profiles on two different dates: (a) subsurface profile (b) lateral deflection profile (c) curvature profile, and (d) flexural moment profile 163

Figure 5.9: Maximum bending moment acting on drilled shafts (positive bending moments indicate bending toward center of bridge as sketched). 165

Figure 5.10: Time-history of changes to east abutment cap position and changes to east abutment cap expansion joint width (arrows indicate abutment cap general displacement direction during highlighted periods). 169

Figure 5.11: Schematic illustration of cyclic p-y behavior of foundation soil in different conditions: (a) period of increase in average daily temperature; (b) period of decrease in average daily temperature decrease; and (c) period of essentially unchanged average daily temperature. 171

Figure A. 1: Assembly of sensor and logger equipment for temporary additional instrumentation of Mack Creek SIAB 183

Figure A. 2: Enclosure assembled for additional monitoring of Mack Creek SIAB 184

Figure A. 3: Testing of the equipment on the rooftop of Civil Engineering department at UT Austin....185

Figure A. 4: Flow chart of the python program developed for data collection, processing and visualization....187

Figure A. 5: New messages received from the datalogger....189

Figure A. 6: Archived messages after they were processed by Python....189

Figure A. 7: Example output of the file management algorithm developed in Python...190

Figure A. 8: Example output of the plotting program developed in Python....192

Figure A. 9: Equipment installed on Mack Creek in January 2020....193

Figure A. 10:Closeup of equipment installed on the south abutment: (a) Logger equipment and laser distance meter (b) crackmeter installed between backwall and pile cap + loggerbox....194

Figure A. 11:Closeup of equipment installed on the north abutment, laser target and crackmeter installed between backwall and pile cap. (a) view from behind (b) top view....195

Figure A. 12: .Closeup of pole mounted equipment on the south abutment, which includes solar panel, climavue50, SI-111SS and lightning protection device: (a) installation of SI-111SS for measuring deck surface temperatures (b) Closeup of SI-111SS....196

Figure B. 1: High water level in China Creek after a precipitation event in August 2018....198

Figure B. 2: Corroded bents under China Creek bridge to be replaced....198

Figure B. 3: Seepage of water through the deck joints....199

Figure B. 4: Cracked edge of pavement at the end of the approach slab due to backfill settlement....200

Figure B. 5: Demolition of the first half of the old China Creek Bridge....201

Figure B. 6: Installation of soil nail wall as temporary support for the active roadway crossing the undemolished half of the bridge (Picture provided by Samuel Groves).....202

Figure B. 7: Casing used for the top portion of the drilled shafts.....204

Figure B. 8: Gray shale covered with powdery red dirt recovered from 8 m depth 205

Figure B. 9: Heap of soil excavated from the drilled shaft. Note the broken pieces of shale on top (depths of 7.5 m and lower) and wetter/plastic material removed beforehand.....205

Figure B. 10:Placement of one of the west abutment drilled shafts' rebar cage 206

Figure B. 11:Forming of abutment walls after placement of girders and precast panels, March 2020 (East abutment) 207

Figure B. 12:Top view of the earth pressure cell (GK-4810) installed on the inside of the form on the west abutment wall, photographer standing on one of the precast panels placed on the deck, March 2020.....208

Figure B. 13: Finished surface of the east abutment wall with the pressure cell (GK-4810) installed between the two girders on the left, March 2020.....209

Figure B. 14:GK-4200L as installed on the deck, perpendicular to the direction of the bridge, March 2020.....210

Figure B. 15:A pair of GK-4200 strain gauges installed on the deck during phase 1 of the construction.....211

Figure B. 16:Identification of strain gauges using colored tapes as binary ID code 211

Figure B. 17:Installation of strain gauges: (a) cables of the strain gauges were routed through a small gap between the foam boards to underneath the bridge, and (b) coiled up wires coming from the strain gauges (red) and earth pressure cell (blue).....212

Figure B. 18:Predrilled block of wood used to help keep track of the cables coming from embedded strain gauges 213

Figure B. 19:Concrete placement on the deck, Phase 1, March 2020 214

Figure B. 20:Finished surface of the deck, Phase 1, March 2020 214

Figure B. 21:Covered deck surface after concrete was placed, Phase 1, March 2020 215

Figure B. 22:1.5 m PVC conduits transported to China Creek Bridge to house SAAV sensors in the drilled shafts. In this picture, 1.5 m conduits are already assembled into 3 m sections using PVC cement and couplers 217

Figure B. 23:PVC conduits assembled into 11 m sections using additional couplers and joint reinforcement. 218

Figure B. 24:Reinforcement of PVC conduit joints: (a) Threaded couplers + Heavy Duty PVC cement (b) Compression couplers + Flexible couplers + Hose clamps 218

Figure B. 25:Attachment of the PVC conduit to the rebar cage: (a) Heavy duty zipties used on either side of the joints (b) combination of steel hose clamps and heavy duty zipties used at the middle of each section. 219

Figure B. 26:Assembled PVC conduits attached to drilled shafts to serve as SAAV housing.....220

Figure B. 27:Strain gauges attached to the long. Rebars of drilled shafts.....221

Figure B. 28:Instrumented rebar cage intended for Center-East drilled shaft (Phase 2) of China Creek bridge.....221

Figure B. 29:Installation of east abutment instrumented drilled shaft: (a) lift and transportation of the rebar cage using a front loader to the drilled shaft location (b) lifting of the rebar cage from the top using a crane (note the bending of the rebar cage and PVC conduit).....223

Figure B. 30:Construction of the instrumented east abutment drilled shaft: (a) concrete being pumped into the drilled shaft (b) Final orientation of the instrumented shaft and sensors 225

Figure B. 31:Formwork for construction of abutment caps and wing walls 226

Figure B. 32:Instrumentation of the abutment caps: (a) west abutment cap pressure cell (before formwork is completed) (b) east abutment pressure cell (after formwork is completed) 228

Figure B. 33:Construction of the west abutment cap: (a) Pouring concrete for abutment cap using a concrete tremie (west abutment) (b) finishing the surface of the abutment cap, notice SAAV conduit sticking out between the two girder pedestals 229

Figure B. 34:Installation of epcs on wing wall forms to measure backfill pressure acting on the wing walls: (a) epcs mounted on the wing wall forms (b) west abutment wing wall after form removal 230

Figure B. 35:Installation of SAAV in the east abutment center drilled shaft 231

Figure B. 36:SAAV verification tool screen (green light indicates successful installation) 231

Figure B. 37:Capped SAAV conduit on east abutment 232

Figure B. 38:Miniature strain gauge next to the drill guide used for installation on the side of the bottom flange of the bridge girder 233

Figure B. 39:Installation of miniature strain gauges on the bridge girder: (a) epoxied strain gauge (b) strain gauge installation, cables are routed along the top flange.....233

Figure B. 40:Mounted miniature strain gauges on the bottom flange of the middle girder 234

Figure B. 41:Location of the 3 pairs of concrete embedded strain gauges on the east abutment wall.....235

Figure B. 42:A pair of earth pressure cells mounted on the back of the form intended for the west abutment wall.....235

Figure B. 43:Placement of precast concrete panels on the deck.....236

Figure B. 44:Phase 2 deck concrete placement 236

Figure B. 45:Instrumented concrete sample cylinders.....237

Figure B. 46:Installation of VW displacement transducers to be used as backfill settlement sensors: (a) excavation of the hole using auger (b) vertical placement of the sensor in the hole.....239

Figure B. 47:Settlement sensor installation locations: (a) west abutment (b) east abutment.....240

Figure B. 48:Installation of soil extensometers in the backfill: (a) west abutment (b) east abutment 241

Figure B. 49:Stainless steel plates attached to the top flange of the settlement sensors..242

Figure B. 50:Crackmeter installed for measuring relative displacement between approach slab and sleeper slab.....243

Figure B. 51:Crackmeter installed for measuring relative displacement between approach slab and wing wall.....243

Figure B. 52: Crackmeter installed for measuring relative displacement between abutment cap and abutment wall + tiltmeter installed on the abutment wall 244

Figure B. 53:Piezometer measuring water pressure in the backfill (prior to installation). The sensor is fully inserted and sealed on the back to prevent water infiltration from the creek side in case of flooding.....245

Figure B. 54:Creekside piezometer installed on the abutment cap.....245

Figure B. 55:The superstrut mounted on southwest wing wall. Infrared radiometer is pointed towards the deck surface to measure surface temperature.....246

Figure B. 56:Solar panel mounted on the south railing of the east end of china creek bridge 247

Figure B. 57:China Creek bridge construction completed and opened to traffic on July 31, 2020.....248

Figure B. 58:Upside-down installation of the logger enclosures below the deck. Enclosure is mounted to the bottom of the deck. To keep water from damaging the equipment housed inside, all cord grip holes need to be as close to the lid as possible.....250

Figure B. 59:Wiring of the east side datalogger station which is equipped with a laser distance meter as well. Fun fact: This battery-operated fan was our best defense against the late-July heat and the large number of mosquitoes and wasps living around the creek area while wiring the loggers.....251

Figure B. 60:PVC pipes used for protection of cables routed on top of abutment caps..253

Chapter 1: Introduction

1.1. BACKGROUND

Conventional bridge construction generally makes use of expansion joints placed at the ends of the bridge and in between the spans. These movable joints are implemented to minimize the development of secondary stresses in the bridge superstructure from many sources, such as thermally-induced strains, shrinkage, creep, or abutment settlement. Moreover, expansion joints at the ends of the deck are implemented to prevent interaction with the abutment that can be caused by the daily and seasonal thermal expansion/contraction of the bridge superstructure. A general sketch of a typical conventional bridge with deck expansion joints in the state of Texas is presented in Figure 1. 1.

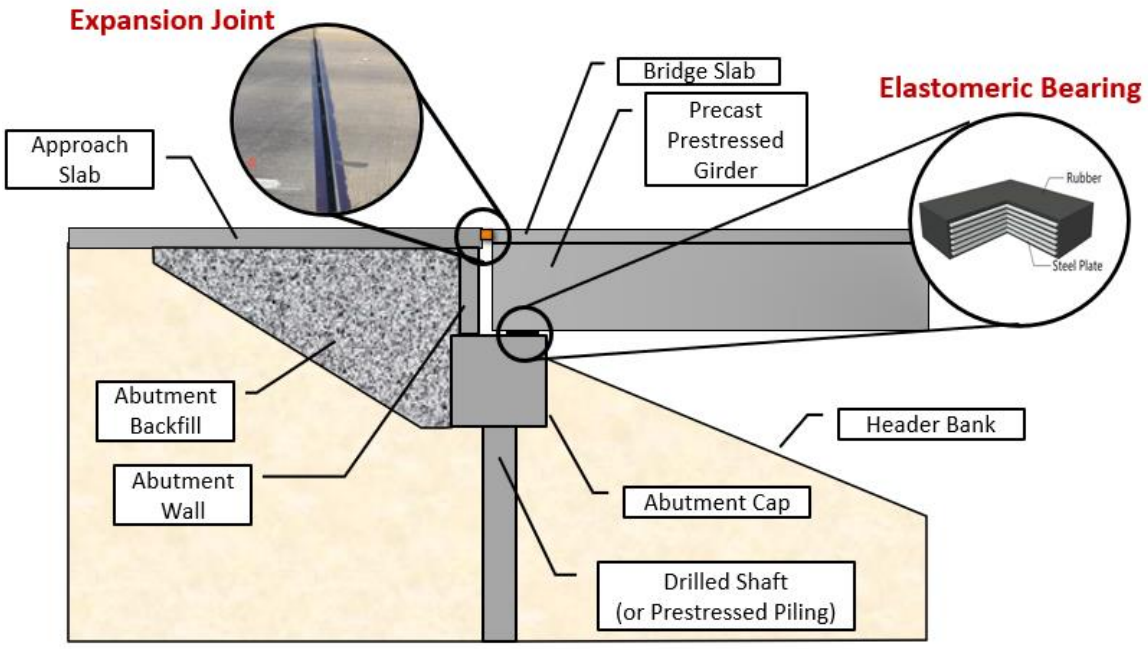

Figure 1. 1: A sketch of a conventional bridge details with deck expansion joints

Decades of experience and countless studies have shown that while expansion joints are a good idea in principle, these components are highly susceptible to in-service deterioration and damage. In addition, expansion joints expose the structure to moisture, deicing salts, abrasives, chemicals, and other debris which leads to extensive damage to the structure and a faster rate of deterioration (Purvis and Berger, 1983). A good example of the long-term structural deterioration caused by the usage of expansion joints can be seen in Figure 1. 2. In this case, the water seepage, happening over several decades, has caused noticeable rust development on the interior bents and has also caused damage to the concrete bent cap.

Figure 1. 2: Seepage of surface runoff through the bridge expansion joint between two adjacent spans in China Creek Bridge, Wichita County, TX

It is worth noting that deicing chemicals are commonly used in many areas across the US, as well as in other countries, that experience snow and frost in the wintertime. Such is the case for the bridge shown in Figure 1.2 which is located in the North Texas region. The usage of deicing chemicals increases the corrosivity of the surface runoff and accelerates the rate of deterioration of various bridge components that come in contact with the surface runoff.

While damaged expansion joints can be replaced periodically to maintain function, the damage to the structural elements is much more difficult to remedy if not entirely unfeasible. Moreover, maintenance of expansion joints is typically considered an expensive cost item and is more expensive than the initial construction cost of the component. As a result, many transportation agencies have begun pursuing jointless bridge designs such as semi-integral and integral bridges.

According to Burke (2009), the adoption of integral and semi-integral bridges began in Ohio in the 1930s with the construction of Teens Run Bridge in Gallia County, Ohio. In semi-integral bridges, the deck, girders, and abutment walls are integrated during construction. In these bridges, the superstructure loads are transferred to the abutment caps and foundation via bearings. A contrasting feature of integral bridges is that the bearings are also eliminated, resulting in a seamless connection between the superstructure and the substructure. A general sketch of these bridge types is shown in Figure 1. 3.

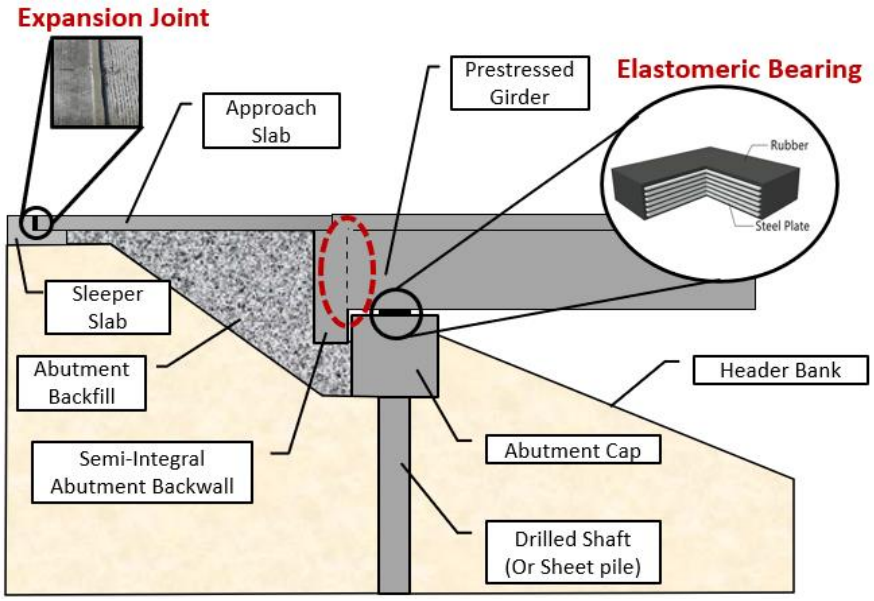

(a)

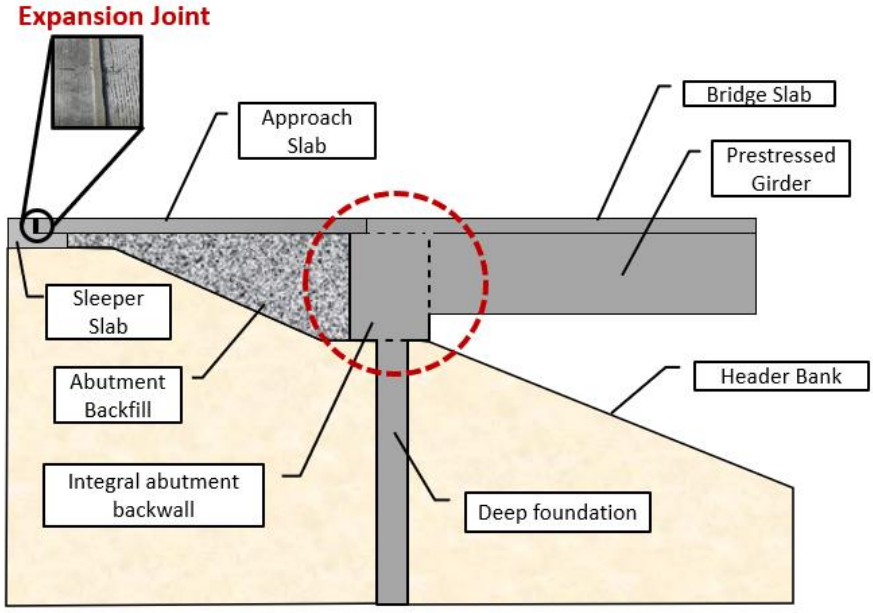

(b)

Figure 1. 3: General sketch of jointless bridge abutments (a) semi-integral bridge abutment (b) integral bridge abutment

Another promising alternative that allows for the elimination of expansion joints is the seamless bridge system. The seamless bridge system has been used in Australia (Bridge et al., 2005) in an attempt to provide a seamless connection between Continuously Reinforced Concrete Pavements (CRCP) and bridge decks. In this system, all transverse joints are eliminated, and the pavement and deck are connected using a reinforced concrete connection that can resist the induced stresses. In this system, additional reinforcement is included in the transition zone between the CRCP and bridge deck to control concrete crack widths and ensure stresses are within the range prescribed by the building codes.

As noted earlier, the elimination of expansion joints from the superstructure can potentially result in the development of secondary stresses in the structure. Despite this issue, the jointless bridge designs have been gaining favor with many transportation agencies, especially for bridges of moderate length and skew, where the distress caused by expansion joints over the service life of the structure exceeds their potential benefits. This has prompted many transportation agencies to develop their own guidelines and design details for the construction of integral and semi-integral bridges, in a process largely guided by experience.

It is worth noting that while Figure 1. 3 shows integral and semi-integral bridges built using stub-type abutments and drilled shaft foundations, their usage is not limited to a specific foundation type. However, given the characteristic differences between the integral and semi-integral bridges, there are some differences between the typical integral and semi-integral bridge foundations. In fact, one of the largest deciding factors between semi-integral and integral bridges is related to the choice of foundation type. Because in integral bridges, superstructure and substructure are “tied” together, integral bridge

foundations need to possess sufficient flexibility to allow for relatively unrestrained thermal expansion/contraction of the structure, otherwise damage may occur. As a result, many transportation agencies in the US require the usage of steel H Piles with the weak bending axis oriented in the direction of the integral bridge. In contrast to the relatively flexible foundations in integral bridges, because semi-integral bridges do not have the rigid connection between the superstructure and substructure, the usage of foundation systems such as large diameter drilled shafts that are comparatively more rigid are commonly permitted. Therefore, semi-integral bridges are often selected where the project can benefit from the elimination of expansion joints, but the site conditions do not permit the usage of flexible foundation systems (e.g., pile driving is not feasible).

However, in either case, thermal expansion and contraction of the superstructure results in a daily cyclic interaction with the abutment backfill. The cyclic soil-structure interaction occurring in semi-integral and integral bridge abutments has been studied by several researchers over the past few decades. Through long term field monitoring programs, it has been found that this interaction causes increased abutment earth pressure (also known as ratcheting) and settlement of the backfill (Mofarraj and Zornberg, 2022; Huntly and Valsangkar, 2013; England et al. 2000; Frosch and Lovell, 2011; Civjan et al., 2013). However, these long-term field monitoring studies have provided mixed results regarding the occurrence of ratcheting in integral and semi-integral bridges. While some researchers have clearly observed yearly increasing earth pressures (Mofarraj and Zornberg, 2022; Huntly and Valsangkar, 2013), others have made contradicting observations (Civjan et al., 2013; Ooi et al, 2020) indicating lateral earth pressures slightly decreasing over time in some cases. Moreover, a consensus regarding the design lateral

earth pressure and its distribution against the abutment walls, wing walls and abutment caps do not currently exist.

According to Oesterle and Tabatabai (2014), the complexity and uncertainty of the behavior of jointless bridges has resulted in the adoption of an experimental design approach for such bridges. As such, jointless bridges were initially constrained to short lengths and the continued success of these structures resulted in increasingly longer structures over time. Consequently, the design procedures and guidelines presented by various transportation agencies have been developed primarily based on empirical rules. Therefore, significant gains can be made by obtaining a better understanding of the long-term behavior of semi-integral and integral bridges and developing a more rigorous design approach for such structures.

In addition to the secondary stresses caused by the soil-structure interaction occurring in the abutment area, variation of temperature across the bridge decks causes additional stresses in these members. These stresses are induced due to rotational and translational distortions of the deck. Several studies have been studied by various researchers in the past. As noted by Imbsen and Vandershaf (1984), the shape of the bridge cross-section as well as the climate conditions can have a significant effect on the distribution of these stresses. Additionally, Chen (2008) notes that other factors such as the orientation of the bridge, distance between the girders and the type of bearings can affect the development of these stresses as well.

With the brief overview provided so far, it is clear that jointless bridge designs hold a lot of promise over the traditional and conventional bridge designs that utilize deck expansion joints. However, as stated, the guidelines for development and construction of

these bridges have been developed somewhat iteratively and based on the experience of local transportation agencies. As such, the range of application of jointless bridges has evolved somewhat conservatively and over several decades due to the limited understanding of their behavior and true limitations. Gaining a better understanding of the factors affecting the long-term behavior of jointless bridges improves the possibility of optimizations in the design process and better definitions of the true application limits of jointless bridges.

The main goal of this dissertation is to improve the knowledge of the factors affecting the long-term behavior and performance of semi-integral bridges, especially the complex soil-structure interaction in the abutment area. To this end, two pilot semi-integral bridges were instrumented during construction using a variety of state-of-the-art sensors and datalogging equipment. The installed equipment was used for continuous monitoring of environmental variables such as ambient air and internal temperature of the bridge deck as well as the stresses and strains developed within various bridge components due to changes in temperature. It is hoped that with the detailed analysis of the data collected from the two semi-integral bridges during nearly 5 years of continuous monitoring, a better understanding of the complex behavior of such structures is gained, leading to more optimized design procedures with improved certainty.

1.2. ORGANIZATION OF DISSERTATION

This dissertation is organized into five chapters. This introductory chapter provides a brief overview of the history of jointless bridges, their advantages and disadvantages and limitations as compared to conventional bridges is provided. Chapters 2 to 5 (main body)

are self-contained chapters prepared as stand-alone journal manuscripts, each with their own abstract, introduction, analysis, conclusions, and references. In the end, a brief summary of the findings from the preceding chapters as well as potential future work are provided in Chapter 6 (Conclusions). A summary of the main body chapters is provided below.

In Chapter 2, the data collected from the monitoring of the Mack Creek Semi-Integral Bridge built in 2017 outside of Palestine, TX is presented. Mack Creek Bridge was the first of the two pilot semi-integral bridges built by TxDOT and instrumented for this research project. The instrumentation for this bridge consists of two phases. Phase 1 focused on collecting abutment lateral earth pressure data and in Phase 2 additional sensors were added to directly measure thermal expansion/contraction of the bridge and other thermal characteristics. These Phase 2 measurements included relative displacement between the abutment caps and abutment walls and climate variables at the site such as ambient air temperature and solar radiation. Among the most notable findings of this investigation was that the lateral abutment earth pressures can significantly increase year-to-year due to ratcheting, having exceeded Rankine's passive earth pressure estimate in only 2 years. Moreover, it was found that the response of the abutments to the thermal expansion of the bridge can be quite asymmetric with one abutment experiencing significantly larger earth pressures compared to the other one. Moreover, it was found that the thermal expansion/contraction of the bridge also results in lateral loading of the substructure, which is typically not considered in the design of semi-integral bridges.

In Chapter 3, an overview of the comprehensive instrumentation system developed for monitoring the China Creek Semi-Integral Bridge is presented. In this chapter, an

overview of the field monitoring studies performed prior to implementation in the China Creek Bridge and the main findings are provided as a guide to the development of the implemented monitoring system. For monitoring the behavior of the China Creek Bridge, more than 70 sensors were installed on the structure during different stages of the construction. Typical data from various sensors are provided in the chapter to discuss the reliability of the instrumentation data and also lay the groundwork for analysis of the data collected from different sensors. Among the notable findings outlined in the chapter are the importance of using an on-site weather station, the benefits of implementing redundancy in the instrumentation scheme for the measurement of critical variables and field validation of the accuracy of the new backfill measurement technique developed for the project.

In Chapter 4, a comprehensive analysis of the soil-structure interaction occurring in the China Creek Bridge abutments is provided using the collected instrumentation data. The instrumentation data was used to estimate the displacement time history of each abutment wall, displacement of the bridge as a whole, changes in abutment backfill lateral earth pressure, backfill settlement and the overall factors causing the asymmetric response of the bridge to changes in temperature. Among the most notable findings of the chapter is that despite the symmetric appearance of this structure, minor differences during construction led to its noticeably asymmetric response. It is also shown that ratcheting in semi-integral bridge abutments similarly affects the wing walls and abutment caps. Moreover, backfill settlement is seen to consistently increase over time with no signs of slowing down after 2 years of monitoring.

In Chapter 5, the primary focus is on the interaction between the superstructure and substructure in the China Creek Bridge. Evidenced by the primary data collected from the Mack Creek Bridge, which indicated lateral loading of the bridge foundations, it was decided to instrument the foundation of the China Creek Bridge to directly monitor lateral loading of the substructure. The collected data clearly indicates that the semi-integral bridge foundations are subjected to cyclic lateral loading due to shrinkage, creep and thermal expansion/contraction of the superstructure. Moreover, it is shown that the accumulation of plastic strains in the foundation soils has resulted in permanent displacement of the bridge towards one of the abutments.

After Chapter 6, which includes a summary of conclusions from Chapters 2 to 5 as well as potential future work, two appendices are also included. Additional details regarding the Phase 2 instrumentation of Mack Creek Bridge are provided in Appendix A. The details regarding various construction stages as well as the instrumentation of the China Creek Bridge are provided in Appendix B.

1.1. References

Bridge, R., Griffiths, S., and Bowmaker, G. (2005). "The concept of a seamless concrete pavement and bridge deck." Australian Structural Engineering Conf. 2005: Structural Engineering: Preserving and Building into the Future, M. G. Stewart and B. Dockrill, eds., Sydney, NSW, Australia

Burke, M. P. (2009). "*Integral and Semi-Integral Bridges*." Wiley-Blackwell.

Chen, Q. 2008. "Effects of thermal loads on Texas steel bridges." Ph.D. thesis, Dept. of Civil, Architectural and Environment Engineering, Univ. of Texas at Austin.

Civjan, S. A., Kalayci, E., Quinn, B. H., Brena, S. F., and Allen, C. A. (2013). "Observed integral abutment bridge substructure response." *Engineering Structures*, 56: 1177–1191. https://doi.org/10.1016/j.engstruct.2013.06.029.

Huntley, S. A., and Valsangkar, A. J. (2013). *"Field monitoring of earth pressures on integral bridge abutments."* Can. Geotech. J., 50 (8): 841–857. https://doi.org/10.1139/cgj-2012-0440.

Imbsen, R. A., & Vandershaf, D. E. (1984). Thermal effects in concrete bridge superstructures. Transportation Research Record, (950)

Mofarraj, B., and Zornberg, J. G. (2022). "Field Monitoring of Soil-Structure Interaction in Semi-Integral Bridges." Geo-Congress 2022, ASCE, Charlotte, NC, 33–42. https://doi.org/10.1061/9780784484067.004.

Oesterle, R., and Tabatabai, H. (2014). "Design Considerations for Integral Abutment/Jointless Bridges in the USA." Civil and Environmental Engineering Faculty Articles. 1. https://dc.uwm.edu/cee_facart/1

Ooi, P. S. K., Lin, X., and Hamada, H. S. (2010). "Field Behavior of an Integral Abutment Bridge Supported on Drilled Shafts." *J. Bridge Eng.*, 15 (1), 4–18. https://doi.org/10.1061/(ASCE)BE.1943-5592.0000036.

Purvis, R. L., and Berger, R. H. (1983). "Bridge Joint Maintenance." *Transportation Research Record,* 899, 1-10.

Chapter 2: Monitoring of Temperature-induced Lateral Earth Pressures in Semi-integral Bridges

ABSTRACT

Despite the increased utilization of jointless bridges, their attributes and overall behavior are still not fully understood. This is particularly because of the uncertainty in the temperature-induced lateral earth pressures behind the abutment walls. This chapter presents the results and analysis of field monitoring data collected over three years from a semi-integral bridge in Texas. The bridge was instrumented using a combination of earth pressure cells, laser distance meters, crackmeters and temperature sensors. The effect of temperature variations on the evolution of lateral earth pressures acting on the abutment walls were studied using the collected field monitoring data. As expected for semi-integral bridges, elimination of the expansion joints at the ends of the deck resulted in thermally-induced backfill movements that were consistent with daily loading cycles due to thermally induced strains, leading to increased lateral earth pressures and settlements in the backfill. However, the monitoring results indicate that the most significant increases in lateral earth pressures actually occur during the colder periods rather than during the warmer periods when the bridge deck have expanded the most. Also, results from abutment crackmeter data revealed signs of cyclic interaction between the superstructure and substructure of the bridge, which is typically not expected to occur and consequently not considered in current design methodologies of semi-integral bridges.

2.1. INTRODUCTION

Most highway bridges include expansion joints at the ends of their decks and in between adjacent spans to accommodate for longitudinal strains induced in the bridge deck by changes in temperature, shrinkage, and creep. While the incorporation of deck expansion joints minimizes the temperature-induced interaction that occurs between the

deck and abutment, they may also pose important disadvantages (Arsoy et al. 1999). Specifically, and in addition to the initial material and construction costs associated with the use of expansion joints, additional costs often result due to maintenance of the expansion joints and associated bridge components. This is because the use of expansion joints increases the exposure of the bridge superstructure and substructure to moisture, deicing salts, abrasives, chemicals, and other debris, often leading to structural damage and a comparatively fast rate of deterioration (Purvis and Berger 1983). While attempts have been made to protect the concrete against these elements by coating the concrete surfaces, adding a flexible seal, or incorporating a drainage trough, such measures have often been unsuccessful. The repair of damage related to expansion joints can often exceed the initial construction costs of the joints, due to factors such as labor-intensive reconstruction, recurrent traffic disruptions and high overhead costs associated with comparatively small repair work. As a result, several transportation agencies have pursued the elimination of expansion joints in bridge structures.

According to Burke (2009), the use of integral and semi-integral bridges began in Ohio in the 1920s. Since then, the design of such alternative bridges has increased significantly, with many transportation agencies having developed specific design guidelines. Unlike conventional bridges, integral and semi-integral bridges do not have expansion joints and, consequently, the abutment wall displacements (caused by the bridge thermal expansion/contraction) result in movements in the abutment backfill and approach roadways.

In semi-integral bridges, the deck, girders, and abutment walls are integrated during construction (see Figure 1.3). However, the superstructure in these bridges is still typically supported on elastomeric bearings resting on abutment caps that ultimately transfer the load to a deep foundation system. Conversely, the elastomeric bearings are eliminated in the case of integral bridges, resulting in a direct connection between the abutment caps and the deck, girders, and abutment walls. However, the integration of bridge components

establishes additional demands on the foundation components of integral bridges, as the foundation elements need to accommodate lateral displacements that result from the thermal expansion and contraction of the integrally-connected bridge deck. Consequently, compared to applications of semi-integral bridges, higher lateral-flexibility in the foundations and shorter maximum lengths are generally recommended in the design of integral bridges (Burke, 2009). Semi-integral bridges are often preferred over integral bridges in sites where it is more feasible to use rigid foundation units such as large diameter drilled shafts considering the subsoil conditions.

The elimination of expansion joints at the ends of semi-integral bridge decks is expected to lead to cyclical lateral loading of bridge abutments due to changes in internal deck temperature. The magnitude of such displacements depends on the bridge length as well as on local weather conditions, with comparatively large displacements anticipated in longer bridges constructed in climates characterized by larger daily and seasonal temperature fluctuations.

A schematic view showing deformation pattern within the backfill soil induced by cyclic displacements of the abutment wall is shown in Figure 2.1. The abutment wall, originally in a neutral position (Figure 2.1(a)), displaces laterally away from the backfill when the bridge deck contracts (Figure 2.1(b)). This situation leads to backfill movements in the active direction, possibly experiencing an active state of stresses, and resulting in backfill settlements immediately behind the wall. Subsequent expansion of the bridge deck causes the abutment to reach the neutral position again (Figure 2.1(c)), however, the lateral earth pressures in this case are expected to be higher than those in the original neutral position (Figure 2.1(a)) because of the rearrangement of soil particles. Moreover, with each cycle, some backfill settlement is expected to also occur. Continued expansion of the bridge deck (Figure 2.1 (d)) may subsequently lead to displacements in the passive direction within the backfill soil. This condition results in additional backfill deformations, increased lateral earth pressures and possibly heaving at some distance from the abutment

wall. While the displacements shown in Figure 2.1 are magnified for clarity, they illustrate the sequence by which changes in daily temperature lead to recurrent displacements of the abutment wall (into and away from the backfill). Considering the plastic behavior of backfill soils, cycles of the abutment wall displacement generally result in the accumulation of plastic strains within the soil mass. Over time, the accumulation of such plastic strains may result in continuously increasing lateral earth pressures and associated backfill settlements over time. The continued accumulation of plastic strains within the soil mass, coupled with increasing lateral earth pressures, is a phenomenon that is often referred to as "ratcheting", "soil ratcheting" or "earth pressure ratcheting" in the technical literature (Civjan et al 2013, Huntly and Valsangkar 2013, Liu et al. 2021).

Previous studies have attempted to quantify the impact of cyclic loading on the continued increase in lateral earth pressures using in-situ field monitoring, numerical and experimental methods (England et al. 2000, Frosch and Lovell, 2011, Civjan et al., 2013). Clayton et al. (2006) evaluated this problem by conducting a series of cyclic triaxial tests and concluded that increases in the lateral earth pressures caused by cyclic loading depends on the number of cycles, strain magnitude, soil relative density, and shape of the soil particles. These past studies reported that even for densely packed sand particles, cyclic loading leads to fabric changes (i.e., rotation and interlocking of particles) and dilatant behavior, resulting in the accumulation of plastic strains and increasing lateral earth pressures.

However, reported field monitoring data from jointless bridges has not always indicated increasing lateral earth pressures within the abutment backfill of integral and semi-integral bridges. For example, Civjan et al. (2013) reported a slight decline in lateral earth pressures based on long-term monitoring data of an integral bridge, with pressures reaching only 20 to 40% of the theoretical passive earth pressures. These results contradict those reported by other studies such as Huntly and Valsangkar (2013), whose records showed the occurrence of ratcheting in the integral abutment of a bridge. The researchers

provided recommendations regarding the applicability of Rankine's (1857) and Coulomb's (1776) passive earth pressure theories to predict the lateral earth pressures in the abutment backfill. It should be noted that not only abutment walls but also wing walls have reportedly experienced continued increases in lateral earth pressures. For example, Steinberg et al. (2004) monitored the lateral earth pressures acting on the wing walls of two semi-integral bridges, ultimately identifying a non-linear relationship between the bridge expansion/contraction and the lateral earth pressures acting on the wing walls.

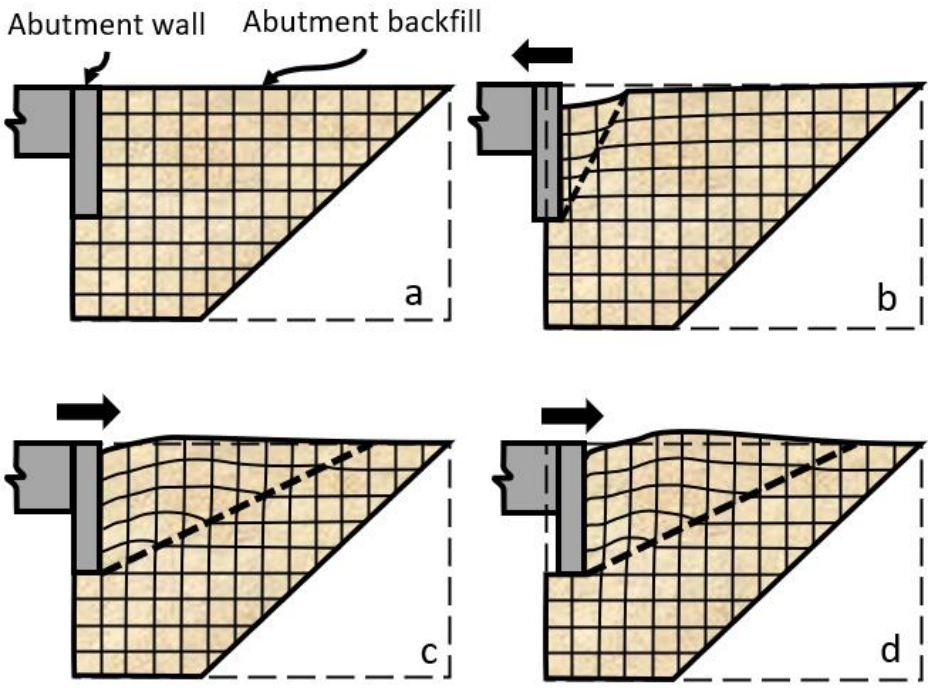

Figure 2.1: Schematic illustrating the phenomenon of "soil ratcheting" within the backfill behind the abutment in a semi-integral bridge: (a) Initial position (neutral) (b) Deck contraction (backfill movement in the active direction) (c) Deck expansion back to initial position (backfill movement in the passive direction) (d) Additional deck expansion (backfill movement in the passive direction)

Some studies have used numerical models to simulate the ratcheting phenomenon and the associated lateral earth pressure increase that result from cyclic loading of granular materials (Xu et al. 2007; Jia and Kong 2015; Liu et al. 2021). These studies have included evaluation of the effect of factors such as the magnitude of temperature cycles, their frequency, and soil relative density on the increase in lateral earth pressures. Notably, numerical simulations reported by Xu et al. (2007) revealed that lateral earth pressure increase occurs in coarse sands with a wide range of relative densities and that ratcheting does not necessarily occur due to soil densification.

Despite the increasing number of jointless bridges being constructed worldwide, there is not a clear consensus regarding issues on a number of factors, such as the design backfill load, expected backfill settlement. In addition, data collected by Burke (2009) reveals that southern US states have been comparatively less inclined to adopt jointless bridge technologies. This may have resulted from the fact that the southern US states experience snowy and icy conditions less frequently and consequently treat roadways with deicing chemicals (a leading cause of expansion joint deterioration) less frequently. In this study, the behavior of jointless bridges under conditions representative of the state of Texas (e.g., climate, standard construction procedures, abutment lateral earth pressures) were evaluated through an instrumentation program implemented on a semi-integral bridge constructed on a rural road in Anderson County, TX in 2017. The instrumentation allowed monitoring of lateral earth pressures and displacements on the abutment wall, deck temperature, and weather parameters. An important objective of the study was to assess the performance of the semi-integral bridges, with particular emphasis in clarifying the contradicting information regarding the magnitude of lateral earth pressures to be considered in their design.

After describing the bridge structure constructed in Anderson County, this chapter summarizes the field data collected as part of the monitoring program and provides an evaluation of the temperature-induced lateral earth pressures acting on the abutment walls.

Ultimately, the collected data provides relevant insight on the performance of semi-integral bridges, including refinements in the design of jointless bridges.

2.2. PROJECT DESCRIPTION

The semi-integral bridge evaluated in this chapter was built to replace an older bridge on County Rd 2133, which overpasses Mack Creek outside the city of Palestine, TX. The replacement bridge is 21 m-long and is striped for two traffic lanes. The cast-in-place deck is 7.98 m-wide and has a thickness ranging of 0.19 m. The deck is supported by six precast, prestressed concrete box girders. The abutment walls of the bridge are 0.91 m-deep and 0.3 m-thick. The topography of the area resulted in a bridge grade ranging from +0.8% (in its northern half) to +1.6% (in its southern half), with the north abutment having an elevation that is 0.25 m below that of the south abutment. The vertical bridge loads are transferred to the foundation soil using 6.7 m-long PZC-18 sheet piles over the entire width of the deck. A schematic of the Mack Creek bridge is shown in Figure 2.2.

The wing walls were constructed using steel sheet piles, which had the same profile adopted for the foundation piles. As a semi-integral bridge, the deck, girders, and abutment walls were integrated during construction. A 12 mm-thick preformed bituminous fiber board was attached to the back of the abutment caps to prevent direct contact between the abutment walls and the pile caps.

The backfill material used for the abutment walls consisted of a crushed rock aggregate. A non-woven geotextile was placed at the bottom and sides of the backfill soils. The access road over the soil backfill involves a flexible pavement that includes a 0.2 m-thick base material and a 0.15 m-thick asphalt concrete layer. A layer of riprap was placed on the bank slopes to protect the sheet piles against the effects of erosion and scour during flooding events at the creek. Due to the semi-integral nature, this bridge does not have expansion joints between the deck and abutment walls; consequently, the thermally-induced abutment wall displacements are transferred to the abutment backfill as well as to

the flexible pavement of the approaching roadway. The Mack Creek Bridge was opened to traffic in July 2017.

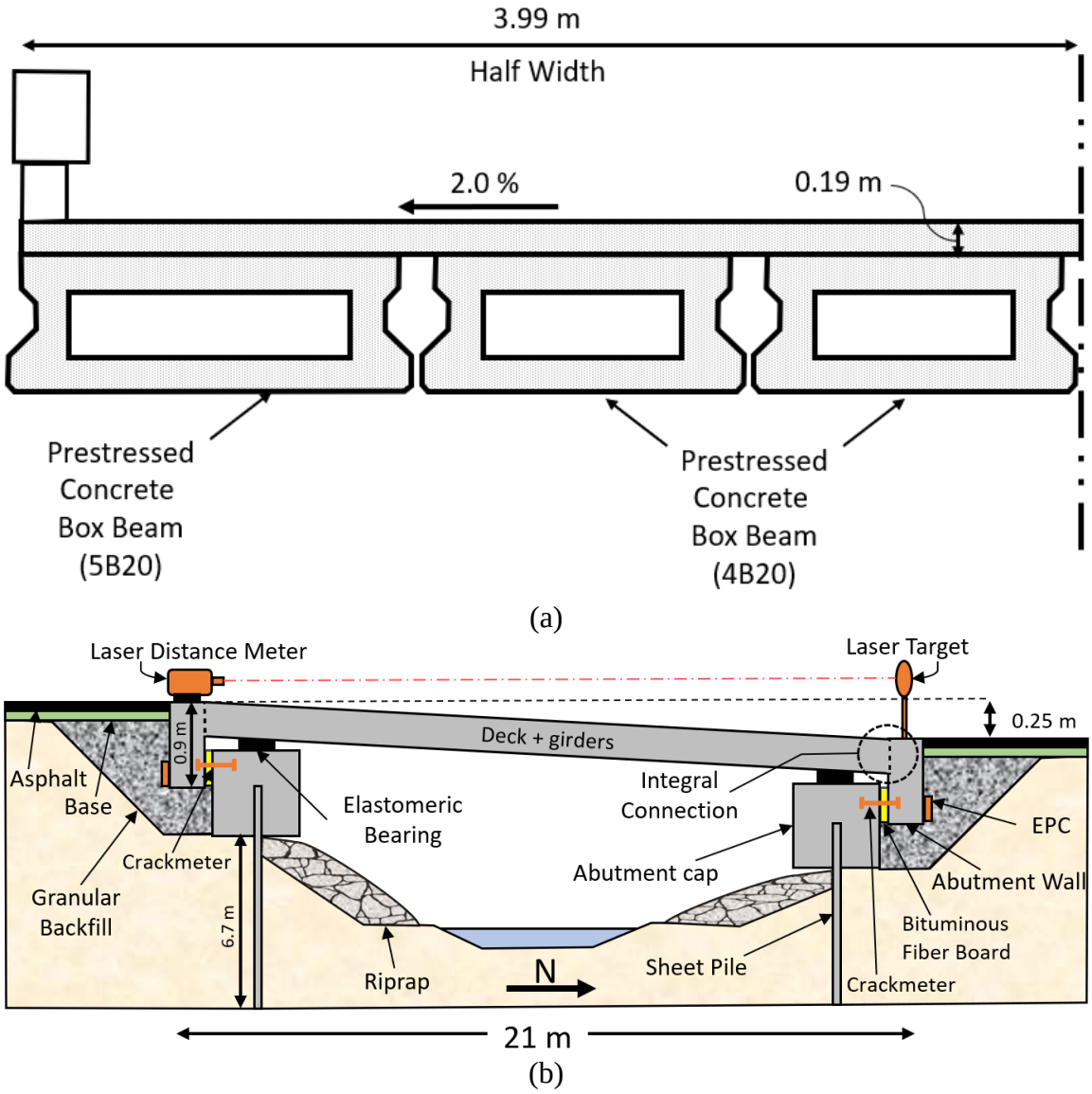

Figure 2.2: Schematic view of the Mack Creek semi-integral bridge: (a) Transverse cross-section (half width); and (b) Longitudinal cross-section with the location of sensors. (Note: EPC stands for earth pressure cell)

2.3. SUBSURFACE GEOTECHNICAL CHARACTERIZATION

To characterize the in-situ soils, 14 m-deep borings were implemented on each side of the bridge. The soil samples recovered from the borings revealed that the top 2 to 5 m consist of silty sand materials and that the deeper layers involve low plasticity sandy and silty clays. Complementing the physical characterization of in-situ soils, a series of Texas Cone Penetrometer (TCP) (TEX 132-E, 1999) tests were performed 1.5 m-deep intervals. A TCP count of 50 was reached for depths below 9 m, which is generally considered an adequate bearing stratum for the sheet pile foundation.

A crushed rock aggregate with a maximum particle size of 16 mm was adopted for the abutment backfill. A series of large-scale consolidated-drained (CD) triaxial tests were performed to characterize this material. Because the maximum particle size of the backfill was 16 mm, a diameter of 150 mm was adopted for the triaxial specimens tested as part of this study (per ASTM D7187-11 requirements). The triaxial test results yielded a shear strength envelope characterized by an internal friction angle of 37° and a cohesion intercept of 12 kPa for confining stresses ranging from 48 to 88 kPa. The shear strength envelope of the abutment backfill is shown in Figure 2.3.

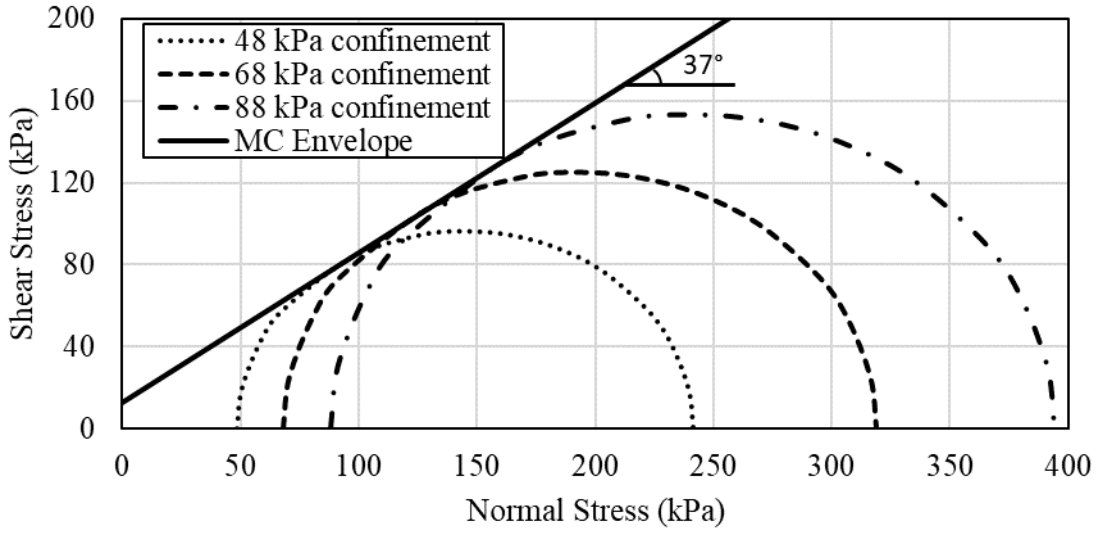

Figure 2.3: Mohr-Coulomb shear strength envelope for the abutment backfill material, as defined from large-scale CD triaxial tests

Complementing the triaxial testing program conducted to characterize the internal shear strength of the backfill soil, the interface shear strength between the backfill soil and concrete was measured by conducting a series of large-scale direct shear tests. A large-scale direct shear testing apparatus, which accommodates specimens with dimensions of 508 mm (W) × 508 mm (L) × 254 mm (H), was used in this interface characterization program. The testing configuration involved placing the backfill in the bottom half of the direct shear box and a precast concrete block on the top half. The tests were performed under normal stresses ranging from 3.5 to 14 kPa, in accordance with ASTM D3080-11. The resulting interface shear strength envelope is shown in Figure 2.4. The interface shear strength between the backfill soils used at the Mack Creek Bridge and precast concrete was characterized by a friction angle of 24° with a negligible cohesive intercept (0.3 kPa) for the range normal stresses considered in the testing program. It should be noted that the concrete-backfill interface friction angle matches well with the typical assumption of

adopting a soil-concrete interface shear strength equal to 2/3 of the internal friction angle of the backfill material (Terzaghi et al., 1996).

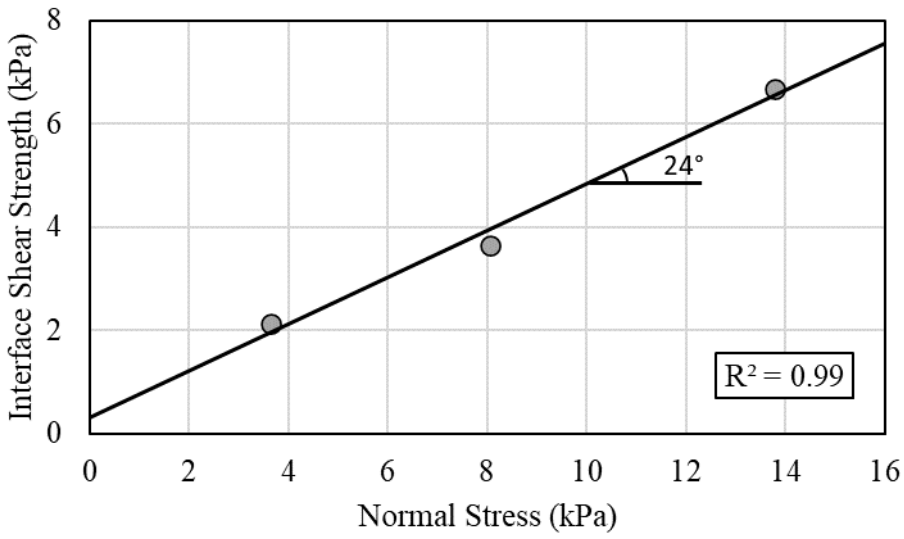

Figure 2.4: Mohr-Coulomb interface shear strength envelope between concrete and abutment backfill, defined using large-scale direct shear tests.

The concrete-backfill interface friction angle and the backfill internal friction angle obtained as part of this testing program were used to predict the theoretical lateral earth pressures at the locations of the earth pressure cells considering the frameworks for active, passive, and at-rest conditions proposed by Rankine (1857), Coulomb (1776) and Jaky (1944).

2.4. FIELD INSTRUMENTATION PROGRAM

The instruments for field performance monitoring of the Mack Creek Bridge were installed in two separate phases, with the initial instrumentation phase carried out during construction of the bridge and the second instrumentation phase implemented 2.5 years later, in 2020.

The initial instrumentation phase included installation of Geokon model 4810 vibrating wire earth pressure cells (EPC) on the abutment walls (see Figure 2.1). Two EPCs were installed on each abutment wall (1.35 m from the center line of the bridge on each side) and measured lateral earth pressures at a depth of 0.75 m. The EPCs were connected to two data loggers (Geokon 8002-4 LC2X4) which were set to collect readings at a rate of once per hour. The data loggers were mounted under the bridge to protect them from potential flooding, rain and direct sunlight. In addition to the lateral earth pressure readings, the temperature of the data logger panel, representing ambient air temperature in the shade, was collected hourly. Additional details about this phase of instrumentation is provided by Walter (2018).

After having collected data from earth pressure cells over the initial two years, a decision was made to install additional sensors at the site to gather complimentary information on the effect of climate variables and thermal deformations of the bridge. The sensors installed during the second phase include:

1. A compact weather station (ClimaVue50), which included a pyranometer, anemometer, temperature sensor, drip counter gauge and a relative humidity sensor. Solar irradiation (Pyranometer) and ambient temperature measurement were expected to be useful to understand different seasonal behaviors of the bridge.
2. An Infrared Radiometer (SI-111SS) was installed to measure the surface temperature of the bridge deck using a thermopile. The deck surface temperature was expected to be a useful parameter to understand the thermal behavior of the bridge.
3. An industrial grade, time of flight laser distance sensor (OptoNCDT ILR 1181-30), which is capable of measuring distances of up to 150 m with a resolution of 0.1 mm.

4. Two crackmeters (Geokon Model 4420) installed at the ends of the bridge, between the abutment caps and the abutment walls. The objective of this instrument is to measure relative displacement between the ends of the bridge deck and abutment caps.

The weather station and infrared radiometer were mounted on top of a pole to conduct the measurements. The laser distance meter was installed on one end of the deck, aiming at a reflective target mounted on the opposite end of the deck, to measure the total length of the deck. The crackmeters were placed with one leg connected to the abutment wall and the other connected to the abutment cap to measure relative displacements between these two components at each abutment. The location of these sensors is also depicted in Figure 2.2.

The data from the Phase 2 sensors were collected by a separate data logger (Campbell Scientific CR6). This data was transmitted daily via cellular modem and was processed automatically by a cloud-based python program developed for this study.

Unfortunately, the earth pressure cells began facing technical difficulties two years after installation and eventually stopped providing data. A field inspection revealed that the sensors started malfunctioning due to damage to the buried portion of the sensor cables. As such, there is no direct overlap between the time histories of the two sets of field monitoring data. However, as both datasets were complemented by ambient air temperature measurements, it is possible to associate the Phase 2 data with the lateral earth pressure data collected during the first phase of instrumentation and reach relevant conclusions.

2.5. PHASE 1 INSTRUMENTATION RESULTS

The EPC and ambient air temperature data collected during the first phase of the monitoring program are presented in Figure 2.5. The figures include the hourly variation (gray lines) of the parameters as well as the 24-hour running average (black lines) of the datasets to help better visualize the trends. Overall, lateral earth pressures ranging from 3

to 70 kPa and ambient air temperatures ranging from -9 to 39°C were observed during the monitoring period.

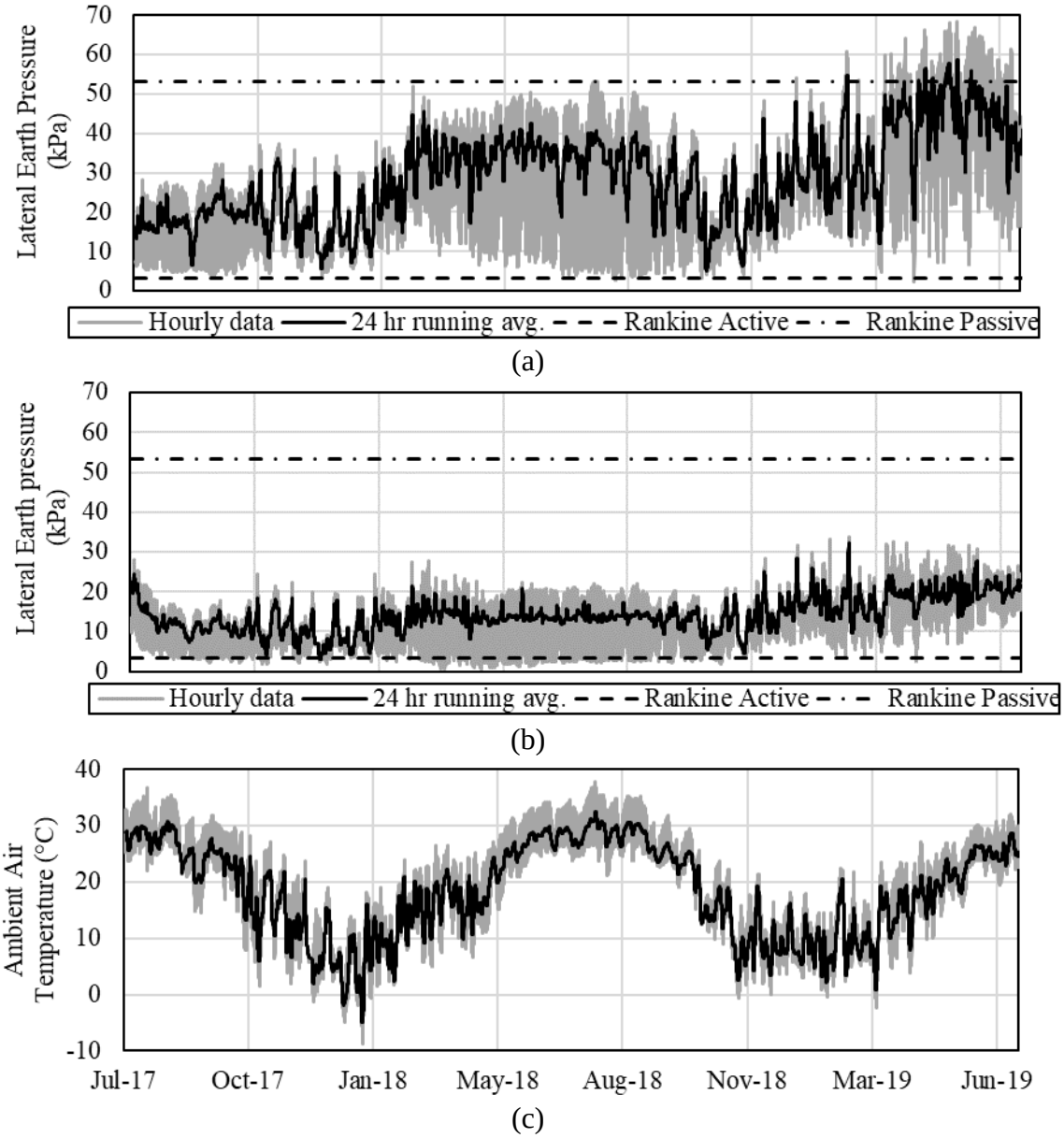

Figure 2.5: Data collected during the first phase of instrumentation: (a) south abutment EPC data; (b) north abutment EPC data; and (c) ambient air temperature

To facilitate the interpretation of the EPC data, theoretical active, passive and at-rest lateral earth pressures at the location of the EPCs are presented in Table 2.1. To facilitate comparison, Rankine's active and passive pressures are included as reference in Figure 2.5. Lateral earth pressure estimates based on Coulomb and Jaky's theories are not included in Figure 2.5 to avoid visual clutter and maintain focus on the field data. As shown in the figure, the pressure values collected from both abutments start at a similar level. The south abutment lateral earth pressures fluctuated within a range of 7 to 25 kPa for the first two months after construction, while the north abutment experienced a decreasing trend in pressures during these two months from 20 kPa to 10 kPa in average. It should be noted that in addition to an average decrease in lateral earth pressures experienced at the north abutment, the magnitude of lateral earth pressure daily variation was also found to decrease. Moreover, for the entire duration of the monitoring period, the south abutment experiences significantly higher lateral earth pressures and larger daily and seasonal fluctuations as compared to the north abutment.

The observed asymmetric behavior continued beyond the first few months of monitoring. The data indicates that the two abutments experienced significantly different levels of lateral earth pressures due to thermal expansion/contraction of the bridge. The south abutment experienced lateral earth pressures as high as 25 kPa in summer 2017, 50 kPa in summer 2018, and 70 kPa in summer 2019. Therefore, the maximum south abutment lateral earth pressure appears to increase by 15 to 25 kPa each summer. On the other hand, the north abutment experienced comparatively smaller levels of lateral earth pressure increases, with an average increase of approximately 5 kPa each year. It is worth noting that the asymmetric behavior of jointless bridges have been noted in several other field monitoring studies such as Laaksonen and Kerokoski (2007).

A possible explanation for the observed asymmetric response of the Mack Creek Bridge is the sloping grade of the bridge (see Figure 2.2). This is because a sloped bridge is expected to expand asymmetrically due to a large fraction of the bridge self-weight being

supported by the lower elevation abutment (north abutment in this case), leading to asymmetric loading of abutment backfills. Additionally, unequal application of compaction efforts was observed during the placement of the abutment backfills, which may be another potential contributor to this behavior. Another potential contributor to the asymmetry was the sequence of construction, which involved placement of the abutment backfill in the south and north abutments several days apart. Placing backfill on one of the abutments while leaving the other abutment unrestrained might cause the bridge to primarily expand towards the side with no backfill, as this side offers no resistance to thermal-induced movements of the bridge. In this case, placing the second backfill while the bridge is at or near its maximum daily thermal expansion, would be followed with the immediate loss of second backfill's compaction when the bridge cools down and contracts when temperature decreases. This phenomenon can potentially result in a significant difference between the stiffness of the two abutments.

An additional important observation that can be drawn from Figure 2.5 is that the lateral earth pressures measured on the south abutment wall slightly exceed the Rankine passive earth pressure (summer 2019), although it still remains below the Coulomb passive earth pressure (see Table 2.1). The passive earth pressures estimated in Table 2.1 were calculated using the laboratory-estimated density and internal friction angle, which may somewhat differ from the in-situ conditions. While comparisons with the theoretical lateral earth pressures are made primarily for comparisons with familiar and practical estimates, for the case of this bridge, Rankine's pressures are consistent with the values collected so far, while Coulomb's pressures would overestimate the range of monitored lateral earth pressure values.

	Coulomb (1776)	Rankine (1857)	Jaky (1944)
Active Earth Pressure (kPa)	3	3.3	-
Passive Earth Pressure (kPa)	160	54	-
At-rest Earth Pressure (kPa)	-	-	5.3

Table 2.1: Predicted lateral earth pressures at the location of the EPCs

Huntley and Valsangkar (2013) report that the lateral earth pressures recorded on an integral bridge exceeded Rankine's passive earth pressure near the top of the wall, while remaining far below such reference pressure at the bottom of the abutment wall, with none of these equations providing a good match to their field observations. While field observations such as those observed in this study indicate that the use of Rankine's passive pressures in design would be slightly unconservative, other researchers such as Civjan et al. (2013) and Kim and Laman (2012) offer a conflicting view by reporting slightly decreasing or relatively constant backfill pressures over time, not reaching Rankine's passive earth pressure. Overall, based on the data collected in this study, and consistent with other monitoring results, the lateral earth pressures acting on the abutment walls in semi-integral are expected to exceed Rankine's passive earth pressures.

Evaluation of the lateral earth pressure data also reveals that the magnitude of daily lateral earth pressure changes during summer months is larger than the magnitude of such pressure changes during winter months. Additionally, the average daily lateral earth pressure remains nearly constant throughout the summer months but changes considerably during the winter months. This contrast in behavior is illustrated by the data presented in Figure 2.6, where daily lateral earth pressure changes in July and November 2018 are compared. As revealed by these results, for daily ambient air temperature changes ranging from 6 to 12 °C, the magnitude of daily lateral earth pressure changes is drastically different for the two months evaluated in this figure (5 to20 kPa in November and 30 to 50 kPa in

July). Therefore, the magnitude of daily lateral earth pressure variation is not correlated with the magnitude of daily ambient air temperature change.

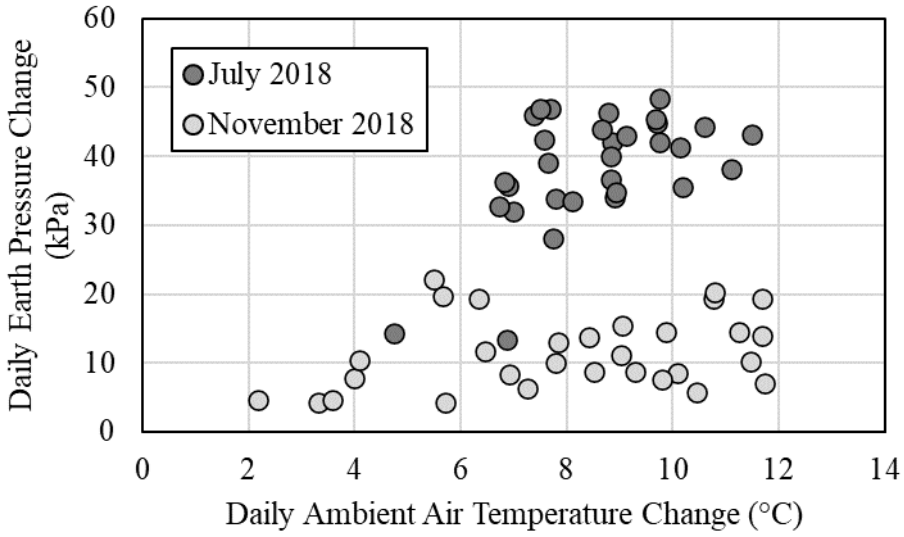

Figure 2.6: Daily ambient air temperature change vs daily lateral earth pressure changes at the south abutment wall (November and July 2018)

In addition to the seasonal contrast in the range of daily lateral earth pressure variation, there also appears to be seasonal differences between how much the average daily lateral earth pressure changes in the colder versus the warmer seasons. For example, inspection of the lateral earth pressures developing at the south abutment (Figure 2.5(a)) and the corresponding ambient air temperatures (Figure 2.5(c)) reveals that the maximum average daily lateral earth pressure (black line) in a given year is actually reached around mid-February, which is a period when the ambient air temperatures are well below the maximum summer temperatures. It is further observed that this lateral earth pressure is barely exceeded during the ensuing warmer months. For example, it can be seen in Figure 2.5 that while the daily average ambient air temperatures remain relatively constant during

the period ranging from November 2018 to February 2019, the lateral earth pressures in the south abutment continuously increased during this period.

To better understand this trend in lateral earth pressures, an algorithm was developed to identify the most prominent periods of sustained lateral earth pressure increase in the lateral earth pressure monitoring results collected from the south abutment. This algorithm aimed at finding the local maxima and minima (extrema) of the lateral earth pressure time-history data with the minimum prominence (Distance between the peak and the base) of 9 kPa in the south abutment lateral earth pressure dataset. To reduce the effect of short-term variations on the analysis and facilitate the selection of instances that represent a period of sustained elevated lateral earth pressures, the algorithm was set to detect such points using a 5-day moving average of the lateral earth pressure data.

The points that satisfy the above-mentioned criteria were used to calculate the percent lateral earth pressure increase between consecutive local extrema, with the results plotted against the average air temperature during that period in Figure 2.7(a). For example, during the period of January 4, 2018, to February 18, 2018, when the average air temperature was 9.5 °C, the 5-day average earth pressures in the south abutment increased by 230% (From 11 kPa to 36 kPa). To help better visualize this data, Figure 2.7(b) was developed as well. This plot shows the average south abutment pressure magnitude versus the average ambient air temperature during the sustained earth pressure increase periods identified by the algorithm. The results plotted in Figure 2.7 indicate that although larger earth pressures were recorded during periods with higher temperatures, larger earth pressure increases have occurred during the period with relatively colder temperatures. In other words, significant ratcheting has occurred at temperatures significantly below the maximum annual ambient air temperature and was a cold season phenomenon.

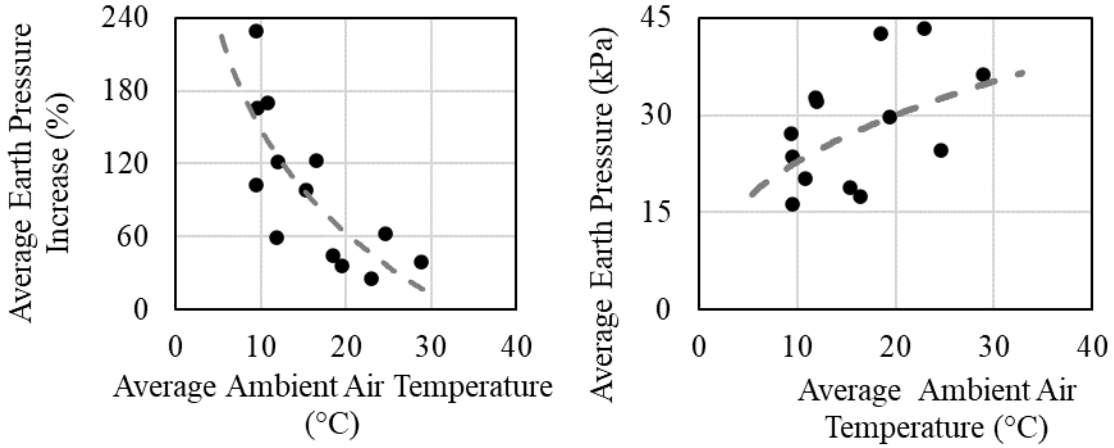

(a) (b)

Figure 2.7: Evaluation of the relationship between ambient air temperature and ratcheting: (a) south abutment average earth pressure increase vs the average ambient air temperature (b) south abutment average earth pressure vs average ambient air temperature

According to the experimental studies of ratcheting by Clayton et al. (2006), one of the leading causes of stress increase in coarse-grained soils is the readjustment of particles at or close to stress conditions corresponding to the active state. Therefore, the increased likelihood of the backfill soil experiencing active or close to active conditions during the winter can explain the larger pressure increases observed during the periods of cold temperatures as characterized in Figure 2.7. It is worth noting that the likelihood of abutment backfills experiencing active conditions is expected to be larger for bridges completed in the hotter times of the year as compared to bridge completed during the colder times of the year.

Based on the previous analysis, the likelihood of occurrence of earth pressure increase or ratcheting is expected to increase with the following conditions:

1. Bridge sites where the magnitudes of daily and annual temperature changes are large as opposed to locations where daily and seasonal temperature variation is small (such as tropical locations)
2. Bridge construction finishing during the warmer periods of the year instead of colder periods.
3. Bridges with a longer total length.
4. Bridges that experience asymmetrical thermal expansion/contraction which can be due to factors such as the bridge geometry, backfill compaction, construction sequence, foundation soil variation, etc.

This hypothesis may explain why despite the expectation of ratcheting and long-term earth pressure increase, not all field monitoring projects have observed such behavior.

2.6. PHASE 2 INSTRUMENTATION RESULTS

As previously mentioned, additional sensors were installed on the Mack Creak Bridge in January 2020 to collect complementary field data. With the added sensors, the changes in the length of the bridge deck were measured using a laser distance meter. Figure 2.8(a) presents the change in deck length measured using the laser distance meter results. These results were calculated using the reference length of 20,395 mm which was measured at the beginning of Phase 2 monitoring using the laser distance meter. The ambient air temperature (obtained using the on-site weather station) and the deck surface temperatures (obtained using the infrared radiometer) are plotted in Figures 8(b) and (c), respectively.

During the first year of monitoring, the Mack Creek Bridge appears to have experienced 25 mm of deck length change from winter to summer. From Figure 2.8(a) it is common to see the bridge length changing 3 to 5 mm in a day during the summer while this value can range between 4 to 15 mm during the winter.

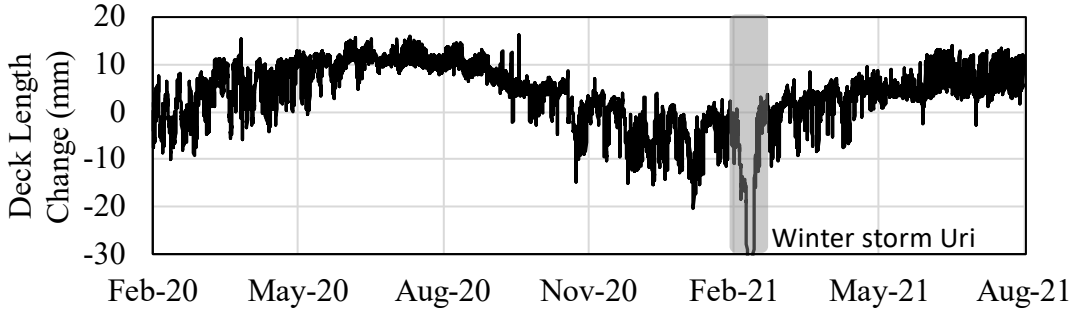

(a)

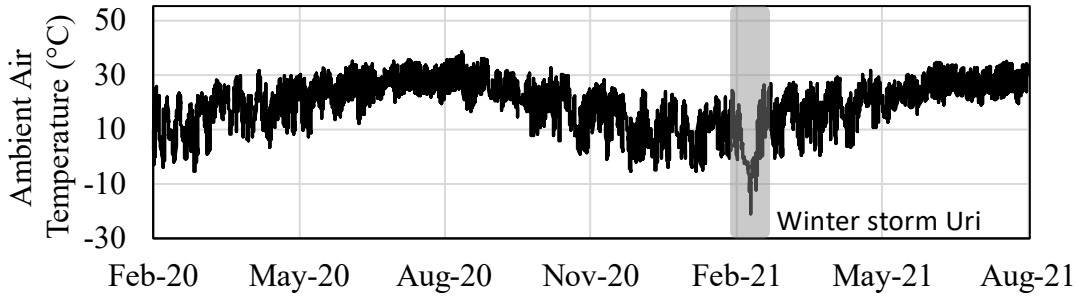

(b)

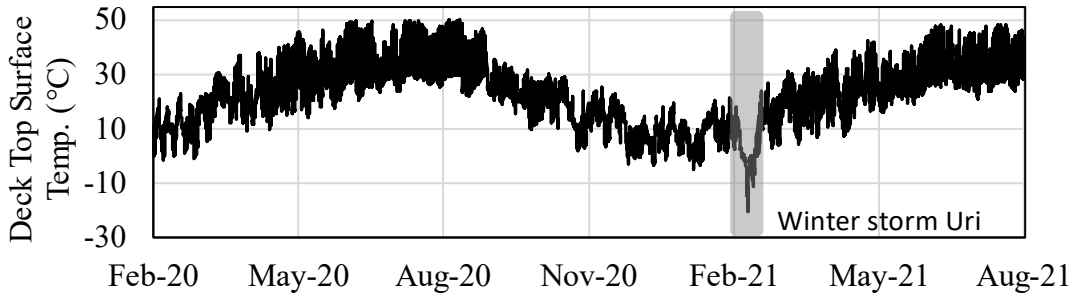

(c)

Figure 2.8: Data collected during the second phase of instrumentation: (a) Deck length changes; (b) Ambient air temperatures; and (c) Deck surface temperatures.

It is worth noting that the second year of monitoring included an event of extreme cold conditions, identified as winter storm Uri. This winter storm is classified as a 100-year return period event, which resulted in significant number of fatalities in Texas as well as financial losses exceeding $200 billion. This weather event occurred from February 13 to 20, 2021, resulting in the largest number of consecutive subfreezing days on record in the state of Texas, causing record low temperatures reaching -20 °C. While readings from the laser distance meter indicated a deck contraction exceeding 50 mm during this winter event, distance meter data during this period is considered invalid because temperatures went below the minimum recommended operating temperature of -10 °C for this sensor. The estimated change in the length of the deck during this period is -30 mm (based on regression analysis of the deck length change against temperature data). Considering this correction, the length of the Mack Creek Bridge decreased by approximately 50 mm from summer 2020 to winter 2021.

To further investigate the difference in the seasonal behavior of the bridge, Figure 2.9 was developed. This plot shows the daily change in the length of the bridge versus the daily change in ambient air temperature in August and December 2020. The collected data shows that the bridge deck experiences larger changes in length during the winter due to any given daily ambient air temperature change. For example, the bridge experienced 8 mm of deck length change on a day with 13.5°C change in temperature in December 2020, while it experienced 2 to 5 mm of deck length change on days with a similar magnitude of temperature change in August 2020. Moreover, the temperature records indicate larger daily temperature changes occurring during the colder months (26 °C maximum temperature change in December 2020 vs. 16 °C in August 2020). This further contributes to the observed difference in seasonal behavior, resulting in larger daily deck length change values during the colder months of the year compared to the warmer months.

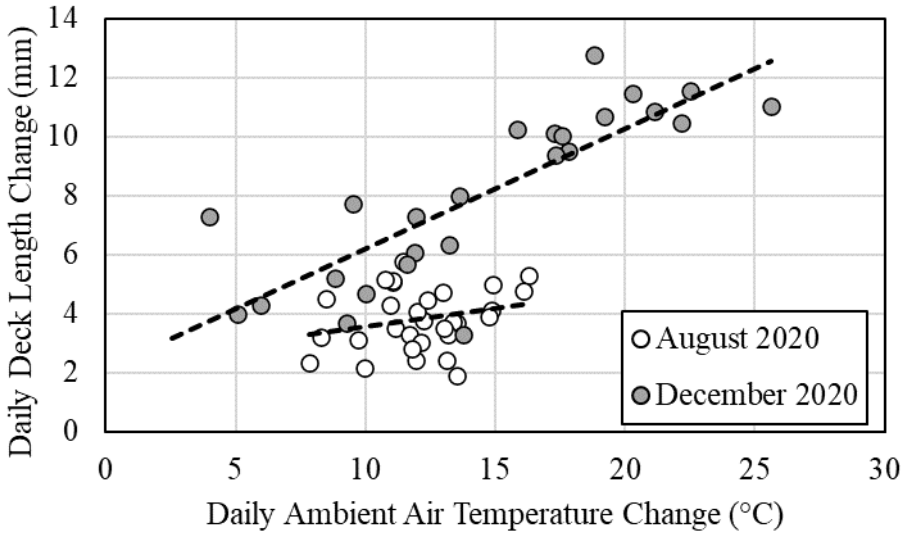

Figure 2.9: Daily changes in deck length as a function of daily ambient air temperature changes (for August and December 2020)

To further investigate the causes of the difference in seasonal thermal expansion/contraction behavior, a comparison between the ambient air temperature, the deck surface temperature and solar radiation during the winter and summer periods was conducted. Figure 2.10 shows the recorded temperature and solar irradiance (solar power density per unit area) for the months of December and August 2020. During the winter, the deck surface temperatures are within 5 °C of the ambient air temperatures. On the other hand, during the summer, the deck surface remains at temperatures that are 5 to 20 °C higher than the ambient air temperatures. It is expected that the longer duration of the days as well as the high magnitude of solar irradiance during the summer causes the internal deck temperature to increase much more than it does during a typical winter day, resulting in the bridge deck remaining warmer than the ambient air temperature during the night. In this case, the elevated core concrete temperature in summer days keep the deck surface warmer than the ambient air temperature, even during the nighttime hours.

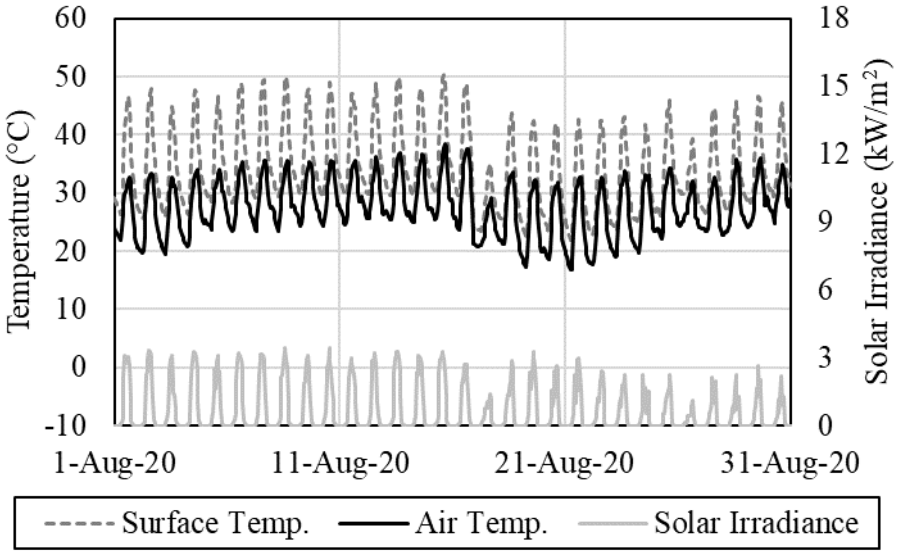

(a)

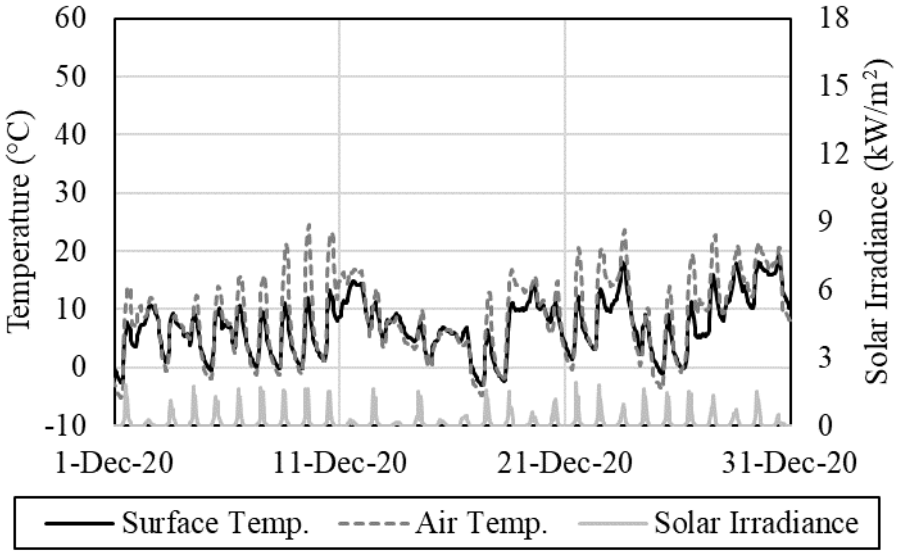

(b)

Figure 2.10: Recorded ambient air temperature, deck concrete surface temperature and solar irradiance at the bridge: (a) August 2020, and (b) December 2020

The factors mentioned above result in the deck remaining consistently at higher temperatures than the ambient air during the warm months of the year, even during the night. On the other hand, in winter the deck surface can be found to be cooler than the ambient air temperature during the night as well as most hours of the day as shown in Figure 2.10. Consequently, deck surface typically experiences smaller magnitude of temperature variation during a day in the summer than it does in winter months and similar trends are expected to have occurred below the deck surface as well. As thermal expansion/contraction is a function of changes in the material's temperature, the observations made based on Figure 2.10 explains why smaller magnitude daily thermal expansion/contraction cycles are observed during the summer months (Figure 2.9). As the bridge length change equals the sum of lateral displacements in the two abutment walls, larger displacement cycles are expected to have affected the abutment backfills during the colder months, in comparison to the warmer months. As shown by studies such as Clayton et al. (2006), higher magnitude displacement cycles can increase the rate of stress increase or ratcheting within the soil mass.

While there was no overlap between the periods during which EPC data and displacement data were collected (i.e., monitoring phases 1 and 2, respectively), the two datasets can still be qualitatively combined given the similar annual temperature records between the two datasets. As previously discussed, the daily average lateral earth pressure in the backfill of the abutment walls increases significantly during cold periods while it remains reasonably unchanged during warm periods. Additionally, the abutment walls tend to exert displacement cycles of comparatively larger magnitude on the backfill during cold rather than during warm periods. Lastly, the backfill soil is more likely to approach active conditions during cold months, especially considering that completion of the Mack Creek Bridge took place during the summer.

It should be noted that several of the aspects that affected the development of lateral earth pressures in the Mack Creek Bridge cannot be generalized to other semi-integral

bridges without careful evaluation of the conditions of each project. These conditions include location of the bridge (climate), bridge geometry, length of the bridge, and season of completion of the bridge construction. That is, a bridge of similar geometric and structural characteristics to the Mack Creek Bridge, located in a climate with different ranges of daily and seasonal temperature variations may not experience similar levels of earth pressure increase. Also, a similar bridge with construction finalized during winter, will generally have a smaller likelihood of the backfill approaching active state conditions and experiencing ratcheting.

As described previously, the Phase 2 instrumentation of the Mack Creek Bridge included the installation of two crackmeters on the abutments. The crackmeters aim at measuring the relative displacements between the abutment walls and abutment caps on each end of the bridge (see Figure 2.2). As previously mentioned, crackmeter measurements are in reference to their position at the time of installation. The crackmeter data collected in the south and north abutments is presented in Figure 2.11. During the first year of monitoring, the relative displacement measured between abutment caps and abutment walls reached 5 and 2.6 mm in the south and north abutments, respectively. Similar to the EPC data collected in the south and north abutments, the crack meters also show asymmetric movements in the two abutments, with larger relative displacements occurring in the south abutment.

Overall, the sum of crackmeter measurements in the two abutments was found to be smaller than the total change in deck length as recorded by the laser distance meter. For example, the crackmeter measurements total 7.7 mm in July 2020 while the laser distance meter recorded changes in deck length of 14 mm at that time. The difference in displacements between the crackmeter and the laser distance meter measurements reveals that the abutment caps should have experienced lateral displacements. In fact, considering the bridge completion time (peak summer temperatures), the seasonal temperature differences (30 to 40 °C), it can be inferred that the magnitude of permanent and seasonal

contraction has caused contact (and consequently, interaction) between the abutment walls and the abutment caps.

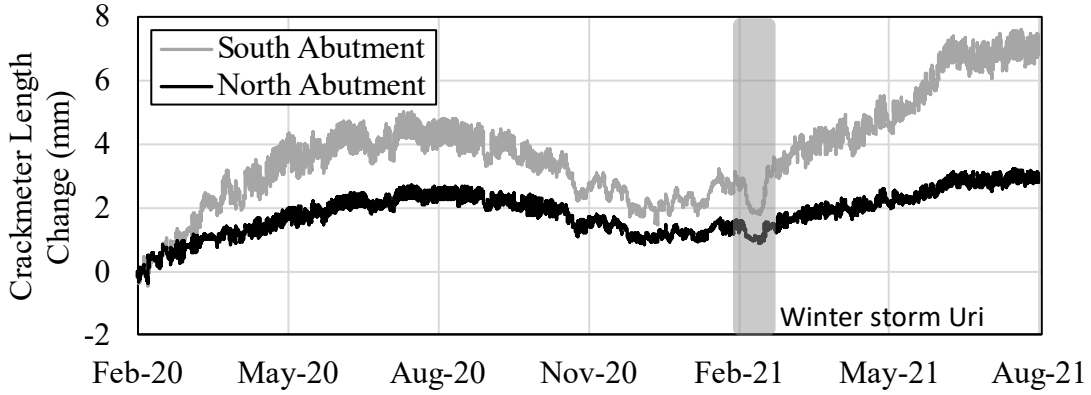

Figure 2.11: Crackmeter measurements in the two bridge abutments, quantifying the relative displacement between abutment walls and caps

Another relevant observation can be made by assessing the crackmeter measurements recorded one year after the installation. As can be observed in Figure 2.11, the north and south crackmeters measurements did not return to 0 mm after one year of operation and measured 1 mm and 2 mm in January and February 2020. Furthermore, the measurements do not drop below these levels even during the February 2021 winter storm, which caused temperatures ranging from 20 to 30 °C below than that at the time of installation. Inspection of the expansion joints being monitored by the crackmeters revealed signs of debris accumulation in these joints. These observations suggest that after the bridge expanded and the joint width between abutment wall and abutment cap increased, debris may have accumulated in this joint and prevented their full closure during winter. Consequently, the magnitude of the displacements of abutment caps are expected to increase with subsequent yearly cycles. This increase in the abutment cap displacement is also expected to lead to increased tension in the deck with subsequent yearly cycles.

As both crackmeter and laser displacement meter measure relative displacements, the absolute displacement of each abutment cap cannot be determined using the available measurements. However, the net displacement of both abutment caps can be determined by subtracting the sum of crack meter measurements from the laser distance meter measurements. The results of this analysis are shown in Figure 2.12. These results correspond to the sum of the displacements of the two abutment caps relative to their position at the beginning of the monitoring program. For example, the 10 mm displacement shown for summer 2020 indicate that the two abutment caps were 10 mm farther from each other at that time, compared to their position in February 1, 2020.

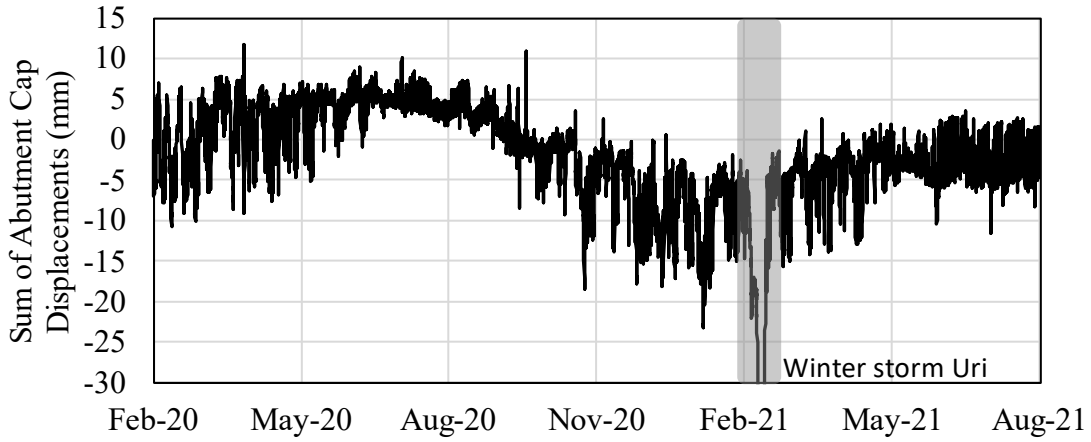

Figure 2.12: Sum of abutment cap displacements. Positive values indicate increasing distance between abutment caps (relative to their position in February 2020).

It is evident from the data in Figure 2.12 that the abutment cap movements occurred daily, and that the cyclic displacement continued through the summer when the bridge was at its maximum length (summer). While the actual fraction of these total displacements that corresponds to each abutment is unknown, the mere identification of the existence of abutment cap movements has major design implications. This is because the presence of cyclical lateral displacements on the abutment caps reveal that cyclical lateral loading

occurred on the foundation elements in spite of the semi-integral nature of the Mack Creek Bridge. To put this in perspective, such loading is expected and designed for when adopting integral bridges, where abutment cap and wall are integrally connected, often leading to the selection of comparatively flexible deep foundations that would be not significantly affected by the expansion/contraction of the bridge. However, in semi-integral bridges, where abutment cap and wall are not integrated, such interactions are not expected nor considered in the design of the deep foundation elements. In fact, comparatively rigid deep foundation elements such as drilled shafts are often adopted for these bridges. Consequently, comparatively long semi-integral bridges may experience long-term performance issues due to this interaction between the abutment wall and cap, especially if the foundation involves comparatively rigid units.

Figure 2.12 data shows that in addition to the caps experiencing daily cyclic relative displacements, the magnitudes of these displacements increase each year, probably due to debris accumulation in the joints (For example, compare May 2020 to May 2021 data). Therefore, the design of the foundation elements may require additional analyses to account for these lateral displacement cycles and their effect on the long-term performance of semi-integral bridge foundations.

The cyclic loading of the foundations in semi-integral bridges is affected by factors such as the season of bridge completion, length of the bridge, abutment details, climate, and drainage conditions. For example, a bridge completed during winter, is less likely to experience lateral loading of abutment caps during the summer, although it may still experience such lateral loading during the winter due to cold spells. Similarly, a bridge with proper drainage design may not be affected by debris accumulation in the joints, which can lead to larger magnitude displacements of the abutment caps. An approach to minimize such effects may involve designing for joints between abutment caps and wall that are comparatively wide. Additionally, the use of a resilient soft compressible inclusion within

this joint may help minimizing undesired interactions between the abutment wall and abutment cap.

2.7. CONCLUSIONS

Field monitoring data was obtained from an instrumented semi-integral bridge located in Anderson County, TX, a state where semi-integral bridge design has not yet been adopted as standard practice. The monitoring results were evaluated to assess the field performance of semi-integral bridges

The instrumentation data collected from this semi-integral bridge led the following conclusions:

- Data from the abutment wall pressure cells showed a clearly increasing trend in lateral earth pressures, revealing the occurrence of ratcheting caused by daily cyclic displacement of abutment walls. The maximum annual earth pressure in the monitored wall was observed to increase by approximately 100% each year during the monitoring period.
- An asymmetric earth pressure response was observed between the two abutments. The south abutment experienced larger magnitude earth pressures, reaching Rankine passive earth pressures, while the north abutment wall experienced comparatively smaller earth pressures. The asymmetry in the performance was attributed to several factors, including the sloping grade of the bridge, unequal application of compaction efforts during backfill placement, and the sequential placement of backfill behind the abutment walls. Accordingly, symmetrical behavior of semi-integral bridges should not be necessarily assumed for the purposes of design or analysis of the structure.
- The highest lateral earth pressures for both abutments developed during the warm season, when the bridge deck is at maximum expansion. The maximum lateral earth pressures were observed to reach Rankine's passive earth pressure during summer 2019, while they were observed to drop to Rankine's active earth pressure regularly

due to contraction of the bridge at night. This resulted in relatively large amplitude earth pressure cycles being experienced over the warmer months, compared to the colder months.

- Analysis of seasonal increase in lateral earth pressures reveals that while the highest yearly lateral earth pressures are observed during the warm periods of the year, the highest lateral earth pressure increases occur during the cold periods of the year. This finding indicates that sustained earth pressure increases occur when the backfill soil experiences active or close to active conditions.
- Analysis of the bridge length change data reveals that the bridge deck tends to experience larger changes in length during the colder months, compared to the warmer months. The observed difference in seasonal behavior is attributed to the difference in solar radiation intensity and duration between the seasons which results in smaller daily temperature variation of deck concrete during the summer months compared to winter months. Therefore, the larger magnitude displacement cycles occurring during the colder months also contribute to the higher rate of earth pressure increase observed during the colder months versus the warmer months.
- Comparison of the crackmeter data (relative abutment wall – abutment cap displacement) with deck length change data revealed that the abutment caps undergo cycling displacement cycles. This is expected to have been caused by the contraction of the deck due to shrinkage, thermal contraction, and accumulation of debris in the joints. As the bridge was completed in the summer, the largest magnitude abutment cap displacements were observed during the winter with the abutment caps being pushed towards the center of the bridge. Therefore, the design of the semi-integral bridge foundation elements may require additional analyses to account for these lateral displacement cycles and their effect on the long-term performance of semi-integral bridge foundations.

- The crackmeter data revealed that the width of the expansion joints on both abutments has increased after one year of monitoring. Accumulation of debris in these joints was confirmed after a visual inspection. These observations suggest that after the bridge expanded and the joint width between abutment wall and abutment cap increased, debris may have accumulated in this joint and prevented their full closure during winter. Consequently, the magnitude of the displacements of abutment caps are expected to increase with subsequent yearly cycles.

2.8. ACKNOWLEDGEMENTS

The authors thank the Texas Department of Transportation (TxDOT) for funding this research under project 0-6936 through the Center for Transportation Research (CTR) at the University of Texas at Austin.

2.9. REFERENCES

Arsoy, S., Barker, R. M., and Duncan, J. M. (1999). "The behavior of integral abutment bridges." Virginia Transportation Research Council, and Jr. Dept. of C. and E. E. Virginia Polytechnic Institute and State University. Charles E. Via, eds.), (FHWA/VTRC 00-CR3).

ASTM D3080 / D3080M-11. (2011). "Standard Test Method for Direct Shear Test of Soils Under Consolidated Drained Conditions.", ASTM International, West Conshohocken, PA, 2011, www.astm.org

ASTM D7181-20. (2020). "Standard Test Method for Consolidated Drained Triaxial Compression Test for Soils", ASTM International, West Conshohocken, PA, 2020, www.astm.org

Burke, M. P. (2009). "Integral and semi-integral bridges." Wiley-Blackwell.

Civjan, S. A., Kalayci, E., Quinn, B. H., Breña, S. F., and Allen, C. A. (2013). "Observed integral abutment bridge substructure response." Engineering Structures, 56, 1177–1191.

Clayton, C. R. I., Xu, M., and Bloodworth, A. (2006). "A laboratory study of the development of earth pressure behind integral bridge abutments." Géotechnique, 56(8), 561–571.

Coulomb, C. A. (1776). "Essai sur une application des règles de maximis & minimis à quelques problèmes de statique, relatifs à l'architecture." De l'Imprimerie Royale, Paris.

England, G. L., Tsang, N. C. M., and Bush, D. I. (2000). "Integral bridges: a fundamental approach to the time–temperature loading problem." Thomas Telford, London, England.

Frosch, R., and Lovell, M. (2011). "Long-Term Behavior of Integral Abutment Bridges." JTRP Technical Reports. https://doi.org/10.5703/1288284314640.

Huntley, S. A., and Valsangkar, A. J. (2013). "Field monitoring of earth pressures on integral bridge abutments." Canadian Geotechnical Journal, 50(8), 841–857.

Jaky, J. (1944). "The coefficient of earth pressure at rest." J. Soc. Hung. Archit. Eng., 355–358.

Jia, P., and Kong, L. (2015). "Modeling of ratcheting accumulation of secondary deformation due to stress-controlled high-cyclic loading in granular soils." Journal of Central South University, 22(6), 2306–2315.

Kim, W., and Laman, J. A. (2012). "Seven-Year Field Monitoring of Four Integral Abutment Bridges." Journal of Performance of Constructed Facilities, 26(1), 54–64.

Laaksonen, A., and Kerokoski, O. (2007). “Long-term monitoring of Haavistonjoki Bridge.” IABSE Symposium, Weimar 2007: Improving Infrastructure Worldwide, International Association for Bridge and Structural Engineering (IABSE), Weimar, Germany, 360–361.

Liu, H., Kementzetzidis, E., Abell, J. A., and Pisanò, F. (2021). “From cyclic sand ratcheting to tilt accumulation of offshore monopiles: 3D FE modelling using SANISAND-MS.” Géotechnique, 1–16.

Purvis, R. L., and Berger, R. H. (1983). “Bridge joint maintenance.” Transportation Research Record, (899).

Rankine, W. J. M. (1857). “On the stability of loose earth.” Philosophical transactions of the Royal Society of London, 147, 9–27.

Steinberg, E., Sargand, S. M., and Bettinger, C. (2004). “Forces in wingwalls of skewed semi-integral bridges.” Journal of Bridge Engineering, 9(6), 563–571.

Texas Department of Transportation. (1999). “Tex-132-E: Test Procedure for Texas Cone Penetration.” Texas Department of Transportation.

Walter, J. R. (2018). “Experimental and numerical investigation of integral/semi-integral bridge abutments for Texas conditions.” Master’s Thesis, University of Texas at Austin.

Xu, M., Clayton, C. R., and Bloodworth, A. G. (2007). “The earth pressure behind full-height frame integral abutments supporting granular fill.” Canadian Geotechnical Journal, 44(3), 284–298.

Chapter 3: Development of an Instrumentation System for Monitoring Long-term Thermally-induced Interactions in Semi-integral Bridges

ABSTRACT

The development and field performance assessment of a comprehensive monitoring system for a semi-integral bridge is discussed in this chapter. The purpose of the instrumentation system is to help quantify loads and displacements acting on the superstructure, substructure, and abutment of a semi-integral bridge due to daily and seasonal temperature variations. The instrumentation system consists of more than 70 sensors, which enable continuous monitoring of more than 200 parameters in the instrumented bridge. The sensors include strain gauges, tiltmeters, crackmeters, laser distance sensors, shape arrays, infrared radiometers, a weather station, piezometer and earth pressure cells. In addition to the commercially available sensors, a new approach was used to measure backfill settlement using a customized displacement transducer, which was proven to be highly accurate after cross-validation with a Ground Penetrating Radar (GPR) survey at the site. Most notably, the early data collected from the sensors indicated that the thermal deformations of the bridge occurred asymmetrically and that the drilled shafts experienced cyclic lateral loading due to thermal contraction of the bridge. The drilled shaft shape arrays were found to be a particular useful component of the instrumentation system as they could be successfully used to estimate bending moments acting on the drilled shafts and to determine absolute abutment wall displacements.

3.1. INTRODUCTION

Semi-integral and integral bridge construction is becoming increasingly common in the USA and around the world. The main characteristic of these bridges is the elimination of expansion joints at the ends of the deck and in between spans. Integral bridges are

continuous single or multi-span bridges where the superstructure is constructed integrally with the substructure. In contrast, the abutment walls and abutment caps are not integrally connected in semi-integral bridges, allowing the superstructure to move independent of the substructure.

The increasing utilization of these structures is due to the number of issues associated with deck expansion joints. Deck expansion joints are typically used to alleviate some of the stresses in the structure caused by issues such as shrinkage, creep, thermal expansion/contraction and differential settlement of piers and abutments (Burke, 2009). As noted by Purvis and Berger (1983), there are several problems associated with deck expansion joints. These problems include a comparatively high rate of wear and tear, exposure of the structure to harmful chemicals, and relatively high cost of initial construction and maintenance. Therefore, many transportation agencies across the world have opted for other alternatives, such as semi-integral and integral bridges, as the cost of deck expansion joints often outweighs the benefits they provide by the alleviating secondary stresses for single and multi-span bridges of moderate length (Burke, 2009).

A review of the semi-integral and integral bridge details within the United States reveals significant differences among the designs adopted in each state. For example, according to Maruri and Petro (2005), while many states require H-pile foundations oriented toward the weak axis for integral bridges for flexibility, some states require it to be oriented toward the strong axis and some states (e.g., Nevada), even permit the use of drilled shafts, which can be much more rigid than H-piles. This information reveals that the design methodology used for these structures has evolved somewhat experimentally by experienced bridge engineers in different regions.

As expected, elimination of expansion joints leads to displacement of abutment walls into and away from the backfill. These cyclic movements, which occurs daily with changes in temperature, can lead to ratcheting, settlement, and an increase in lateral earth pressures within the backfill (Mofarraj and Zornberg, 2022; Huntly and Valsangkar, 2013).

This complex soil-structure interaction has been studied by researchers using numerical, experimental, and field investigation methods. While a trove of valuable information has been gathered through these efforts, the behavior of semi-integral and integral bridges is still not fully understood. Moreover, many transportation agencies prefer to learn about the performance of their designs in their respective areas of jurisdiction to evolve their current methods of bridge construction and support the construction of jointless bridges.

With the increased availability and affordability of instrumentation equipment, many transportation agencies have begun utilizing long-term monitoring programs to better understand the performance and behavior of sensitive infrastructure, such as roadways and bridges. Consequently, an increasing number of publications detailing the information found through various studies about the performance of semi-integral and integral bridge structures are being made available. A summary of the relevant publications, which includes long-term field instrumentation data from semi-integral and integral bridges, is presented in Table 3.1.

Reference	**Location**	**Bridge type**	**Sensors**	**Duration (yrs)**	**Notable Conclusions**
Abendroth et al. (2007)	Iowa, US	34 m-long, single span, precast girder, skew, precast piles, integral	strain gauges, displacement sensors, thermocouples	1.5	asymmetric abutment displacement, in-plane deck rotation
Huffaker (2013)	Utah, US	97 m-long, 3 spans, skewed, pre-stressed girders, driven steel piles, integral	survey targets (reflectors)	1	asymmetric displacement records for skewed abutments

Table 3.1: Summary of studies on the field performance of integral and semi-integral bridges. (Continues)

Reference	Location	Bridge type	Sensors	Duration (yrs)	Notable Conclusions
Abendroth et al. (2007)	Iowa, US	34 m-long, single span, precast girder, skew, precast piles, integral	strain gauges, displacement sensors, thermocouples	1.5	asymmetric abutment displacement, in-plane deck rotation
Huffaker (2013)	Utah, US	97 m-long, 3 spans, skewed, pre-stressed girders, driven steel piles, integral	survey targets (reflectors)	1	asymmetric displacement records for skewed abutments
Jorgenson (1974)	N Dakota, US	137 m-long, 6 spans, concrete box girders, integral	manual measurements using steel tape, slope indicators and thermocouples	1	asymmetric abutment movements with large movements observed in south abutment
Ooi et al. (2010)	Hawaii, US	24 m-long, single span, integral, drilled shaft, precast girders	strain gauges (deck, girder, abutment, foundation) inclinometer array (abutment wall, foundation), pressure cell (abutment wall)	4	shrinkage and creep dominated compared to thermal strains, asymmetric abutment displacement, backfill pressures below active pressure, asymmetric bridge response to flooding

Table 3.1: (Continued)

Reference	**Location**	**Bridge type**	**Sensors**	**Duration (yrs)**	**Notable Conclusions**
Huntly and Valsangkar (2013)	New Brunswick, Canada	76 m-long, 2 spans, piles, integral	strain gauges (piles, deck, girder), thermocouple (deck, girder), pressure cell (abutment wall), tiltmeter (abutment wall), deformation meter (abutment wall), fiber optic sensors (backfill)	3.5	asymmetric abutment wall pressure, asymmetric abutment displacement, lateral earth pressure increase in one abutment, translational abutment wall movement
Lawver et al. (2000)	Minnesota, US	66 m-long, integral, prestressed concrete girders, 3 spans, H piles	abutment displacement & rotation, abutment earth pressure, strain gauges (pile, girder, deck), thermal gradients, approach settlement, frost depth, weather	2	abutment motion was mainly translational, abutment expansion was effectively unrestrained, effect of environmental loads found to be larger than live load in some cases
Hoppe et al. (1996)	Virginia, US	98 m-long, semi-integral, 2 spans, steel girder, 5-degree skew	pressure cells (cap and backwall), strain gauge (girder), temperature (ambient, steel, soil)	2	passive pressures, large settlement of backfill, large daily variation in girder stresses

Table 3.1: (Continued)

Reference	Location	Bridge type	Sensors	Duration (yrs)	Notable Conclusions
Hoppe (2005)	Virginia, US	100 m-long, semi-integral, 3 spans, steel plate girders	abutment wall pressure, strain gauge (girder), displacement sensor (girder), abutment wall rotation, EPS thickness	5.5	abutment wall EPS reduced earth pressure, backfill settlement, asymmetrical abutment displacement
Abendroth et al. (2005)	Iowa, US	61 & 96 m-long, integral, skewed (30 & 15 degree), 3 spans, precast girder, steel piles	longitudinal, translational and rotational movement of abutments, strain gauges (girder, pile, deck), temperature, pile cap rotation	2.5	abutment motion was asymmetrical, data indicates that skewed abutment was subject to flexural bending in horizontal plane
Steinberg et al. (2004)	Ohio, US	26 & 96 m-long, semi-integral, steel girders, 65 & 25 degree-skews	load cells (wing walls), displacement sensors (survey points, manual), temperature (abutment wall and girders)	1.5	wing wall earth pressure change, asymmetric wing wall pressures and abutment displacement

Table 3.1: (End of Table)

As summarized in Table 3.1, the field-based studies conducted on integral and semi-integral bridges have been quite varied in terms of methodologies, parameters of interest and conclusions. Some of the notable conclusions from this group of studies include documented cases of increased lateral earth pressure and passive earth pressures

reached and cases where the lateral earth pressure has dropped to levels below the estimated active earth pressure. Also, several studies have reported asymmetric displacement of the bridge abutments. In skewed bridges, in-plane bridge deck rotation and increased asymmetric earth pressure on the wing walls have been observed. Moreover, the contrast seen in bridge construction, given the range of girder types (e.g., steel plates, pre-stressed, etc.) and foundations (e.g., H-piles, drilled shafts, precast, etc.) used, reflects the typical bridge construction practice of each region.

Considerable differences among the approaches adopted can be identified among the monitoring programs developed for each study. One of the most common characteristics among them has been the measurement of lateral earth pressures and strains. Earth pressures have been primarily measured at the interface between abutment wall and backfill, though some researchers have also measured wing wall pressures. While not all studies include strain measurements, typical strain measurement efforts have included gathering such data from bridge components such as the deck, girder, and foundations.

As the abutment – backfill interaction problem is primarily driven by daily and seasonal temperature changes, temperature measurement has also been adopted in the studies. However, the approach adopted to measure temperature has been quite varied. As summarized in Table 3.1, some studies have relied on official local weather station data (from nearby airports and cities), while some have installed thermistors and thermocouples inside the deck, girder, or abutment walls to measure temperature distribution in different bridge components.

Experimental studies have indicated that the magnitude of abutment wall displacement affects the rate of soil pressure increase and backfill settlement (Clayton et al., 2006, England et al., 2000). Accordingly, past studies have attempted to measure the displacement and rotation of bridge components using a variety of methods. As summarized in Table 3.1, bridge movement and rotation characterization efforts have ranged from manual measurement of displacements of survey targets using tape or a total

station to adoption of abutment wall tilt sensors, inclinometer arrays on backwall and foundation, or displacement measurement of abutments relative to a nearby reference point.

The review of studies summarized in Table 3.1 reveals one notable difference between the instrumentation programs designed for semi-integral bridges and the ones designed for integral bridges and that is related to the monitoring of the foundations. Integral bridge foundations and abutment walls have sometimes been instrumented using one or more tilt sensors to capture their displacement profiles. However, foundation monitoring was not found to be a component of any of the field monitoring studies for semi-integral bridges. This is because semi-integral bridges do not include a rigid connection between the substructure and superstructure, their foundations have been assumed to be unaffected by thermal expansion/contraction of the deck and so they have not been instrumented to capture lateral deformations. Nonetheless, as stated in Mofarraj and Zornberg (2022), it is possible for semi-integral bridge foundations to interact with the superstructure during thermal expansion/contraction of the bridge. Therefore, for semi-integral bridges, it has become necessary to complement instrumentation programs with a foundation monitoring system as well to successfully understand the behavior of the bridge.

In addition to choosing which parameters to track while studying the long-term behavior of integral and semi-integral bridges, it is also important to establish the frequency of data logging and duration of monitoring. A majority of the studies summarized in Table 3.1 indicated data collection rates ranging from once every 20 minutes to once every six hours. The studies that relied on manual measurements reported a data collection rate of once per month.

Overall, there appear to be significant differences among the approaches of various researchers in studying the long-term behavior of integral and semi-integral bridges in the past few decades. While some of these differences can be attributed to changes in instrumentation technology, a majority thereof are likely due to project-specific decisions

(e.g., funding agency interests or research team interests, capabilities and thought processes).

The design and implementation of a large-scale monitoring program is only the beginning of the efforts for such studies, as the proper utilization of this data for the broader civil engineering community depends on the type of analysis performed and final presentation of the data. The complexity of this task depends on the quantity and number of different types of sensors used. A successful interpretation of the data not only requires well-executed data collection and conversion of sensor measurements to physical parameters, but also establishing adequate correlations among various data sources to gain an in-depth understanding of the bridge behavior.

This chapter focuses on the development of the instrumentation plan for long-term monitoring of the China Creek Bridge, which is a semi-integral bridge constructed on State Highway 240 in Texas, USA. This monitoring program was developed with a focus on capturing the response of the substructure, superstructure, and abutments, as well as the interactions among these components due to daily and seasonal changes in temperature. As part of a larger research initiative, this monitoring program assesses the performance of semi-integral bridges in Texas conditions and provides recommendations for future jointless bridge construction projects. In particular, this chapter outlines novel approaches used in developing the bridge monitoring program and describes the type of analysis performed using the collected data.

3.2. DESCRIPTION OF CHINA CREEK SEMI-INTEGRAL BRIDGE

The China Creek semi-integral Bridge was built on Texas State Highway 240, near Wichita Falls, TX, during the summer of 2020. A schematic of the bridge is shown in Figure 3.1. This bridge is 27.5 m-long and involves two traffic lanes. The deck consists of six Tx34 pre-stressed concrete I-beam girders, 0.1 m-thick partial depth prestressed concrete panels (PCPs) between the girders, and a 0.32-m thick cast-in-place concrete

overlay. The abutment walls are integrally connected to the deck and are 1.25 m-deep. The bridge is supported by four 11 m-deep drilled shafts on each side, each of which are 0.9 m in diameter. The deck connects to the approaching roadway via 6 m-long reinforced concrete approach slabs that are structurally connected to the deck and abutment wall on one end and rest on sleeper slabs on the other. As the abutment wall extends below the top of the abutment cap, the gap between the abutment wall and abutment cap was filled with a 50 mm-thick closed cell foam.

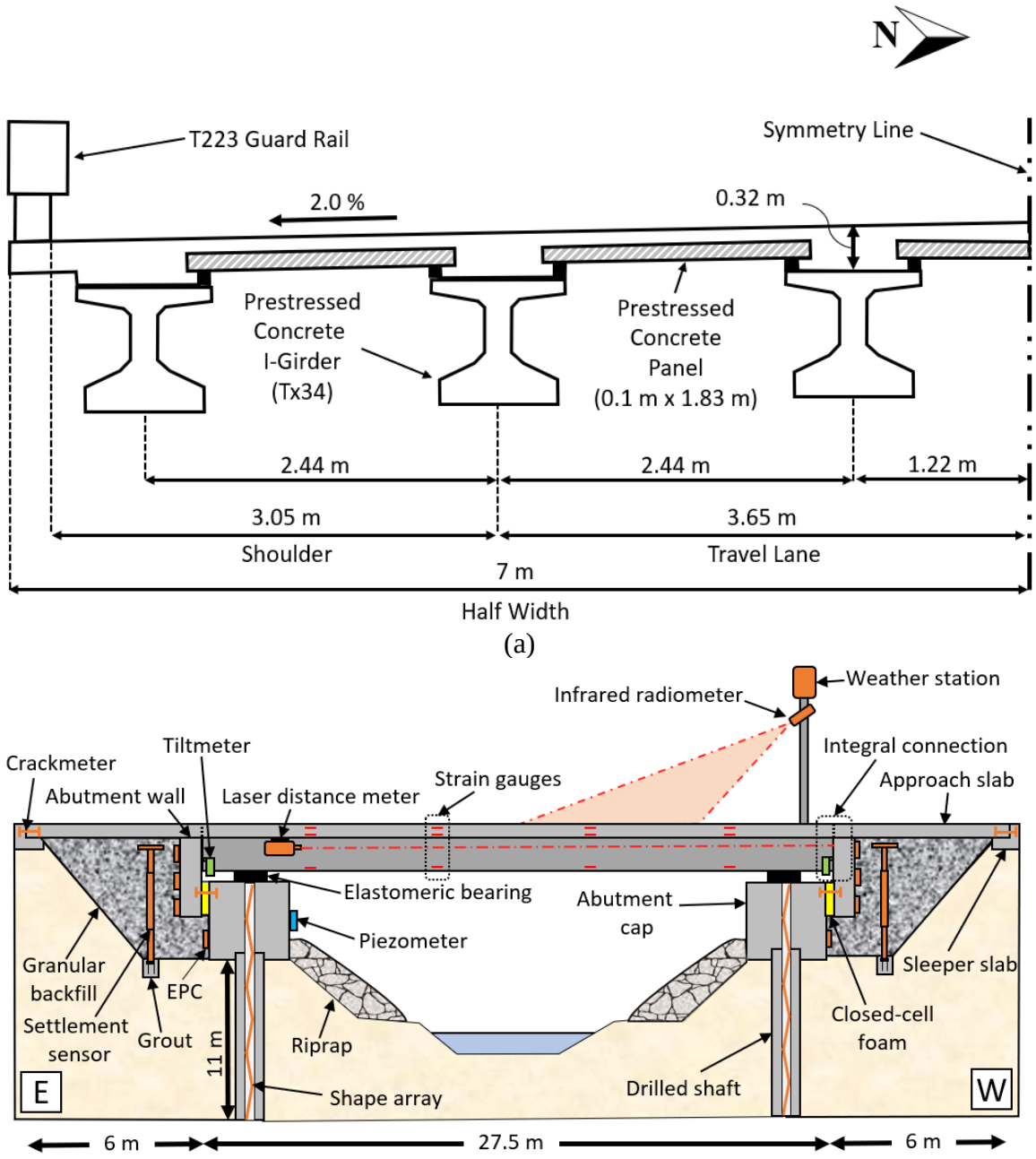

Figure 3.1: Schematic of China Creek Semi-integral Bridge: (a) Transverse cross-section (half-deck); and (b) Longitudinal cross-section showing the location of installed sensors. (EPC: Earth Pressure Cell)

3.3. GEOTECHNICAL CHARACTERIZATION OF CHINA CREEK SEMI-INTEGRAL BRIDGE

To characterize the in-situ soil properties, a 12 m-deep boring log was obtained from each side of the bridge. The materials recovered from the boring logs indicated the existence of lean soft clay deposits for the top 4.5 m. The deposits from depths ranging from 2.7 to 4.5 m appeared very soft and saturated. Below 4.5 m, the soil profile consisted mainly of stiff and dry lean clay, with soil appearing very hard and blocky below 7.5 m.

In addition to the physical characterization of the in-situ soils, a series of Texas Cone Penetration (TCP) (TEX 132-E, 1999) tests were conducted at 1.5 m deep intervals. A TCP count of 50 (maximum blow count) was reached for depths below 6 m, making this a suitable bearing stratum for the drilled shaft foundation. However, the top 4.5 m of the boring logs revealed soils with TCP counts ranging from 3 to 7, which is associated with soft to medium soils, according to Touma and Reese (1969).

Per TxDOT specifications, type AS select fill was used as backfill material for the bridge abutment. Type AS backfill is the coarsest backfill material typically used in the construction of retaining walls by TxDOT. This material is largely composed of crushed gravel particles, with 50% or more larger than 12 mm (TxDOT Item 423) and smaller than 75 mm. The fines content (% passing #200 sieve) in this fill is limited to a maximum of 5%.

3.4. SEMI-INTEGRAL BRIDGE MONITORING PLAN

The China Creek Bridge is one of the first semi-integral bridge prototypes in the State of Texas. As previously stated, semi-integral bridges may exhibit complex long-term behavior. Furthermore, the authors have had the opportunity to monitor the behavior of another semi-integral bridge in Texas for nearly four years (Mofarraj and Zornberg, 2022) prior to construction of the China Creek Bridge. A synthesis of the information gained

through prior bridge monitoring programs resulted in the following objectives for the China Creek Bridge monitoring program:

1. To capture the changes in both magnitude and distribution of lateral earth pressures that develop due to the interaction between abutment fill and abutment wall
2. To quantify the potential settlements and permanent deformations of the backfill retained behind the abutment walls.
3. To measure the changes in ambient air temperature as well as the temperature gradient within various bridge components.
4. To measure deformations and relative displacement of various bridge components.
5. To capture and characterize the potential interaction between the superstructure and substructure due to changes in temperature.
6. To capture potentially asymmetrical thermal expansion/contraction of the bridge.
7. To capture flood events in the creek below the bridge and investigate their potential effect on the behavior of the bridge.
8. To include a degree of redundancy in the instrumentation system to increase confidence in the measurement of important variables and counter loss of data due to potential failure of some sensors.

In order to achieve the goals of the instrumentation program, over 70 sensors were ultimately installed on the China Creek Bridge. These sensors allowed for the measurement of over 200 parameters, which include displacements, strains, temperatures, and stresses at various locations on the structure. A summary of the utilized sensors, their installation locations, and the intended measurement to be recorded is shown in Table 3.2. The installation locations of each sensor are shown in Figure 3.1. The instrumentation data was recorded using two CR6 data loggers (Campbell Scientific) and four 32-channel multiplexers which were mounted to the underside of the bridge deck in IP68-rated enclosures. This location was chosen to hide the monitoring equipment from passersby and provide adequate protection against flooding of the creek.

The monitoring system was set up to support remote data collection. Accordingly, the data logger stations were connected using radio modules, and the system was programmed to measure sensors every 30 minutes and transmit the data via a cellular modem each day. The system is powered using a set of 12V rechargeable batteries connected to two 20W solar panels.

Sensor type	**Installation location**	**Measurement**
Concrete embedded strain gauge	Bridge deck, foundation, approach slabs	Load and thermal strain, temperature gradient
Surface mount strain gauge	Bridge girders	Load and thermal strain
Earth pressure cell	Abutment wall, abutment cap, wing wall	Earth pressure acting on component
Crackmeter	Abutment cap, abutment wall, approach slab, sleeper slab, wing wall	Relative displacement of components
Shape array	Drilled shaft foundation	Lateral displacement profile of drilled shafts
Laser distance sensor	Bridge deck	Deck length change
Tiltmeter	Abutment walls	Abutment wall rotation
Piezometer	Abutment cap	Flood level measurement
Settlement sensor	Abutment backfill	Backfill settlement
Weather station	Bridge deck	Temperature, solar irradiance, relative humidity, rain, wind speed
Infrared radiometer	Bridge deck	Deck surface temperature
Soil extensometers	Abutment backfill	Horizontal backfill displacements

Table 3.2: Sensors used on China Creek semi-integral Bridge.

As anticipated, installation of such a large number of sensors and successful interpretation of the recorded data is a highly involved task. The following sections discuss the approaches used to effectively instrument different components of the bridge and share details regarding data processing.

3.5. TYPICAL OUTCOMES OF THE BRIDGE DECK INSTRUMENTATION

The configuration of the bridge deck (e.g., slab thickness, length, girder type, material) is a key factor influencing the thermally-induced behavior of semi-integral bridges. It is therefore crucial to capture the behavior of the bridge deck as well as the environmental parameters that might impact the behavior.

To measure the total change in deck length, different alternatives were considered. Considering the objective of implementing automatic measurement of changes in length across the 27.5 m distance with sub-millimeter accuracy, solutions such as displacement transducers, linear potentiometers and fiber optics were dismissed. This is largely due to the potential variation in temperature across the length of these sensors, which would be very difficult to measure and correct. Consequently, the Micro-Epsilon OptoNCDT ILR-1181-30 industrial laser distance sensor was adopted, which offers 0.5 mm precision in measurements for objects as distant as 50 m. The sensor was installed inside a data logger enclosure, with a custom peephole for the laser beam, to protect the sensor from the environment. The installation location of the laser distance sensor is shown in Figure 3.1. As the figure shows, the laser distance sensor was attached to the bottom of the deck, in between the girders and close to the east abutment wall. This sensor measures the distance to the west abutment wall using time-of-flight technology.

In addition to the laser distance sensor, strain gauges were selected to better understand the thermal behavior of the deck. To this end, 16 vibrating wire strain gauges were installed in the deck area. As shown in Figure 3.2, five pairs of concrete-embedded strain gauges (GK-4200) were installed within the deck and five surface mount strain gauges (GK-4150) were installed on the bottom girder flange of the middle girder. These strain gauges were distributed evenly across the length of the deck so that each set is approximately 4.5 m apart along the length of the bridge on one of the central girders (third girder from the south). This array of strain gauges was used to measure strain, temperature distribution and curvature across the length of the bridge.

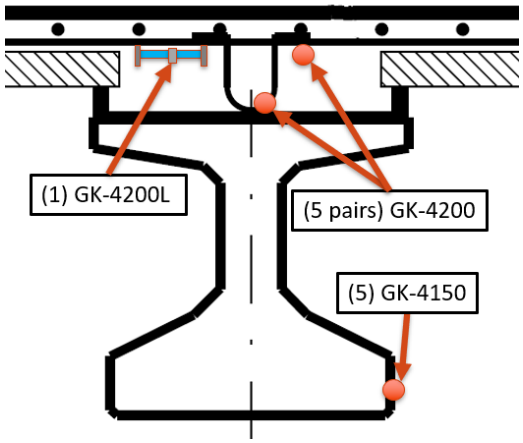

Figure 3.2: Deck strain gauge installation locations.

The deck strain gauges provide the longitudinal strain as well as the temperature measurements at their installation locations. Considering the distribution of strain gauges in the deck, it is possible to calculate the temperature distribution within the deck, longitudinal strains, and changes in deck curvature at five equidistant cross-sections along the bridge. Therefore, it is possible to use the strain measurements to predict the changes in length of the deck by integrating the changes in strain along its length. This process provides an alternate measurement of deck length change, which can be used to verify the laser measurements, adding redundancy to the system.

To measure the unrestrained thermal expansion/contraction of the deck, three low modulus, concrete-embedded strain gauges (GK-4200L) were also selected for installation. One was embedded in the deck near the west abutment, perpendicular to the bridge direction (Figure 3.2) to minimize dead and live load effects on its measurements. The purpose of this strain gauge is to help understand the restraint imposed by the abutment backfills against deck expansion by comparing the gauge measurements to those of other strain gauges embedded in the direction of the deck. If the thermal expansion/contraction of the deck is unrestrained and there are no variations in thermal strains across the bridge

deck, then the thermal expansion of the bridge can also be accurately predicted using this single strain gauge.

The two other low modulus strain gauges were installed within cylindrical concrete specimens that were cast from the same concrete utilized in the cast-in-place deck. One of the specimens was kept under the bridge and on the abutment cap, while the other was kept on top of a wing wall exposed to direct sunlight. The purpose of these strain gauges is to measure the coefficient of thermal expansion as well as shrinkage strains within the concrete of the deck.

To compare the performance of the different approaches adopted to measure changes in deck length, early data was collected and analyzed. In this analysis, the changes in the length of the deck were calculated using laser distance sensor data, longitudinal deck strain gauge data (GK-4200) and the low modulus strain gauge (GK-4200L) installed perpendicular to the bridge direction (see Figure 3.2). The results of this analysis are presented in Figure 3.3(a), which indicate that the changes in deck length among all three sources match well against each other on most instances. However, on some dates the laser distance sensor appeared to have measured deck length changes that exceeded the results predicted using both strain gauge-based methods by more than 10 mm.

To identify the method that recorded the correct measurements, the Coefficient of Thermal Expansion (CTE) of the deck was calculated using each set of data. Per AASHTO (2020), the CTE of a concrete deck typically ranges between 5.4×10^{-6}/°C to 14.4×10^{-6}/°C and it can be assumed to be equal to 10.8×10^{-6}/°C for design in absence of direct laboratory measurements. Back analysis of strain gauge data yields a CTE of 9.4×10^{-6}/°C, which is similar to the value proposed in AASHTO (2017). In contrast, the laser distance sensor data yields a highly non-linear CTE, which can be approximated to 35×10^{-6}/°C for the range of data shown in Figure 3.3(a). Since the CTE obtained using laser distance sensor data is unrealistically large, it may be concluded that the spikes in the laser distance sensor data were due to operational errors and should be ignored.

The instances of significant mismatch between the laser-based and strain gauge measurements may be explained by the installation location of the laser distance sensor (Figure 3.1). Specifically, a potential cause of this error may be the changes in curvature of the deck at the sensor location. Such curvature changes may have occurred due to changes in the thermal gradient within the deck. This possible explanation can be validated by strain gauge data from the set closest to the laser distance sensor. The bending curvature data obtained from the girder and deck strain gauges is shown in Figure 3.3(b). This data indicates changes in curvature of approximately 5×10^{-6} rad/m over one day during this period. This change in curvature may have resulted in the laser beam taking a longer path back to the laser distance sensor by reflecting off additional surfaces, making the target appear farther than it actually was.

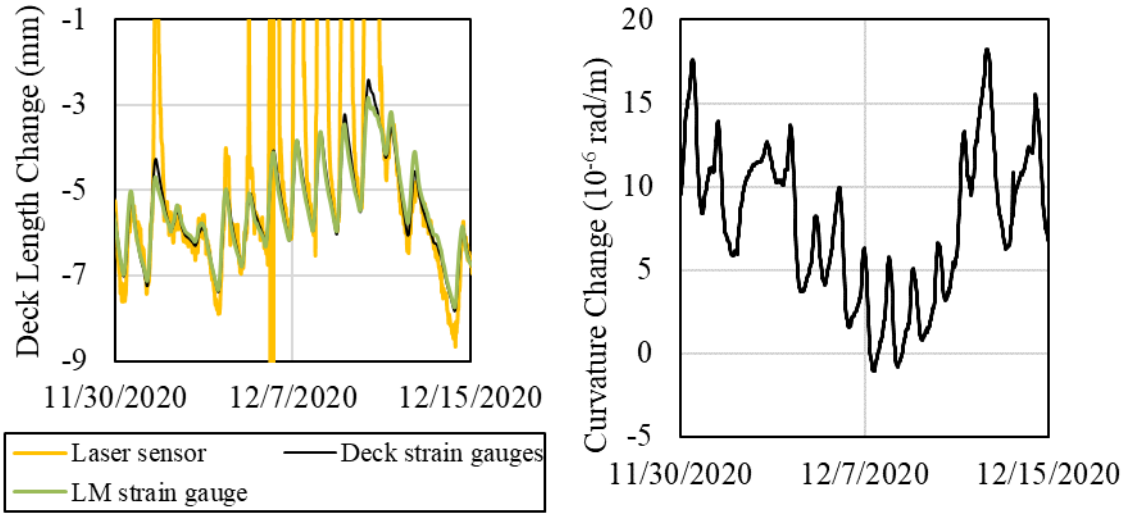

(a) (b)

Figure 3.3: Typical time history of data collected in the bridge deck: (a) Deck length changes measured by laser distance sensor, longitudinal deck-embedded strain gauges and perpendicular low modulus (LM) strain gauge (Note: Vertical axis range is truncated and does not display full range of laser sensor measurements); and (b) Changes in deck curvature near the location of the laser distance sensor.

Overall, a comparison of the longitudinal deck strain gauge array data and perpendicular low modulus strain gauge data reveals that both sets provide virtually the same measurements. Therefore, it can be concluded that the thermal expansion/contraction of the bridge was mainly unrestricted during this period. Furthermore, in this case, one strain gauge was sufficient to measure the changes in length of the bridge deck with high precision. Additionally, the strain gauge array facilitated the measurement of thermal gradients within the deck and calculating changes in curvature of the deck as well.

3.6. TYPICAL OUTCOMES OF THE ABUTMENT AREA INSTRUMENTATION

The interaction between abutment walls and abutment backfill in semi-integral bridges has been recognized as a relevant issue, and often constituted the main focus of previous semi-integral bridge studies. An important issue arising from the cyclic interaction is the development of the "bump at the end of the bridge" due to settlement of the granular abutment backfill. To investigate the backfill settlement issue, it was deemed necessary to measure backfill settlement as well as the displacement of the abutment walls. The measurement of abutment wall movements is especially important as one of the primary causes of settlement and ratcheting of the abutment backfill.

While experimental studies have previously investigated the development of a bump at the end of the bridge in jointless bridges (Walter, 2018; England et al. 2000), the authors have not come across documented field studies that provide information about backfill settlement in integral and semi-integral bridges. Abutment backfill settlement monitoring is considered a challenging endeavor as the backfill area becomes inaccessible after the completion of the bridge and even manual surveying is typically not possible in projects involving rigid approach slabs.

A novel approach was developed in this study for automatic measurement of the backfill surface settlement. Figure 3.1 presents the settlement sensor, a 2.3 m-long displacement transducer (Geokon model 4430) that is used to measure the backfill surface

settlement. The transducer is a long-base strain gauge placed inside a housing with telescopic joints to measure axial deformation between the two end flanges. In this case, the bottom of the transducer was fitted with two 0.5 m-long threaded rods, which were grouted in the foundation soils below the backfill. The top end of the transducer was fitted with a stainless-steel plate (to avoid corrosion) and placed on the top of the backfill. The steel plate installed on the top flange facilitated the changes in transducer length with vertical movements of the soil surrounding the steel plate. Figure 3.4(a) shows typical measurements of backfill settlement collected from one of the west abutment backfill settlement sensors. Specifically, the results in this figure show the changes in transducer length relative to its initial length, as recorded on the day of sensor installation. Overall, the results indicate a time history of comparatively small, yet continued settlements over time. Moreover, the results indicate that the sensors were also able to capture a small magnitude of heave occurring each day (likely due to bridge expansion), although with an overall trend of increasing settlements.

In order to provide a redundant measurement of backfill settlements, a GPR survey of the approach slab was also conducted. The processed GPR subsurface profile is shown in Figure 3.4(b). This subsurface image shows the vertical profile of the reinforced concrete approach slab, the void between the bottom of the slab and abutment backfill, and part of the backfill soil. Among the notable detected features are the top reinforcement bars, bottom of the slab and top of the backfill surface as identified on Figure 3.4(b). The subsurface GPR profile revealed a gap of approximately 50 mm between the bottom of the approach slab and top of the backfill. Therefore, the GPR data validated the adequacy of the approach adopted in this study to continuously track backfill settlements. Overall, four settlement sensors were installed for this field monitoring project.

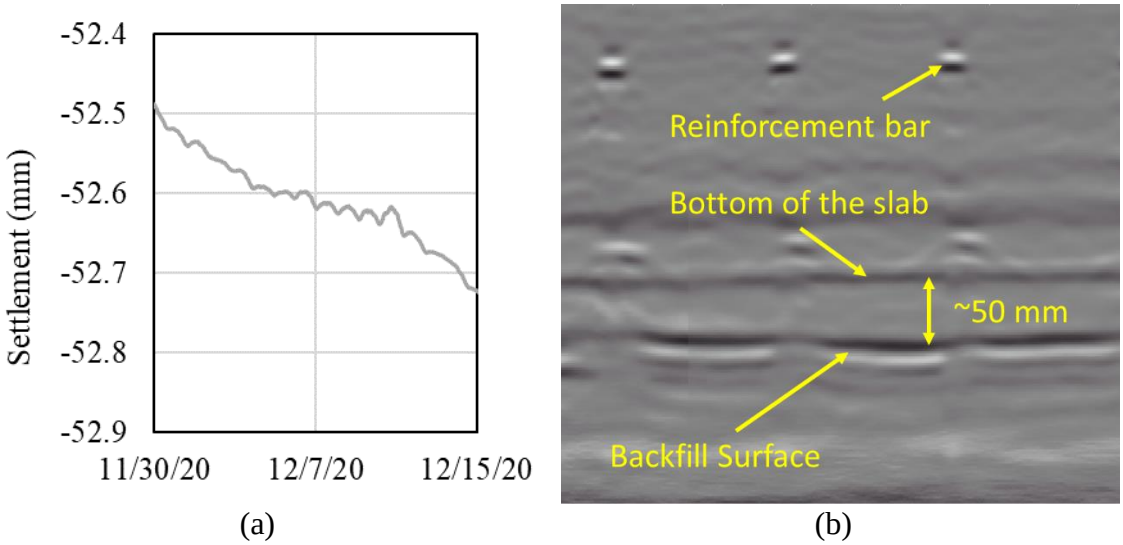

Figure 3.4: Field monitoring results of backfill settlements: (a) West abutment settlements as recorded by the settlement sensor; and (b) west abutment GPR survey profile showing a 50 mm gap between backfill and approach slab at location of settlement sensor.

As previously discussed, an important objective of the monitoring program in the abutment area involved quantification of the abutment wall displacements and defining its motion profile (e.g., purely translational, rotational, or a combination of both). To this end, tiltmeters and crackmeters were installed in the abutment area, as shown in Figure 3.1. Typical data collected using these sensors is shown in Figure 3.5. As illustrated by the typical data collected with these various sensors during early stages in the monitoring program, the movements in the two abutment walls of the China Creek Bridge were clearly different. As illustrated by the results in Figure 3.5(a), the east abutment cap crackmeter measured negligible changes in the width of the joint between abutment cap and wall, while the west abutment cap crackmeter registered nearly 2 mm of width changes during a period of only 15 days shown in the figure. A similar trend can also be observed with the tiltmeter data presented in Figure 3.5(b), which shows that the east wall experienced tilt levels ranging from 0.02 to -0.03 degrees, while the west abutment wall has changed from -0.06

to -0.15 degrees during this period. The observed asymmetry was likely caused by the difference in the stiffness of the abutment backfills.

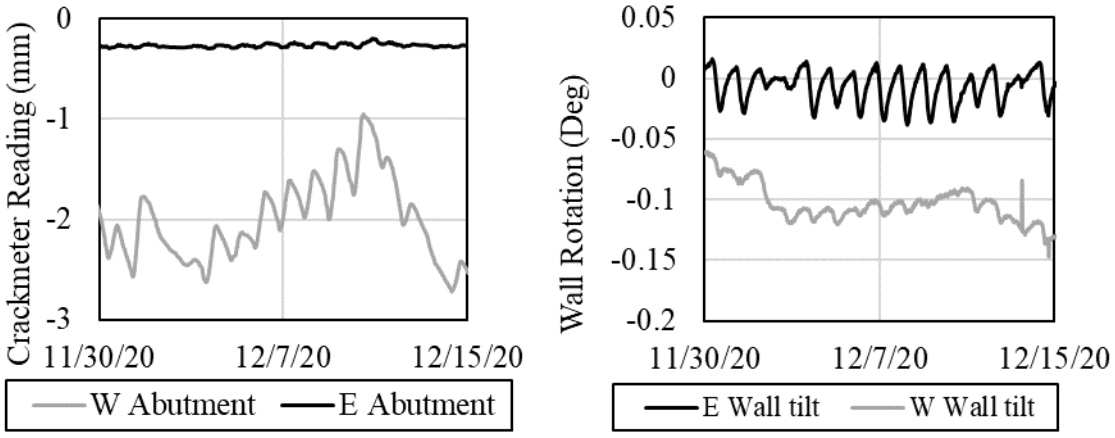

(a) (b)

Figure 3.5: Typical time history of movements in the abutment walls: (a) Changes in width of the abutment cap joint as measured by a crackmeter; and (b) abutment wall rotation as measured by a tiltmeter (Note: Positive values indicate tilting towards the backfill)

Specifically, the east abutment backfill was placed and compacted several days before the west abutment backfill. In the period in which only the east side was backfilled, the bridge was expected to only expand and contract in the west direction, as there was no resistance in that direction. Therefore, when the west backfill was placed during an afternoon, several days after the east abutment backfill, the bridge had already expanded in the west direction. With the daily bridge contraction occurring after the placement of the second backfill, the west backfill likely experienced active or near-active conditions, which can result in softening of the west backfill soil. Due to the particular sequence of construction activities in this project, the bridge likely ended up with a comparatively less dense backfill on the west side, which offered lower resistance to bridge expansion. This

explanation is consistent with the significant difference observed between the crackmeter and tiltmeter data obtained in the two abutments.

Based on the typical data provided so far it appears that thermal expansion/contraction of a semi-integral bridge can result in an asymmetrical response from the abutments. Therefore, an assumption of symmetry can lead to significant loss of data and ultimately an incomplete picture.

3.7. TYPICAL OUTCOMES OF THE SUBSTRUCTURE INSTRUMENTATION PLAN

The potential interaction between the foundation units and the superstructure resulting from temperature changes was also investigated in this study. Specifically, Measurand SAAV shape arrays were selected for installation within one of the drilled shafts constructed on each side of the bridge. Per the manufacturer's recommendation, the shape arrays were installed in PVC conduits 70 mm in diameter inside the drilled shafts using a special top compression assembly provided by the manufacturer. The 11 m shape arrays consist of 22 jointed sensorized segments that provide a 3D displacement profile of the drilled shafts. The deflection data is calculated relative to the position of the node at the bottom of the shaft. As indicated in the foundation profile shown in Figure 3.6(a), the top half of the drilled shaft is permanently encased using a steel pipe, while the bottom is not encased. The steel casing was necessary due to the presence of a soft and saturated clay deposit in the top 4.5 m of the foundation soil.

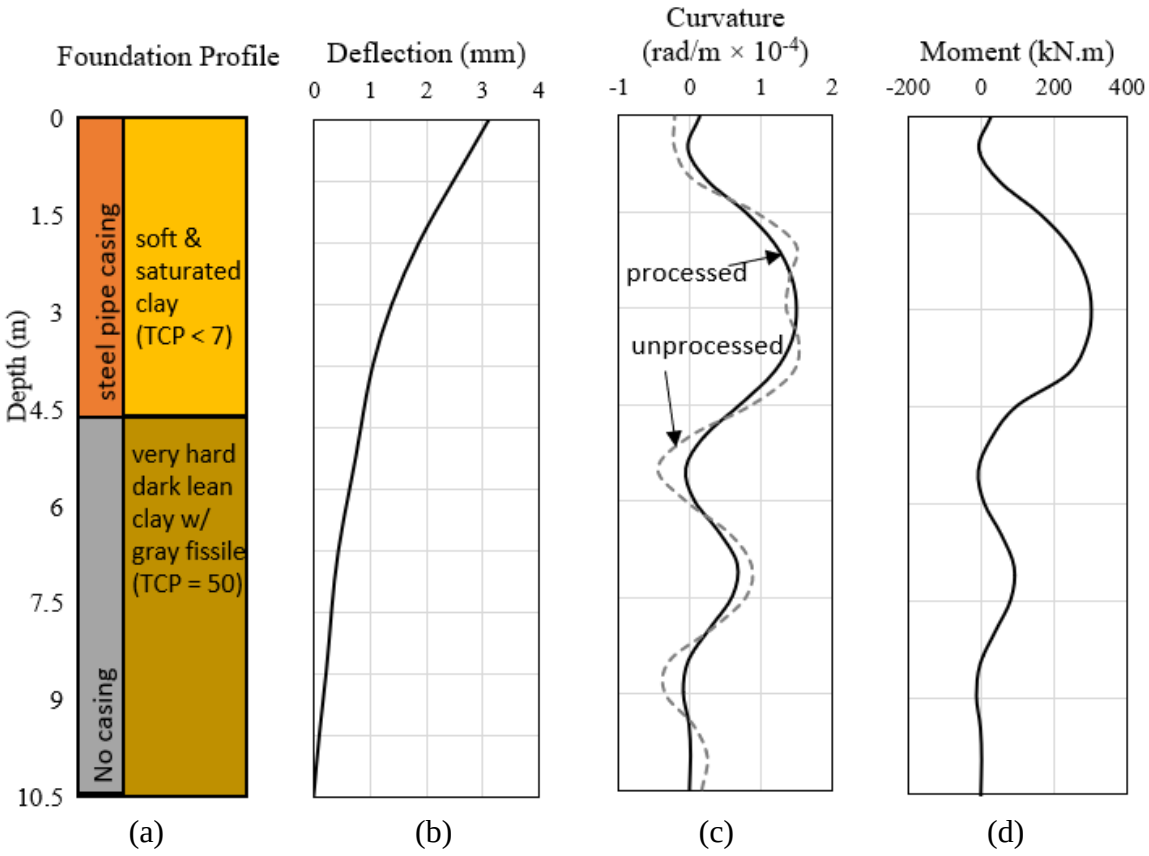

Figure 3.6: West abutment drilled shaft profiles: (a) foundation profile; (b) deflection profile; (c) curvature profile; and (d) moment profile (shape array data captured at 7:30 pm on December 5, 2020).

The shape arrays installed within the drilled shafts allow prediction of their deflection profile by determining the change in position of each node compared to its position at the time of installation. A typical deflection profile of the instrumented west abutment drilled shaft is presented in Figure 3.6(b). As the data indicates, the west abutment cap had moved 3 mm toward the center of the bridge at the time of reading (7:30 pm on December 5, 2020) likely due to the bridge thermal contraction that has occurred since the time of construction.

In addition to the deflection profile of the drilled shafts, other parameters of interest can also be estimated, including the moments profile. This requires determination of the curvature profile of the foundation units. The curvature profile can be obtained by taking the second differential of the deflection profile, as follows:

$$\frac{d^2y}{dx^2} = \frac{y_{m+1} - 2y_m + y_{m-1}}{h^2} \qquad \textbf{(Equation 1)}$$

where "*y"* is the nodal deflection in the y-direction, "x" is the nodal position in the x-direction, "*h*" is the distance between the nodes (or shape array segment length) and "m" is the node number as shown in Figure 3.7.

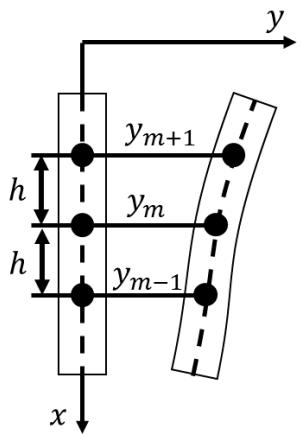

Figure 3.7: Schematic of a deflected segment of the drilled shaft.

Because the shape array only measures displacement at the nodal locations, calculating the second derivative of the unprocessed deflection profile using the finite difference method can result in unrealistic spikes in the profiles. Accordingly, several filters were evaluated to smoothen the data, including rolling average, rolling median and Savitzki-Golay (Savitzki and Golay, 1964) algorithms. For the typical data collected, processing the deflection data with a moving average filter with a window size of three was found to be effective for removing the noise in the curvature results. The small window

size of the applied filter resulted in minimal distortion of the unprocessed deflection data, while also minimizing noise in the curvature profile. The calculated curvature profile for the instrumented drilled shaft in the west abutment is shown in Figure 3.6(c).

To obtain the moment profile, flexural stiffness properties of the instrumented sections were calculated using the LPILE software (Wang et al., 2022). As previously mentioned, the top 4.5 m of the drilled shafts are permanently encased, while the bottom section consists only of reinforced concrete, resulting in greater flexural rigidity for the top section. Consequently, the bending moment profile of the west abutment drilled shaft was calculated using the shape array data and flexural stiffness analysis conducted using LPILE. The resulting profile is shown in Figure 3.6(d). The figure displays that a maximum bending moment of 300 kN.m occurred at a depth of 3 m within the encased section of the drilled shaft. The bending moment within the bottom segment of the drilled shaft, which is embedded in the hard clay deposit was significantly smaller and reached a maximum of 90 kN.m. It is noteworthy that the moments and curvature values displayed in Figure 3.6 were within the elastic range of behavior for the drilled shaft, according to the moment-curvature diagram obtained for each section.

The analysis described above can be extended to the time-history of the maximum bending moment acting on the drilled shafts for a given period of time. Additionally, to understand the significance of the lateral loads imposed on the drilled shafts due to thermal expansion/contraction of the bridge, the calculated moment profiles can be compared with the cracking moment of the section. Such a comparison provides a measure of the level of the elastic flexural section capacity that has been reached. The results for typical data collected from the instrumented west abutment drilled shaft are shown in Figure 3.8. As the figure displays, during this period the abutment cap displacements ranged from 2.6 to 4.1 mm toward the center of the bridge, which resulted in maximum bending moments ranging from 195 to 310 kN.m in the drilled shaft. For reference, the calculated concrete cracking moment for this section is 493 kN.m, which indicates that the calculated bending

moments are still within the elastic range but reach values as high as 63% of the cracking moment for the section during this period. This could be cause for concern as more extreme weather conditions may be experienced in the future, leading to larger bending moments in this section. Also of note is that the maximum moments during this period all occurred within the top (steel encased) segment of the drilled shaft.

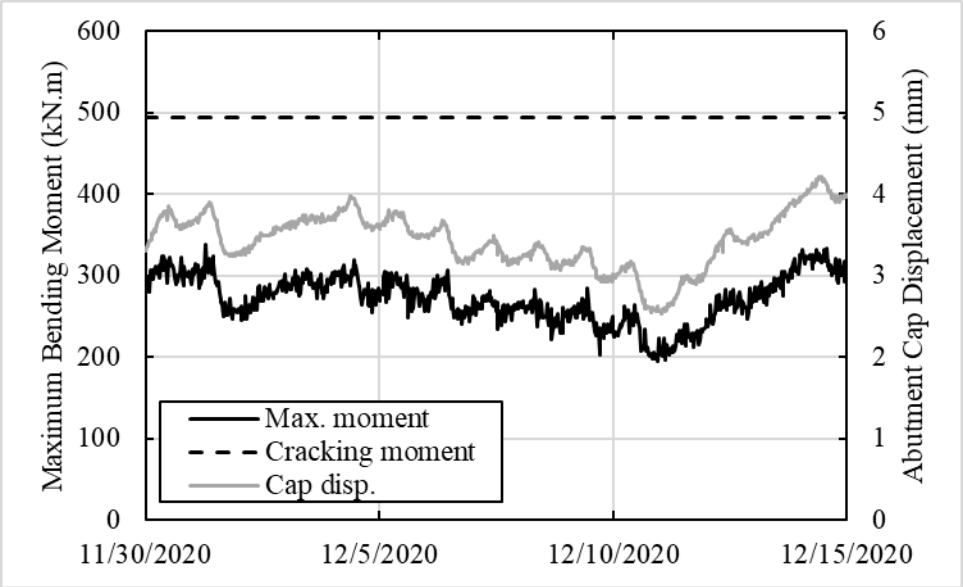

Figure 3.8: Instrumented west drilled shaft's maximum moment and abutment cap displacement data (Note: Positive displacements correspond to drilled shafts bending toward the center of the bridge).

As previously summarized in Table 3.1, no instances are documented in the available literature regarding the cyclic lateral loading of semi-integral bridge foundations. This is because semi-integral bridge foundations are not generally expected to experience significant lateral loading due to changes in bridge length, as the superstructure and the foundations in semi-integral bridges are not integrally connected. However, the authors' prior experiences with semi-integral bridges in Texas (Mofarraj and Zornberg, 2022) indicated the possibility of such interaction. The shape arrays facilitated continuous

monitoring of deflections in the drilled shafts and estimation of the lateral loads, which can help improve future semi-integral bridge design guidelines.

In addition to allowing the prediction of lateral loads acting on the drilled shafts, information from the shape arrays also can be used for estimating the absolute displacement of different bridge components. As shown in Figure 3.1, each shape array extends to the bottom of the drilled shaft, because the bottom of the drilled shaft is expected to experience little-to-no movement due to the thermal expansion/contraction loads, the calculated shape array node displacements relative to the bottom of the drilled shaft can be considered absolute displacement measurements. Consequently, it is possible to calculate the absolute abutment wall displacements by using the data collected from the abutment cap crackmeters and shape arrays. For example, the movement of the abutment walls can be calculated using the shape array data and the crackmeter data measuring the relative displacement of the abutment wall and cap. A typical graph of displacement time-history data of an abutment wall is presented in Figure 3.9(a). The results shown in this figure correspond to the lateral displacement of each abutment wall relative to its position at the beginning of the monitoring program.

Figure 3.9(a) illustrates that the displacements experienced by the east and west abutment walls are significantly different. During this period, the west abutment wall experienced movements ranging from 2.5 to 5.5 mm toward the center of the bridge (eastward), with daily displacement cycles of approximately 0.5 to 1 mm in magnitude. In contrast, the east abutment wall movements ranged from 1 to 2 mm toward the center of the bridge (westward), with daily displacement cycles of approximately 0.25 mm in magnitude. Overall, movement of both abutment walls toward the centerline of the bridge is evident. The abutment wall displacement data indicates that while both abutment walls moved toward the center of the bridge due to bridge deck thermal contraction, this contraction primarily affected the west abutment.

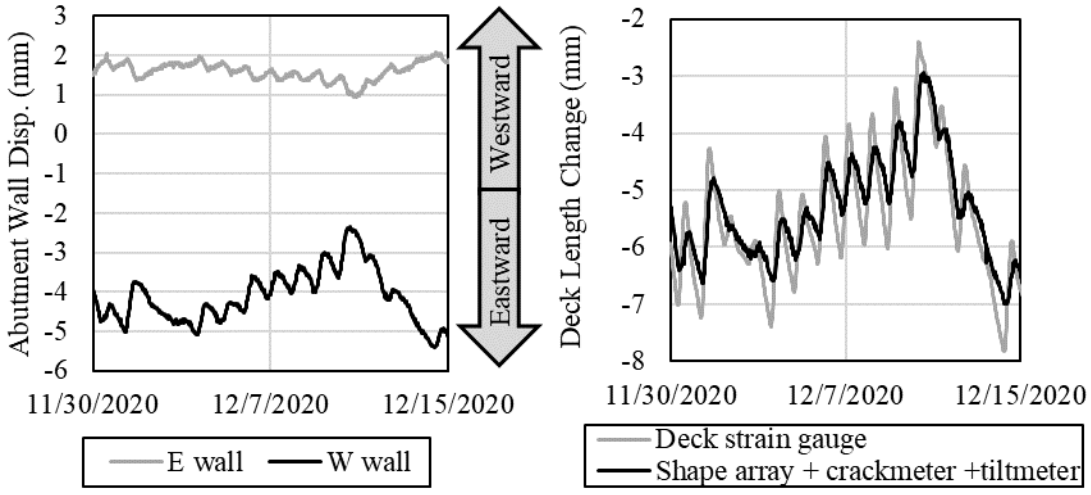

(a) (b)

Figure 3.9: Effect of daily temperature variation on expansion/contraction of the bridge: (a) Abutment wall displacement calculated by adding results from the drilled shaft shape arrays to those obtained from the abutment cap crackmeters; and (b) Comparison between the changes in deck length calculated using data from shape arrays, abutment cap crackmeters, and abutment wall tiltmeters versus the data from the deck strain gauges.

To verify and assess the accuracy of the abutment wall displacement data, the bridge deck length change was also calculated by adding the displacement data collected from the shape arrays, crackmeters and tiltmeters. The deck length changes predicted this way can be compared against the length changes calculated by integrating the data collected from the deck strain gauges. The change in bridge length calculated using these two independent methods is presented in Figure 3.9(b). Despite the significantly different data sources for these two calculation methods of bridge deck length, a very good match can be observed between the results obtained from these two methods. The comparatively minor differences between the results obtained using the two methods may be attributed to the fact that the strain gauges are not individually calibrated by the manufacturer and can

potentially have up to 5% error in measurements according to the manufacturer specifications. Despite the minor differences between the two datasets, the good match between the two datasets further confirms the accuracy of the instrumentation data.

As previously stated, the abutment wall displacement magnitude is one of the main parameters that affects backfill settlement and ratcheting over time. The shape arrays and abutment cap crackmeters are demonstrably reliable in measuring the absolute displacement of the abutment walls. Therefore, the installed sensors can provide very valuable information for investigation of the soil-structure interaction in semi-integral bridge abutments due to the daily and seasonal thermal expansion/contraction of the bridge.

3.8. TYPICAL OUTCOMES FROM TEMPERATURE MEASUREMENTS

Proper interpretation of the thermally-induced behavior in semi-integral bridges relies on accurate measurement of environmental variables, namely temperature information. These monitoring efforts can generally be grouped into two categories, as follows:

1. Measurement of the internal temperature distribution within bridge components, such as the deck and girders.
2. Measurement of weather data, including ambient air temperature, solar irradiance, and wind speed.
3. The magnitude of thermal expansion/contraction of a bridge deck can be defined as:

$$\Delta L = CTE \times \Delta T \times L_0 \qquad \textbf{(Equation 2)}$$

where ΔL is the change in bridge length, "CTE" stands for the coefficient of thermal expansion, "ΔT" is the change in temperature and L_0 is the initial length of the bridge.

Therefore, the deck's coefficient of thermal expansion can be obtained from the measured changes in deck length and its internal temperature. As previously described, in this study such data is collected using an array of strain gauges embedded within the deck.

Consequently, it is possible to use this information to calculate CTE of the deck and possibly predict the performance of this bridge under extreme weather events. This information can also be used to predict the behavior of a bridge with similar sectional properties, but different length, in the same geographic location. However, additional information may be needed to predict the performance of semi-integral bridges located in a region with significantly different weather patterns or bridges with different deck cross-sections.

It is also possible to use the monitoring data to extend the lessons learned to hypothetical scenarios that are not directly comparable with the instrumented bridge by using accurate weather data measurements and validating a heat transfer model for the deck. As outlined in Branco and Mendes (1993), temperature distribution within the deck is affected by ambient air temperature, solar radiation, wind speed, bridge surface temperature, geometry, and material properties, such as convection heat transfer coefficient and irradiation heat transfer coefficient.

Considering that the long-term goal of this study is to evaluate and improve the semi-integral bridge design guidelines, it is deemed beneficial to record weather-related parameters to extend the data specific to the China Creek Bridge to other design scenarios. As summarized in Table 3.1, past studies have applied different approaches to measure temperature in the respective field monitoring investigations. Each approach offers advantages and disadvantages in terms of performance, cost, and ease of implementation. For example, data from nearby weather stations may be readily and freely available but would not offer the greatest accuracy depending on the distance to the site. Conversely, an on-site weather station can provide accurate measurements, but can be costly and difficult to maintain. Another approach to measuring ambient temperature involves relying on temperature measurements from the data logger panel, which is sometimes argued to represent the ambient air temperature if the data logger panel is kept in the shade. However, there can be significant differences in the actual ambient temperature if the data loggers

are maintained in an enclosure that provides some insulation and the air inside the enclosure is warmer or cooler than the outside air temperature.

As previously stated, the instrumentation plan on the China Creek Bridge includes an on-site weather station, infrared radiometer for deck surface temperature and deck-embedded thermistors that are included in the vibrating wire strain gauges. This arrangement of sensors was selected to enable measurement and calculation of the parameters required for developing a heat flow model such as that described in Branco and Mendes (1993).

A typical ambient air temperature dataset from the local Wichita Falls airport weather station (40 km from the bridge site), on-site weather station (ClimaVUE50) and data logger panel thermistor (same location as the laser distance sensor in Figure 3.1) is shown in Figure 3.10. A comparatively short time span is shown in the figure to focus on the subtle differences among the various sources of temperature. As can be seen in the figure, the local weather station ambient air temperature measurements are very similar to the on-site weather station's measurements for the daytime but tend to deviate by up to 5°C during the nighttime for this period. In contrast, the data logger panel temperature does not generally match the ambient temperature, as the daytime temperatures tended to be up to 5°C lower than the ambient temperature, while the nighttime temperatures tended to be up to 8°C higher. As a result, it can be argued that in the absence of an on-site weather station, even a somewhat distant weather station significantly outperformed the data logger internal thermistor for ambient air temperature measurements.

Along with the ambient air temperature measurements, the deck surface temperature (infrared radiometer) and internal deck temperature data (concrete embedded strain gauge thermistors) are also plotted in Figure 3.10. In this case, the deck surface temperature records, which serve as an important boundary condition in heat flow analysis, appear to significantly differ from the ambient air temperature and data logger panel temperature. Therefore, for proper analysis of the thermal expansion/contraction of the

bridge, direct measurement of the deck surface temperature is necessary instead of approximations based on ambient air temperature data. Similarly, the average internal deck temperature appears to significantly differ from ambient air and deck surface temperature records.

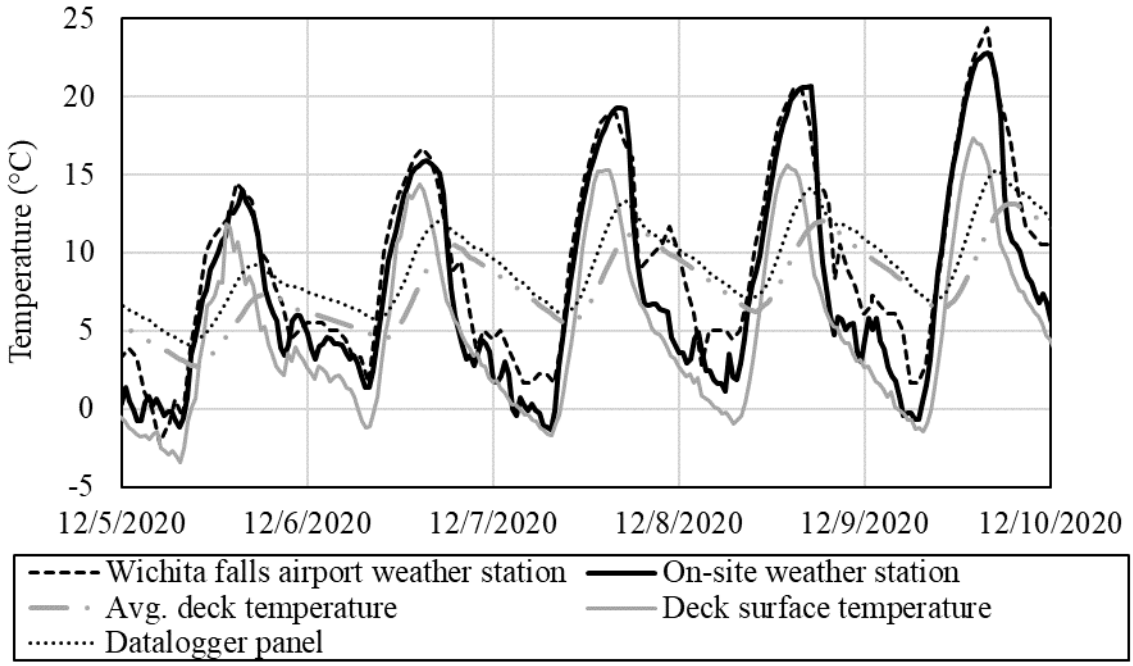

Figure 3.10: Comparison of different temperature records collected at the China Creek Bridge site.

Overall, the temperature data discussed above indicates that the on-site weather station is certainly advantageous over the local weather station and data logger panel thermistor. Consequently, inclusion of an on-site weather station in the instrumentation package for maximum reliability in the measurement of weather parameters. Moreover, the evaluation of the internal deck temperature, deck surface temperature and weather data confirm that these parameters cannot be approximated with one another without a significant loss in accuracy.

3.9. CONCLUSIONS

This chapter describes the basis for the design of an instrumentation program to monitor the behavior of a new semi-integral bridge in Wichita Falls, TX. The details of the resulting field monitoring program of the bridge abutment walls, deck and foundation units are also summarized. Early instrumentation data is used to provide insight into the performance of the monitoring system as well as on the response of the bridge structural components resulting from changes in temperature. The following conclusions are drawn based on the early data collected through this field monitoring program:

- The generation of accurate and redundant measurements of deformations and displacements of different bridge components proved to be crucial to assess the behavior of the semi-integral bridge, particularly considering the need to interpret its complex soil-structure interaction.
- The data collected from many sensors (e.g., shape arrays, crackmeters, tiltmeters, etc.) on the bridge indicate that even though the bridge was designed as a symmetric structure, its thermal behavior was clearly asymmetric, with the west abutment having experienced larger displacements due to changes in temperature.
- Because some components of a semi-integral bridge are not integrally connected (e.g., the abutment caps are not connected to the abutment walls), the use of crackmeters proved to be a relatively inexpensive, yet invaluable instrument to measure the relative displacement of such components. Early crackmeter data indicates that temperature changes led to thermal expansion of the bridge predominantly in the westward direction.
- A reliable measurement of the absolute displacement of abutment walls could be achieved using a combination of data collected from shape arrays, crackmeters and tiltmeters. Measurement from these sensors allowed prediction of the displacement

of abutment caps relative to the bottom of each instrumented drilled shaft, which can be deemed as stationary under normal operating conditions.

- The use of shape arrays provides the opportunities to assess the effect of thermal expansion/contraction of the deck on the foundation units. The analysis of the shape array deflection data reveals that deep foundation units in semi-integral bridges may experience significant lateral loads. In the specific case of the China Creek semi-integral bridge, the instrumented west abutment drilled shaft experienced bending moments as high as 60% of its cracking moment due to bridge contraction.
- Prediction of changes in deck length using measurements from concrete strain gauges was found to be more accurate than the data from laser distance meters. Although both methods can provide sub-millimeter accuracy levels, proper alignment of laser distance meters and ensuring that the alignment is maintained under operating conditions can be challenging under field conditions. Moreover, the errors due to laser misalignment are expected to increase for longer bridges. Therefore, the usage of strain gauges for this purpose is highly preferred.
- Ambient temperature measurements constitute a relevant information to be accurately collected as part of the monitoring plan of a semi-integral bridge. Comparison of the data collected in this study through an on-site weather station, data logger thermistors and a nearby weather station revealed that the data logger thermistor did not provide a good representation of the ambient air temperature. Additionally, while the local weather station ambient air temperature data closely matched the on-site weather station data for most hours of the day, there was a mismatch of up to 5°C between the two datasets.
- The custom-made sensors implemented to measure backfill settlements were found to provide valuable, continuous data on the development of settlements of the granular abutment backfill. The use of GPR subsurface profiles was found to provide valuable complementary information on backfill settlements. Data from the

settlement sensors can facilitate an understanding of the evolution of backfill settlement due to thermal expansion/contraction of the bridge and define the unsupported length of the approach slabs.

3.10. ACKNOWLEDGEMENTS

The authors thank the Texas Department of Transportation (TxDOT) for funding this research under project 0-6936 through the Center for Transportation Research (CTR) at the University of Texas at Austin.

3.11. REFERENCES

AASHTO. (2020). "AASHTO LRFD bridge design specifications", Washington, DC. American Association of State Highway and Transportation Officials

Abendroth, R. E., Greimann, L. F., Lim, K.-H., Sayers, B. H., Kirkpatrick, C. L. and Ng, W. C. (2005). "Field Testing of Integral Abutments." Iowa State University Center for Transportation Research and Education, Ames, IA.

Abendroth, R., Greimann, L., and LaViolette, M. (2007). "An Integral Abutment Bridge with Precast Concrete Piles." Iowa State University Center for Transportation Research and Education, Ames, IA.

Branco, F. A., and Mendes, P. A. (1993). "Thermal Actions for Concrete Bridge Design." Journal of Structural Engineering, 119 (8): 2313–2331. https://doi.org/10.1061/(ASCE)0733-9445(1993)119:8(2313).

Burke, M. P. (2009). "Integral and Semi-Integral Bridges." Wiley-Blackwell.

Civjan, S. A., Kalayci, E., Quinn, B. H., Brena, S. F., and Allen, C. A. (2013). "Observed integral abutment bridge substructure response." Engineering Structures, 56: 1177–1191. https://doi.org/10.1016/j.engstruct.2013.06.029.

Clayton, C. R. I., Xu, M., and Bloodworth, A. (2006). "A laboratory study of the development of earth pressure behind integral bridge abutments." Géotechnique, 56 (8): 561–571. https://doi.org/10.1680/geot.2006.56.8.561.

England, G. L., Tsang, N. C. M., and Bush, D. I. (2000). "Integral bridges: a fundamental approach to the time–temperature loading problem". Thomas Telford Ltd, London.

Frosch, R., and Lovell, M. (2011). "Long-Term Behavior of Integral Abutment Bridges." JTRP Technical Reports. https://doi.org/10.5703/1288284314640.

Hoppe, E. (2005). "Field study of integral backwall with elastic inclusion." Viriginia Transportation Research Council.

Hoppe, E. J., Gomez, J. P. (1996). Field study of an integral backwall bridge." Virginia Transportation Research Council.

Huffaker, C. D. (2013). "Behavior and Analysis of an Integral Abutment Bridge." Master's thesis, Utah State University.

Huntley, S. A., and Valsangkar, A. J. (2013). "Field monitoring of earth pressures on integral bridge abutments." Can. Geotech. J., 50 (8): 841–857. https://doi.org/10.1139/cgj-2012-0440.

Jorgenson, J. L. (1974). "Behavior of Abutment Piles in an Integral Abutment in Response to Bridge Movements." Transportation Research Record, (903): 72–79.

Lawver, A., French, C., and Shield, C. K. (2000). "Field Performance of Integral Abutment Bridge." Transportation Research Record, 1740 (1): 108–117. SAGE Publications Inc. https://doi.org/10.3141/1740-14.

Maruri, R. F., and Petro, S. H. (2005). “Integral abutments and jointless bridges (IAJB) 2004 survey summary.” Integral Abutments and Jointless Bridges 2005, FHWA, Baltimore, MA, 12-29.

Mofarraj, B., and Zornberg, J. G. (2022). “Field Monitoring of Soil-Structure Interaction in Semi-Integral Bridges.” Geo-Congress 2022, ASCE, Charlotte, NC, 33–42. https://doi.org/10.1061/9780784484067.004.

Ooi, P. S. K., Lin, X., and Hamada, H. S. (2010). “Field Behavior of an Integral Abutment Bridge Supported on Drilled Shafts.” J. Bridge Eng., 15 (1), 4–18. https://doi.org/10.1061/(ASCE)BE.1943-5592.0000036.

Purvis, R. L., and Berger, R. H. (1983). “Bridge Joint Maintenance.” Transportation Research Record, 899, 1-10.

Savitzky, A., and Golay, M. J. E. (1964). “Smoothing and Differentiation of Data by Simplified Least Squares Procedures.” Anal. Chem., 36 (8): 1627–1639. https://doi.org/10.1021/ac60214a047.

Steinberg, E., Sargand, S. M., and Bettinger, C. (2004). “Forces in wingwalls of skewed semi-integral bridges.” J. Bridge Eng., 9 (6): 563–571. https://doi.org/10.1061/(ASCE)1084-0702(2004)9:6(563).

Touma, F. T., and Reese, L. C. (1972). “The Behavior of Axially Loaded Drilled Shafts in Sand.” Center for Highway Research, The University of Texas at Austin.

Texas Department of Transportation. (1999). “Tex-132-E: Test Procedure for Texas Cone Penetration.” Texas Department of Transportation.

Texas Department of Transportation. (1993). “Item 423: Retaining Walls” Texas Department of Transportation.

Walter, J. R. (2018). “Experimental and numerical investigation of integral/semi-integral bridge abutments for Texas conditions.” Master’s Thesis, University of Texas at Austin.

Wang, S. T., Vasquez, L. G., Arrellaga, J. A., and Isenhower, W. M. (2022). “LPILE v2022 User’s Manual.” Ensoft Inc., Austin, TX.

Chapter 4: Field Investigation of Soil-Structure Interaction in Semi-integral Bridge Abutments

ABSTRACT

Semi-integral bridges can be an excellent alternative to conventional bridges with potential benefits because these systems do not utilize deck expansion joints. Such elimination of expansion joints has been shown to significantly reduce maintenance costs throughout a bridge's service life, leading to the adoption of jointless bridge construction by many transportation agencies. However, elimination of expansion joints has also raised concerns regarding potential problems that may result from the soil-structure interaction between the bridge structure and abutment backfill. Such interaction is expected from daily thermal expansion/contraction of the bridge, which has not been well understood. This chapter presents data collected from a pilot semi-integral bridge in Texas, USA monitored for nearly two years. The effects of daily and seasonal temperature changes on the displacement of the abutment walls, changes in abutment earth pressure, ratcheting, backfill settlement and changes in backfill stiffness over time were successfully captured. Relevant findings from the monitoring data and its interpretation include the identification and quantification of effects that should be considered in the bridge design, including the time-dependent increase in backfill lateral earth pressure due to ratcheting, continuous backfill settlement, loss of vertical support for approach slabs, and the development of an asymmetric expansion/contraction bridge response that favors displacement of the bridge superstructure toward one of its ends. The asymmetric behavior of the bridge was found to be in response to the difference in the stiffness of the abutment backfills.

4.1. INTRODUCTION

Conventional bridge construction often includes expansion joints placed at the ends of the bridge and in between spans. This design choice is made to minimize the development of secondary stresses in components of the bridge superstructure due to movements such as those induced by thermal strains, shrinkage, creep, and abutment settlement (Burke, 2009). Moreover, expansion joints can potentially prevent interaction between the abutment and the bridge superstructure during its thermal expansion and contraction. However, many studies have shown that bridge expansion joints are highly susceptible to deterioration and damage while in service. In particular, expansion joints expose the abutment caps, girders and bearings to moisture, deicing salts, abrasives, chemicals, and other debris, causing extensive damage to the structure and an accelerated degradation rate (Purvis and Berger, 1983). While periodic replacement of damaged expansion joints can maintain their intended function, potential damage to the structural elements is comparatively difficult, if not entirely unfeasible, to remedy. Furthermore, maintenance of expansion joints is typically expensive and can exceed the initial cost of construction of these joints. As a result, many transportation agencies have pursued jointless bridge designs, such as semi-integral and integral bridges.

In semi-integral bridges, the deck, girders, and abutment walls are integrated during construction, and superstructure loads are transferred to the abutment caps and foundation via bearings. On the other hand, in integral bridges, the bearings are also eliminated, resulting in a seamless connection between the superstructure and substructure. According to Burke (2009), the adoption of integral and semi-integral bridges in the US began in Ohio nearly a century ago.

A key factor in selecting between adoption of a semi-integral or integral bridge is the foundation type of the bridge. Integral bridges require comparatively flexible foundation elements that provide limited restraint against thermal expansion of the superstructure. As a result, many transportation agencies in the US require the use of steel

H-piles with the weak axis oriented toward the integral bridge. In contrast, semi-integral bridges are often preferred when site conditions preclude the use of flexible foundation systems (e.g., pile driving is unfeasible or uneconomical). However, in either case, thermal expansion and contraction of the superstructure may result in daily cyclic interaction of the abutment walls with the abutment backfills.

The cyclic soil-structure interaction that develops in semi-integral and integral bridge abutments has been investigated through several studies over the past few decades. Through long-term field monitoring programs, this interaction has been found to cause increased abutment earth pressure (also known as ratcheting) and settlement of the backfill (Mofarraj and Zornberg, 2022; Huntly and Valsangkar, 2013; England et al. 2000; Frosch and Lovell, 2011; Civjan et al., 2013). Based on a series of cyclic triaxial tests, Clayton et al. (2006) attributed the ratcheting in sand particles to an accumulation of plastic strains and gradual changes in the fabric structure due to cyclic loading of the sand particles. Accordingly, ratcheting was observed in both densely- and loosely-packed specimens. However, long-term field monitoring studies have provided mixed results regarding the occurrence of ratcheting in integral and semi-integral bridges. While some researchers have clearly observed seasonal increases in lateral earth pressures (e.g., Mofarraj and Zornberg, 2022; Huntly and Valsangkar, 2013), others have reported contradicting observations (Civjan et al., 2013; Ooi et al, 2020).

A summary of notable findings from numerous previous studies is provided in **Chapter 3** of this dissertation**.** While summarizing such efforts is beyond the scope of this chapter, it can be stated that research reported so far indicates that factors such as variable site conditions, local construction practices, instrumentation schemes and data interpretation efforts have produced different conclusions on the long-term performance and behavior of integral and semi-integral bridges.

According to Oesterle and Tabatabai (2014), the complexity and uncertainty in the behavior of jointless bridges resulted in the adoption of an empirical design approach for

these structures. Jointless bridges were initially limited to short lengths and their continued success led to increasingly longer bridge structures over time. Accordingly, the design procedures and guidelines established by various transportation agencies were developed primarily based on empirical rules. Therefore, significant insight can be gained by generating detailed field results on the long-term behavior of semi-integral and integral bridges, which can enable the development of a rigorous design approach for such structures.

The purpose of this study is to provide additional insight into the long-term behavior and performance of semi-integral bridges. To this end, a pilot semi-integral highway bridge was constructed in Wichita County, TX in 2020 by the Texas Department of Transportation (TxDOT). This structure was instrumented with over 75 sensors that operated during and after construction. A detailed description of the instrumentation system and its development is provided in **Chapter 3** of this dissertation**.** The focus of this chapter is on providing insight specifically into the quantification of the soil-structure interaction occurring in the abutments and on the evaluation of the affects that such interaction has on the behavior of the superstructure and abutment backfill.

In the following sections, a description of the instrumented semi-integral bridge structure is presented, followed by a detailed analysis and discussion of the instrumentation data relevant to the soil-structure interaction in the abutments. The insight provided by such analysis into the effect of daily and seasonal temperature variations on the bridge behavior is finally discussed in detail.

4.2. BRIDGE DESCRIPTION

The semi-integral China Creek Bridge was built on Texas State Highway 240 outside Wichita Falls, TX, in summer 2020. A schematic of this bridge is shown in Figure 4.1. The bridge is 27.5 m long and 14 m wide with two traffic lanes. China Creek Bridge was constructed to replace an older bridge, and it was constructed in two phases to keep

the road open to traffic during construction. The eastbound lane was completed in April 2020 and the westbound lane in July 2020.

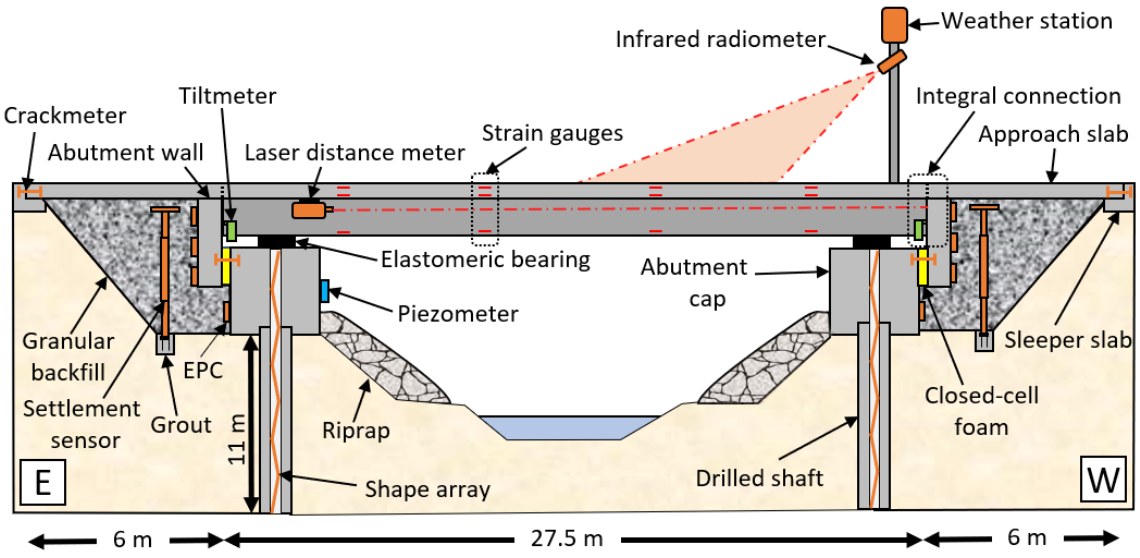

Figure 4.1: Schematic of semi-integral China Creek Bridge and location of installed sensors.

The bridge superstructure consists of six Tx34 prestressed concrete I-beam girders, 0.1 m-thick precast concrete panels between the girders, and a 0.32 m-thick cast-in-place concrete deck. The abutment walls are integrally connected to the deck and measure 1.25 m deep. The deck connects to the approaching roadway via 6-m-long reinforced concrete approach slabs that are structurally connected to the deck and abutment wall on one end and rest on the sleeper slabs on the other. Because the abutment wall extends below the top of the abutment cap, the gap between the abutment wall and abutment cap was filled with a 50-mm-thick closed-cell foam, which was also initially used as formwork for the construction of the abutment walls.

The bridge is supported by four 11-m-deep drilled shafts on each side, each of which are 0.9 m in diameter. Per TxDOT specifications, Type AS select fill (TxDOT Item

423) was used as abutment backfill, which involves a crushed gravel with 50% or more of the particles ranging between 12 and 75 mm in size and a fines content that does not exceed 5%. Figure 4.2 pictures the abutment backfill material. Additional details regarding the backfill and foundation soil are provided in **Chapter 3** of this dissertation.

4.3. INSTRUMENTATION DESCRIPTION

As depicted in Figure 4.1, a large array of geotechnical, structural and climate-related instruments were installed on various bridge components. The bridge monitoring program was developed to provide a comprehensive overview of the development of stresses and strains in and around the structure. Moreover, this instrumentation scheme allows for the measurement of displacements of multiple bridge components (such as abutment walls and caps) independently.

Since this study aims at understanding the soil-structure interaction in the abutment area, data analysis and discussion focuses primarily on movements of the abutment walls, backfill earth pressure distribution, backfill settlement and ratcheting. Figure 4.2 presents the primary instrumentation and abutment backfill sensors prior to placement of the backfilling on the west abutment.

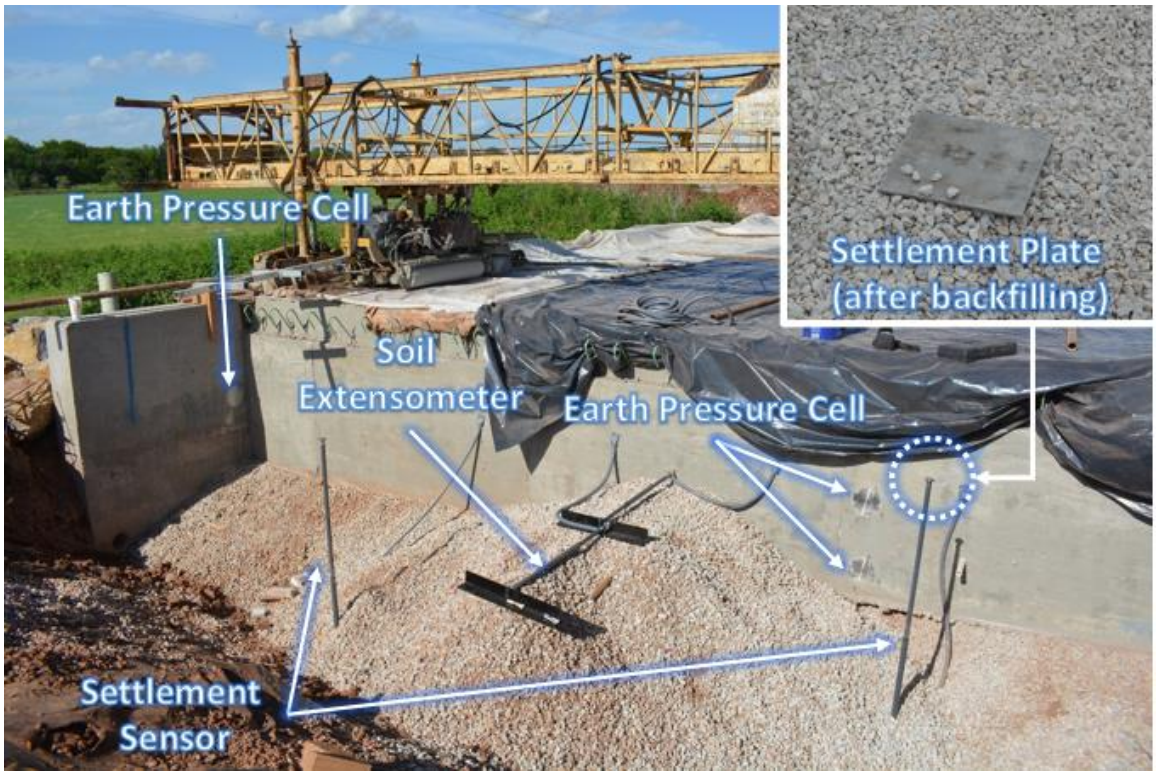

Figure 4.2: Instrumentation and backfilling of China Creek Bridge's west abutment. Top right picture shows a close-up view of the steel plate attached to the top of settlement sensors after completion of backfill placement.

The earth pressure cells (Geokon model 4815) measure the lateral earth pressures acting on the abutment walls (at three different depths), abutment caps (mid-height) and wing walls (mid-height, close to the abutment walls). The vertical settlement sensors consist of 2.3-m-long telescopic displacement transducers (Geokon model 4430) installed vertically within the abutment fill. The bottom of these sensors was grouted below the backfill (Figure 4.1) and the top was attached to a 0.3-m x 0.3-m stainless steel plate seating at the top of the backfill (Figure 4.2). The data collected from the settlement sensors was validated using Ground Penetrating Radar (GPR) measurements, as documented in **Chapter 3** of this dissertation**.**

To estimate the lateral compression of the backfill material, two daisy-chained 1-m-long horizontal soil extensometers (Geokon model 4435) were installed on each abutment. One end of each set of soil extensometers was attached to the abutment wall and the other end was placed within the backfill, as shown in Figure 4.2. These sensors can measure the average compression and extension of the backfill at the sensor locations. The data collected by these sensors can provide stiffness information of the abutment backfill as well as additional insight on the factors affecting the thermal expansion of the bridge.

In addition to the aforementioned sensors in the abutment area, shape arrays, abutment cap crackmeters and deck strain gauges were also installed as part of this project. The data measured by these additional instruments were used to calculate abutment cap and abutment wall movements, which provide further detail on the soil-structure interaction in this semi-integral bridge abutment. The instrumentation data was collected every 30 minutes by Campbell Scientific CR6 data loggers. While the sensors' zero measurements correspond to readings taken immediately after their installation (during bridge construction), the data collection campaign began in October 2020, after construction had been completed, data loggers had been installed and measurement issues were successfully troubleshot.

The discussion of instrumentation data presented in this chapter is grouped into four main categories: thermal expansion of the superstructure; backfill earth pressures; and backfill settlements. The analyses are complemented with a discussion on the new information discovered from the long-term monitoring of the China Creek Bridge abutments.

4.4. THERMAL EXPANSION AND CONTRACTION OF THE BRIDGE

The ambient air temperature data (Figure 4.3) was collected using the weather station installed on site, as shown in Figure 4.1. This data indicates temperature changes ranging from -23°C to 45°C during the monitoring period. The lowest temperature

recorded as part of this study was caused by winter storm Uri in February 2021, which resulted in record low temperatures and snowfall across the state of Texas for nearly a week. As revealed by the ambient air temperature data, temperature fluctuations are significantly larger during the colder fall and winter months of the year compared to the warmer spring and summer months. For example, the ambient air temperature over one week in winter 2021 was observed to fluctuate by 30°C, while temperature changes of more than 20°C during the summer were not typically observed, with the temperature remaining consistently high.

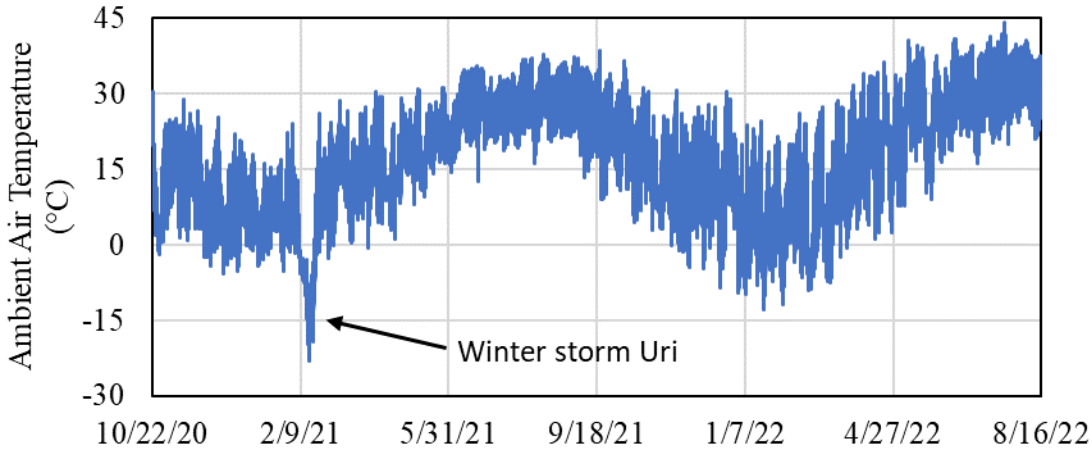

Figure 4.3: Ambient air temperature time-history data collected from the China Creek Bridge site

As illustrated by the monitoring results presented in Figure 4.4, changes in climate conditions affected the thermal expansion and contraction of the bridge. The design of the monitoring program facilitated the determination of the changes in bridge length through two independent, redundant methods. The first method requires using the average strain measurements from the strain gauges installed on the bottom flange of the girder (see Figure 4.1). The second method involves tracking the displacement of abutment walls via the drilled shaft shape arrays and abutment cap crackmeters and determining the change in

their distance at each measurement (**see Chapter 3**). As illustrated by the two methods of measuring length changes presented in Figure 4.4, both methods rendered very similar predictions during fall, winter, and spring (when ambient temperature remained below 25°C), while a slight mismatch in daily variations is observed during the warmer months. However, the strong overall correlation between the two sets of measurements ($R^2 = 0.91$), which were obtained independently, provides good evidence of the high reliable field data collected as part of the monitoring program.

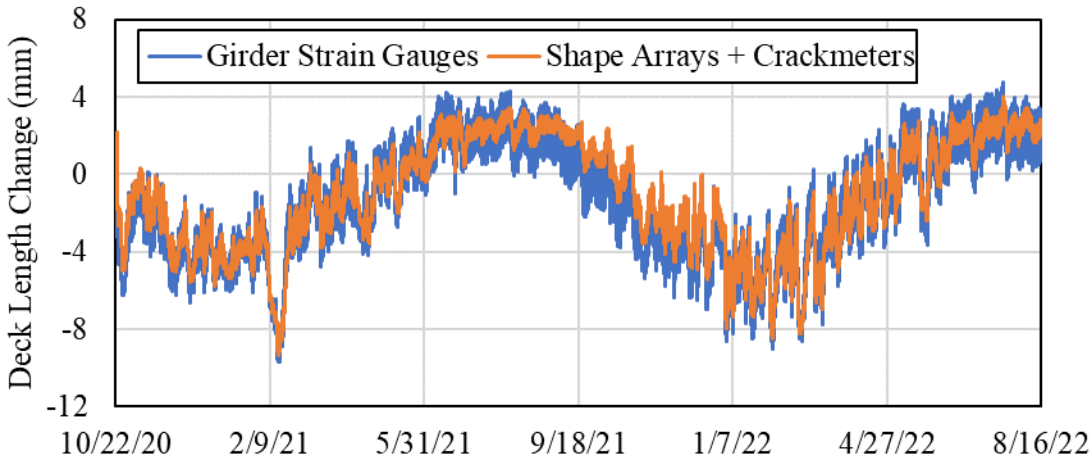

Figure 4.4: Time-history of changes in the bridge length measured using strain gauges mounted on girders compared to foundation shape array and abutment cap crack meter measurements.

Overall, the data shown in Figure 4.4 indicates that the 27.5-m-long bridge experienced approximately 13 mm of thermal expansion/contraction over the monitoring period. Using as a reference the bridge length at the time of construction completion (July 2020), the bridge experienced a maximum thermal expansion of 4 mm during both summers (2021 and 2022) in the monitoring program, and a maximum thermal contraction of approximately 9.5 mm during the winter storm of February 2021. On a smaller timescale, thermal expansion/contraction behavior is observed to vary distinctively

depending on the season. The consistently high temperatures of the summer months typically produce comparatively smaller changes in bridge length, of 1 to 2 mm, happening daily and the average length of the bridge typically not changing by more than 2 mm over the summer months. On the other hand, during the cold winter months, daily changes of 4 mm or more in bridge length were commonly observed and the average bridge length was observed to change by up to 8 mm during the winter months.

The availability of field temperature and displacement data allows the back-calculation of the Coefficient of Thermal Expansion (CTE) of the structure. Specifically, the thermal expansion of a linear structure can be calculated as follows:

$$\Delta L = CTE \times \Delta T \times L_0 \qquad \textbf{(Equation 1)}$$

where *"ΔL"* is the change in bridge length, *"ΔT"* is the change in the structure's internal temperature, and *"L_0"* is the initial length of the structure at the time of construction.

Therefore, the CTE can be obtained by finding the slope of the linear regression line fitted to the average strain measurement ($\Delta L/L_0$) recorded by the deck strain gauges versus the average internal deck temperature measured by their thermistors. The deck-embedded strain gauges were selected for this analysis because they are expected to provide a more accurate measurement of the concrete temperature than the girder strain gauges, as the latter are mounted on the concrete surface.

Figure 4.5 presents the deck strains and corresponding concrete temperature data. According to the AASHTO LRFD Bridge Design Manual (2020), the CTE of normal weight concrete ranges from 5.4 to 14.4×10^{-6}/°C. In absence of project-specific data, a CTE of 10.8×10^{-6}/°C is recommended by AASHTO (2017). Therefore, the estimated CTE of 9.0×10^{-6}/°C based on linear regression analysis of the strain gauge data (Figure 4.5) falls well within the expected range and very similar to AASHTO's recommended design value, which adds further confidence to the field monitoring data.

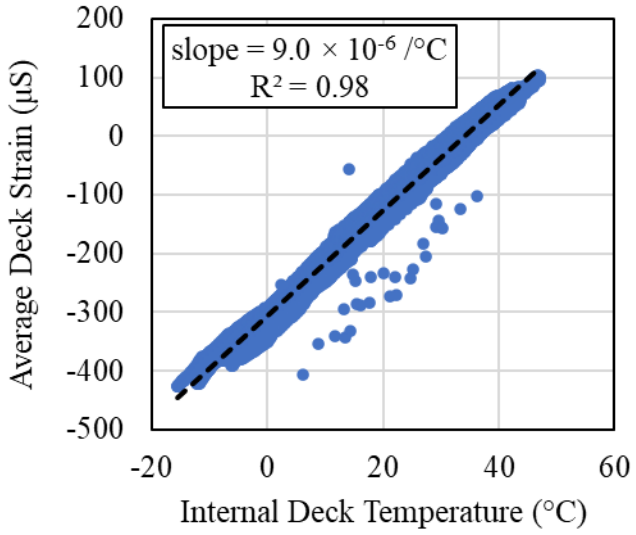

Figure 4.5: Coefficient of Thermal Expansion (CTE) calculation based on deck strain gauges.

As stated previously, the positions of both abutment walls were tracked independently using the installed shape arrays and crackmeters. The abutment wall displacement data is shown in Figure 4.6. The plotted data shows the time-history of the positions of the east and west abutment walls relative to their original positions upon completion of construction. Positive displacement values in this figure indicate that the abutment wall has displaced toward the backfill (passive backfill movements) while negative values indicate that the abutment wall has displaced away from the backfill (active backfill movement).

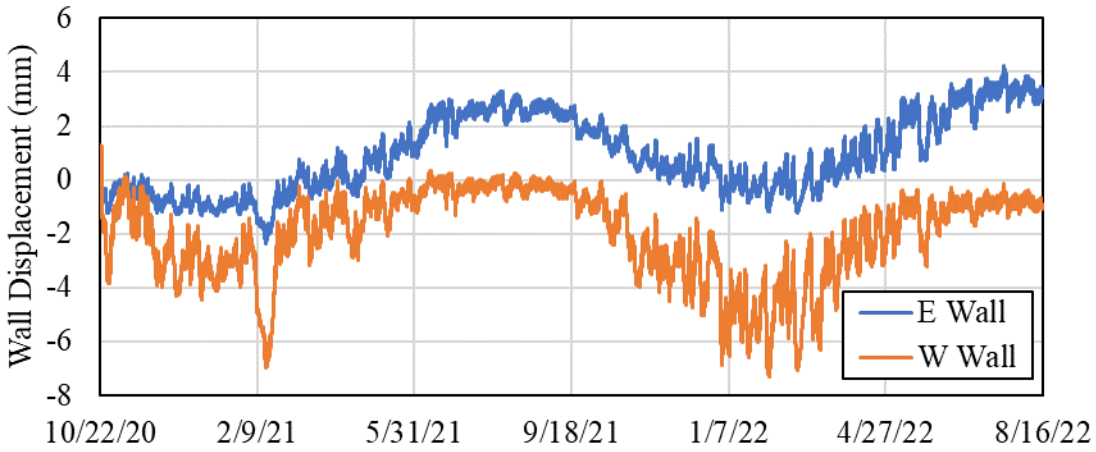

Figure 4.6: Time history of east and west abutment wall displacement relative to their original positions at completion of construction.

The displacement data in Figure 4.6 shows that thermal expansion and contraction in the west abutment wall was comparatively larger than in the east abutment wall, revealing an asymmetric displacement response of the bridge. In addition to the observed difference in abutment wall displacement magnitudes, the direction of displacement and the seasonal behavior observed appears to be asymmetrical as well. It is observed that the west abutment wall primarily moved from its initial position to positions up to 7 mm away from the abutment backfill which occurred during both winters in the monitoring period. On the other hand, the east abutment wall moved among positions 1 to 2 mm away from the abutment backfill (winter months) to 3 mm toward the abutment backfill (summer months). Consequently, while both abutment walls experienced cyclic displacement toward and away from the abutment backfills due to thermal expansion/contraction of the bridge, their behavior was highly asymmetrical. This behavior was unexpected because the structure is geometrically symmetrical as shown in Figure 4.1. For design purposes, the displacement magnitudes of the two bridge abutments due to bridge deck expansion and contraction are often considered to be the same (e.g., for design of joints and bearings).

However, it should be noted that asymmetrical displacements of abutment walls have been previously reported in field monitoring studies of jointless bridges (Abendroth et al., 2007; Huffaker, 2013; Ooi et al. 2010).

An evaluation of the data recorded during winter storm Uri (February 2021) illustrates this asymmetry well: the east abutment wall displaced approximately 2 mm away from the east abutment backfill, while the west abutment wall displaced some 5 mm (i.e., 2.5 times more) away from the west abutment backfill. The results also reveal that from spring to summer 2021, the east abutment wall displaced approximately 3 mm towards the east abutment backfill, which is somewhat larger than the 2 mm displacement recorded for the west abutment wall.

Overall, the east and west abutment walls have experienced displacements of up to 4 and 7.5 mm since construction was completed, respectively. Consequently, the typical design assumption of attributing half the total expected thermal displacements to each abutment is neither a conservative nor realistic assumption considering the total 13 mm thermal expansion/contraction of the bridge length (Figure 4.4). The thermal displacement data collected in this study indicates that an appropriate design approach would be to consider that a single abutment wall may experience displacements consistent with approximately 70% of the expected total change in bridge length. Among the bridge design manuals published by various transportation agencies in the United States, design recommendations have been identified in the State of Ohio's Bridge Design Manual (ODOT, 2020), which recommends considering 2/3 of the total bridge length as expansion length for each abutment wall. The following analysis, based on abutment wall displacement records, demonstrates how the direction of thermal expansion and contraction of the bridge changes throughout the year, resulting in the asymmetrical wall displacement behavior shown in Figure 4.6.

Considering that thermal strains cause the two abutment walls in a bridge to always move in opposite directions, there will be a point along the length of the bridge deck that

experiences zero displacement at any given time. Figure 4.7 shows a schematic view of a bridge with the ends of deck moving by ΔL_1 and ΔL_2 in the opposite directions due to thermal expansion of the bridge deck. Consequently, a point can be imagined along the length of the bridge which does not experience any displacement due to thermal expansion/contraction of the bridge. This Neutral Thermal Expansion Point (NTEP) is positioned such that the displacement of each abutment wall is proportional to the distance of that abutment wall to the NTEP. In this analysis, the distance of each abutment wall to the NTEP is identified as the effective thermal expansion length (L_e). While it is conceivable that the NTEP may fall outside the bridge deck (e.g., if the west sleeper slab is fully anchored causing the bridge to only expand eastward), observing that the abutment walls have always moved in the opposite direction due to thermal expansion/contraction of the bridge reveals that the NTEP lies within the length of the bridge. Consequently, the sum of the effective thermal expansion lengths would be equal to the total length of the deck (L_0), as shown in Figure 4.7.

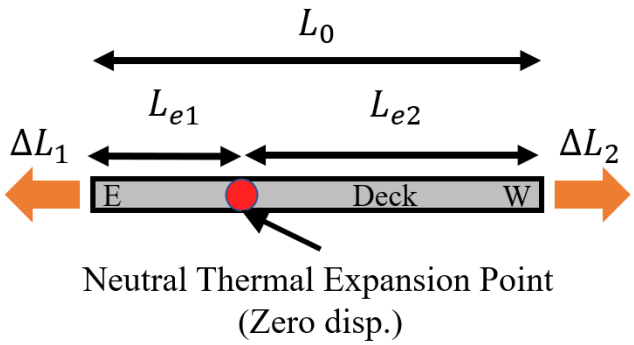

Figure 4.7: Diagram showing neutral thermal expansion point and effective expansion length for each abutment wall.

Having determined the magnitude and direction of displacement at each end of the bridge, the relative position of the NTEP at the China Creek Bridge was calculated and is shown in Figure 4.8. The results in this figure correspond to the distance from the east

abutment wall to the NTEP normalized in relation to the total bridge deck length. For example, L_{e1}/L_0 equal to 50% indicates that the effective expansion length for both abutment walls is the same and the bridge is expanding/contracting symmetrically. As illustrated by the results in Figure 4.8, the position of the NTEP varied considerably over the monitoring period, ranging from 25% to 70%.

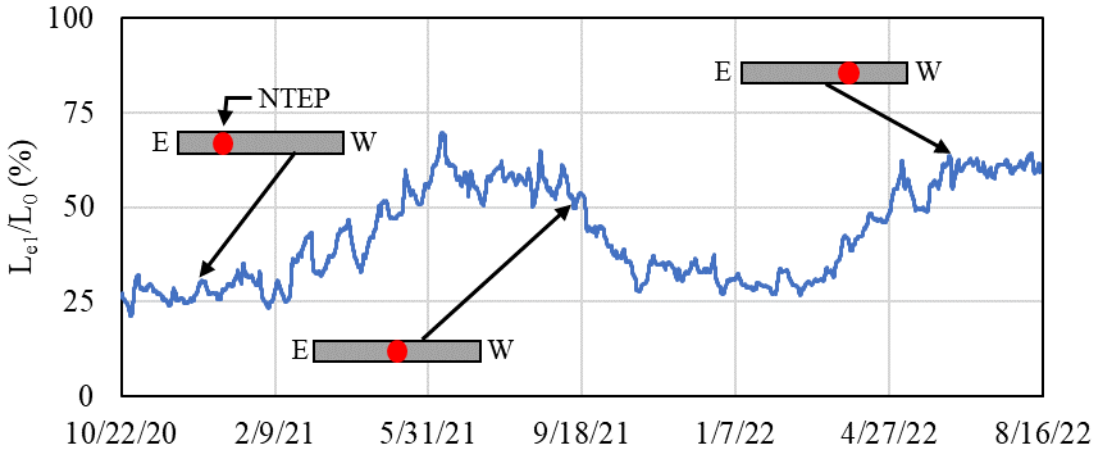

Figure 4.8: Time history of the distance of the neutral thermal expansion point from east abutment wall, normalized to total length of bridge.

During the colder winter months, the NTEP distance has remained within 25 to 35% of the bridge length, meaning that the effective expansion length for the west abutment wall is three to four times larger than that that for the east abutment wall. This observation implies that during the colder months, when the bridge length has decreased due to contraction, the majority of the temperature-induced changes in bridge deck length resulted in displacements of the west abutment. During the warm summer months, the NTEP distance ranged from 60 to 70% of the bridge length, which indicates that bridge thermal expansion resulted in larger displacements of the east abutment wall compared to the west abutment wall.

Overall, it appears that the bridge only experienced symmetrical thermal expansion/contraction (L_{e1}/L_0 = 50%) during a comparatively small period during the monitoring period. Instead, the bridge primarily experienced expansion toward the east abutment and contraction away from the west abutment. Given this trend of monitoring results, it would be worthwhile to investigate whether the bridge experiences a permanent shift over time or returns to the same position after a yearly cycle.

Having established the position of both abutment walls relative to the time of construction, the position of the bridge midpoint can also be tracked at any given time. Such results are shown in Figure 4.9. In this figure, positive values indicate that bridge midpoint has moved towards the east abutment. Figure 4.9 data indicates that the bridge midpoint has experienced displacements of 2 to 3 mm during each annual cycle. While much of the displacements are recovered (see for example the midpoint position changing from 1.5 mm in October 2021 to 3 mm in February 2021 and returning back to 1.5 mm in April 2021), there appears to be a small seemingly permanent shift occurring during the summer months. For example, the bridge midpoint position has changed from 0.8 mm in April 2021 to 1.5 mm in August 2021, indicating a seemingly permanent eastward shift in the bridge midpoint position.

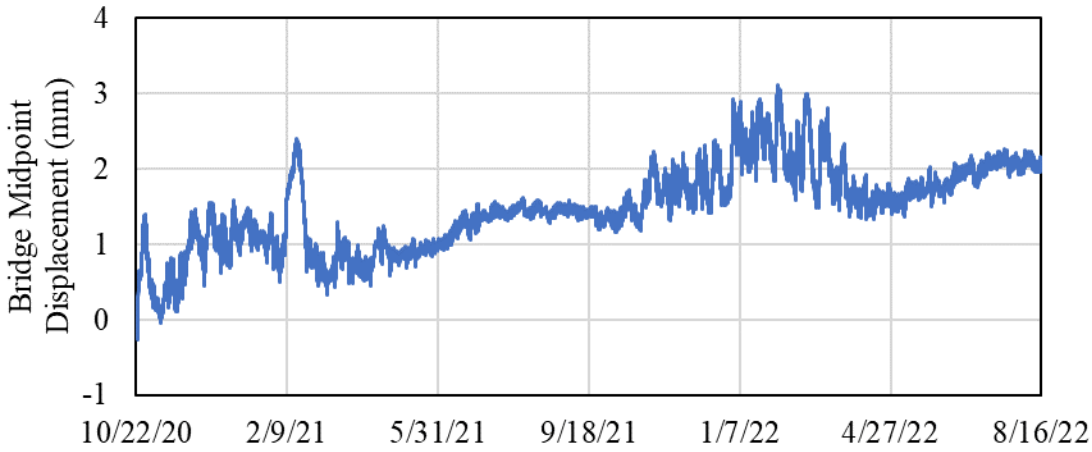

Figure 4.9: Time history of the change in position of bridge midpoint relative to time of construction (positive values indicate that midpoint has moved eastward).

To better understand the reasons behind the asymmetrical response to changes in temperature exhibited by China Creek Bridge, factors that could potentially affect the direction of the bridge thermal expansion/contraction were evaluated. Figure 4.10(a) displays a simplified soil-structure interaction diagram showing the elements that resist a bridge's thermal expansion/contraction. The resisting elements include abutment backfill, foundation, bearings, and approach slab. Typical load-displacement behavior of these components is shown in Figure 4.10(b). To satisfy force equilibrium, the sum of the reaction forces from the approach slab, backfill, bearings, and foundation from the two abutments should be equal. A symmetrical response can be expected if the different resisting elements exhibit the same stiffness on both ends of the bridge. Consequently, considering the asymmetrical behavior described previously, it may be concluded that some of these resisting elements exhibit a higher stiffness on one of the abutment walls than on the other. While it may be reasonable to consider that the elastomeric bearings exhibit a similar shear-deformation behavior because they are manufactured under rigorous

quality control standards, several of the other elements may be a source of unequal resistance in the two abutments, including the following:

1. Difference in the backfill compaction can result in a difference in the stiffness of the abutment backfills against lateral loading
2. Differences between the foundation soil stiffnesses between the two abutments
3. Differences in the sliding resistance of the approach slabs due to factors such as backfill settlement

Considering the potential role of the backfill stiffness variation as a cause for asymmetric thermal expansion/contraction of the bridge, the next section in this chapter presents and discusses the data collected from the earth pressure cells installed in the abutment area.

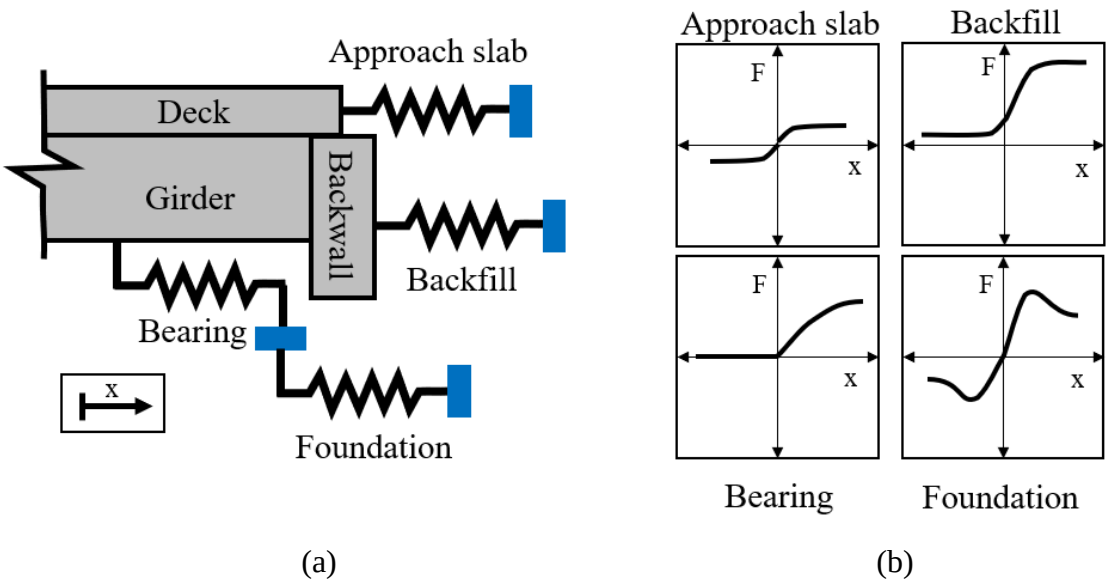

Figure 4.10: Semi-integral bridge abutment resistance model: (a) Diagram showing elements that resist thermal expansion/contraction of a semi-integral bridge; and (b) hypothetical force-displacement diagram of resisting elements (positive ‘x’ signifies abutment wall displacement toward backfill).

4.5. LATERAL EARTH PRESSURES ON ABUTMENT WALLS

The lateral earth pressure data collected from the east and west abutment walls are presented in Figures 4.11(a) and 4.11(b), respectively. Specifically, the graphs show the time histories of lateral earth pressure measurements from the five Earth Pressure Cells (EPCs) installed in each abutment wall. Three EPCs were installed on the 1.25-m-deep abutment walls at depths of 0.36 m, 0.61 m, and 1.07 m from the top, and are referred to in Figure 4.11 as "top backwall", "mid backwall" and "bot backwall", respectively. In addition, one EPC was installed at mid-height of each abutment cap and at mid-height of the north wing walls, approximately 0.35 m from the abutment walls.

Overall, the lateral earth pressures measured by the EPCs can be observed to vary considerably depending on the location and time of year. The lowest earth pressures were recorded during each fall and winter (ranging from 10 to 50 kPa depending on the location), while the highest earth pressures were recorded from late spring to early fall each year (ranging from 100 to 300 kPa depending on the location). These trends are expected, as comparatively higher earth pressures are consistent with the expected expansion of the bridge deck during summers toward the abutment backfill (overall movements in the passive direction) while lower earth pressures are anticipated with the expected contraction of the bridge deck during winters, with abutment walls retracting from the backfill (overall movements in the active direction).

It should be noted that the data recorded over the nearly two years of abutment earth pressure monitoring show signs of ratcheting in both abutments. For example, the maximum earth pressure recorded at the location of the top EPC on the east abutment wall increased by 50 kPa (i.e., about 20%) from summer 2021 to summer 2022. A similar trend can be observed among other EPC records as well. This indicates that the earth pressures acting on the abutment walls, abutment caps and wing walls have shown an overall increasing trend with time. It is noteworthy that the abutment wall displacements have slightly changed from summer 2021 to summer 2022 due to bridge shifting over time

(Figure 4.9). As a result, the east abutment wall has moved slightly more in the passive direction (expected to cause relatively larger lateral earth pressures) in summer 2022 compared to summer 2021 and the west abutment wall has moved slightly more in the active direction (expected to cause relatively smaller lateral earth pressures) in summer 2022 compared to summer 2021. However, ratcheting is clearly observed in the EPC data collected from both abutments.

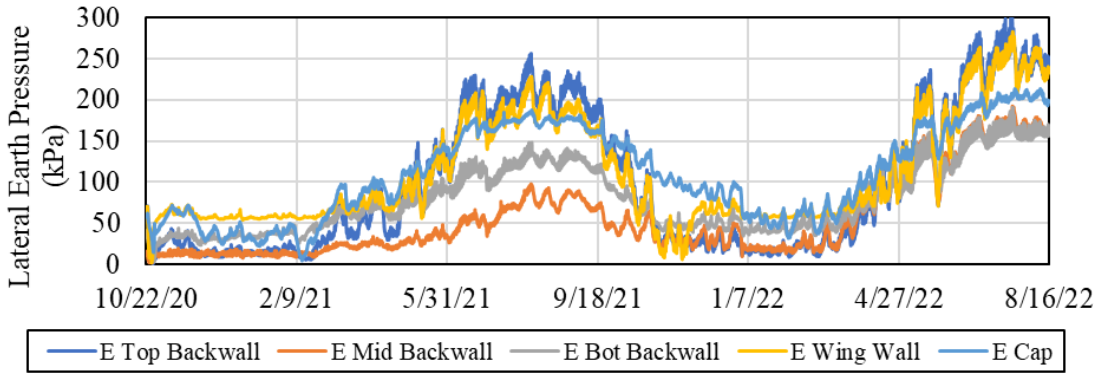

(a)

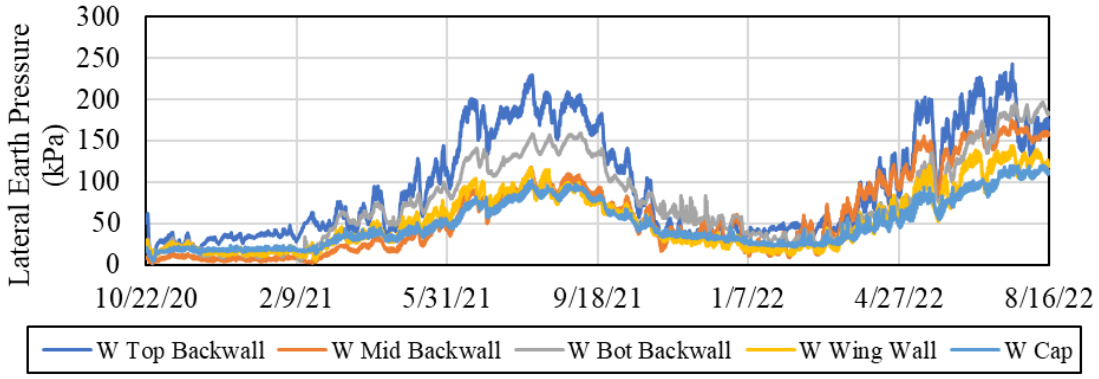

(b)

Figure 4.11: Time history of lateral earth pressures recorded in (a) east abutment; and (b) west abutment.

The data on lateral earth pressures acting on the wing walls and abutment caps, also presented in Figure 4.10, indicate that the thermal expansion of the bridge also significantly affects the earth pressure acting on these components. It bears reiterating that the wing wall

EPCs on China Creek Bridge are installed very close to the abutment wall. The higher confinement of the backfill in this region can potentially explain the similar trends between the readings collected by the wing wall EPCs and those collected by the EPCs installed in the abutment walls. However, the earth pressure acting on the far end of the wing walls is expected to be comparatively lower, and the plotted data should therefore not be considered the representative average earth pressure acting on this component. In the case of the abutment caps, the change in lateral earth pressure is attributed to the displacement of the abutment caps themselves. The recorded data indicates that earth pressures as high as 200 kPa were recorded on the east abutment cap due to thermal expansion of the bridge.

Regarding the variation of lateral earth pressures with depth, the results in Figure 4.11 indicate that the highest earth pressure readings were recorded by the top EPC (i.e., the shallowest), with earth pressures reaching 300 kPa. While this trend with depth may appear inconsistent with typical lateral earth pressure distribution in conventional walls (i.e., lateral earth pressure increasing linearly with depth), several studies (e.g., Huntly and Valsangkar, 2008), Civjan et al.,2004), have also found a non-linear distribution of earth pressures with depth while monitoring integral bridge abutment walls. While this observation is not consistent with expected earth pressure distribution based on classic earth pressure theories (e.g., Rankine, 1857), there are other factors that can help explain why lateral earth pressure behind semi-integral bridge abutment walls would not increase linearly with depth.

Firstly, it is established in the available literature that the lateral earth pressure magnitude behind retaining walls is a function of the displacement of the wall (e.g., Clough and Duncan, 1991). Therefore, the points along the semi-integral bridge abutment wall can be expected to experience different lateral earth pressure magnitudes if the movement of the abutment wall is not purely translational, but a combination of rotation and translation. Furthermore, it has been shown that the magnitude of earth pressure increase due to

ratcheting is a function of lateral compression/extension cycle magnitude (e.g., Clayton et al., 2006). Accordingly, larger displacement cycles can result in a faster rate of ratcheting.

Lastly, the top 2/3 of the abutment wall is directly supported by the girders while the bottom third of the wall is cantilevered and consequently more flexible, which can potentially affect soil arching and stress redistribution, especially as the backfill material is granular (crushed gravel). This arrangement is also analogous to a shallow footing with an off-centered axially-loaded column. Therefore, similar to how soil reaction is expected to decrease from directly below the column to the far edge of the shallow footing, larger magnitude lateral earth pressures can be expected near the top of the abutment wall compared to the bottom of the abutment wall.

While traditional lateral earth pressure concepts do not completely explain the development of higher lateral earth pressures near the top of the abutment walls during the summer months, the other concepts explained above can potentially explain the observed variation of lateral earth pressure with depth. According to the bridge deck temperature distribution model proposed in Branco and Mendes (1993), the deck concrete on top of the girders is expected to experience a wider range of temperatures on most days due to the effect of environmental factors such as solar radiation, thermal convection at the concrete surface, wind, and thermal radiation. As such, the deck concrete, in comparison with the bottom of the girder, is expected to heat up faster and to a higher temperature as well as cool down quicker during the night. This difference in the range of temperatures is also expected to result in a slightly different magnitude of thermal expansion cycles, with larger magnitude cycles occurring near the top of the bridge in comparison with the bottom of the girder.

Since strain gauges were installed at three different depths within the bridge superstructure (girder and deck slab), it is possible to directly verify whether larger thermal expansion cycles occur near the top of the deck. For this purpose, the ratio of daily thermal strains between the top of the deck and bottom of the girder was determined. Figure 4.12

presents these results. For reference, the approximate location of the strain gauges used in the analysis is depicted in the bottom right corner of the figure. Values greater than one in Figure 4.12 indicate that the top of the girder has experienced more thermal expansion than the bottom (in a 24-hour period), meaning that the top of the abutment walls have moved farther than the bottom. Furthermore, the opposite holds true for the few instances where the thermal expansion ratio is seen to fall below one.

Overall, the points near the top of the wall not only experienced larger displacement magnitudes, but also larger daily displacement cycles compared to the bottom of the wall. These two observations along with the potential effect of soil arching and variation of the abutment wall's rigidity with depth due to how it is connected to the girders can potentially explain why significantly higher earth pressures were recorded near the top of the abutment wall in comparison to the bottom of the wall.

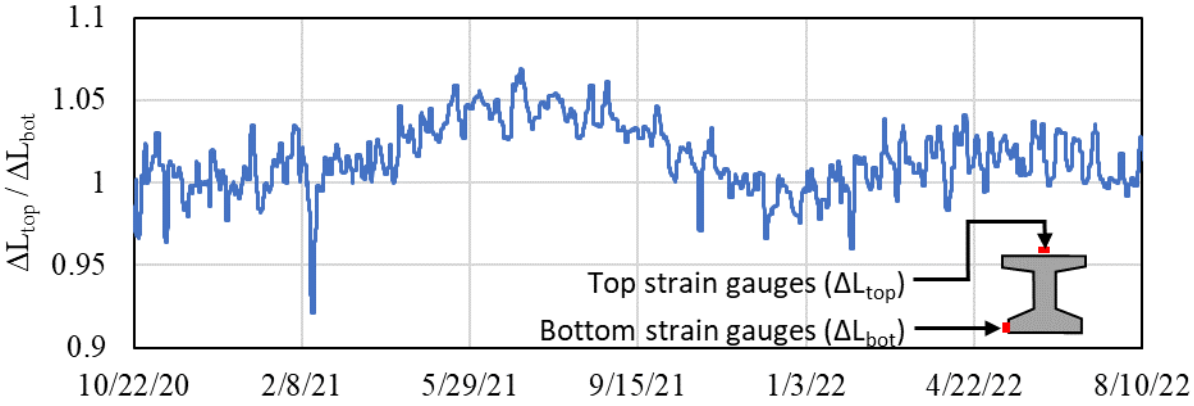

Figure 4.12: Time history plot of ratio between the thermal expansion of deck slab right above the girder's top flange relative to the bottom of girder (girder top-to-bottom thermal expansion ratio).

With the earth pressure data recorded during the monitoring period, it is possible to investigate the causes of the bridge asymmetric thermal expansion/contraction, as previously discussed in Section 4. Specifically, the lateral thrust (i.e., total force) acting on

each abutment was estimated using the lateral earth pressures defined by the EPCs installed on each wall. The lateral thrust results are presented in Figure 4.13. For reference, the lateral thrust predicted using the conventional Coulomb (1776) and Rankine (1857) lateral earth pressure theories (considering the backfill friction angle of 42°) are also shown in Figure 4.13. The results indicate that the lateral thrust acting on both abutment walls reached values that were 2 to 2.5 times higher than Rankine's passive thrust estimate. However, these values are still below the value corresponding to Coulomb's passive thrust force. Moreover, it can be observed that the ratcheting phenomenon resulted in an increase of the average summer lateral thrust of approximately 25%, from summer 2021 to summer 2022.

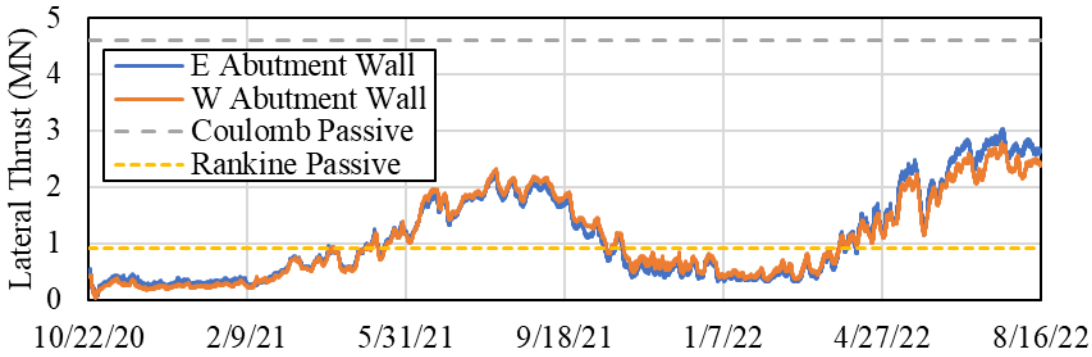

Figure 4.13: Time history plot of lateral thrust force acting on abutment walls estimated from EPC readings.

The results in Figure 4.13 also indicate that the time history of lateral thrust corresponding to the backwalls of the west and east abutments are remarkably similar. Consequently, the difference between the ultimate resistance offered by the backfill on either end of the bridge is essentially negligible. This is revealing, particularly considering the asymmetric abutment wall displacement records discussed in Section 4. Consequently, the stiffness of the abutment backfills is expected to be notably different to result in a nearly identical amount of lateral thrust in response to different magnitudes of abutment wall

movement. The horizontal soil extensometers installed at the mid-depth of each abutment wall (Figure 4.2), allow defining the relationship between the average lateral compression and extension of the backfill soil mass within 1 m of the abutment walls and the lateral earth pressures acting at mid-depth of the abutment walls. Figure 4.14 displays the results of such an evaluation. To facilitate the discussion of observed trends, the data is grouped into warming and cooling periods. In this analysis, "warming period" refers to the period when the bridge primarily experienced thermal expansion (i.e., April to August) and the cooling period is when the bridge primarily experienced thermal contraction (i.e., October to March). In this analysis, positive strain measurements correspond to lateral compression of the backfill the approximate stiffness of the backfill material is defined for the two warming periods on record using linear regression.

The seasonal stress-strain behavior presented in Figure 4.14 indicates that the stiffnesses of the abutment backfill in the east and west abutments are very different. For example, during the first warming period (orange markers), the predicted east abutment backfill stiffness (6 MPa) was less than half that of the west abutment backfill (15 kPa). While the stiffness of the east abutment backfill increased significantly over the second warming period (yellow markers), it was still slightly less than that of the west abutment backfill. The identified discrepancies in backfill stiffness are consistent with the bridge's tendency for eastward thermal expansion during the warming period.

The results presented in Figure 4.14 also provide further evidence of ratcheting and the impact of cyclic lateral loading on the stiffness of the abutment backfill. Specifically, Figure 4.14 results show that during the second warming period (yellow markers), the stiffness of the east abutment backfill had increased by 200% and the stiffness of the west abutment backfill increased by 33% compared to the stiffness estimated for the preceding year. The results in the figure also indicate that the discrepancy in backfill stiffnesses between the east and west abutments decreased significantly from the first to the second year. Therefore, while such discrepancy in backfill stiffness is deemed to be a significant

factor affecting the asymmetrical thermal expansion of the bridge, it is possible that such thermal response will becomes more balanced (i.e., symmetrical) over the long-term. This is considering that the increasing trend of backfill stiffnesses will lead to east and west backfill stiffness values becoming closer in magnitude.

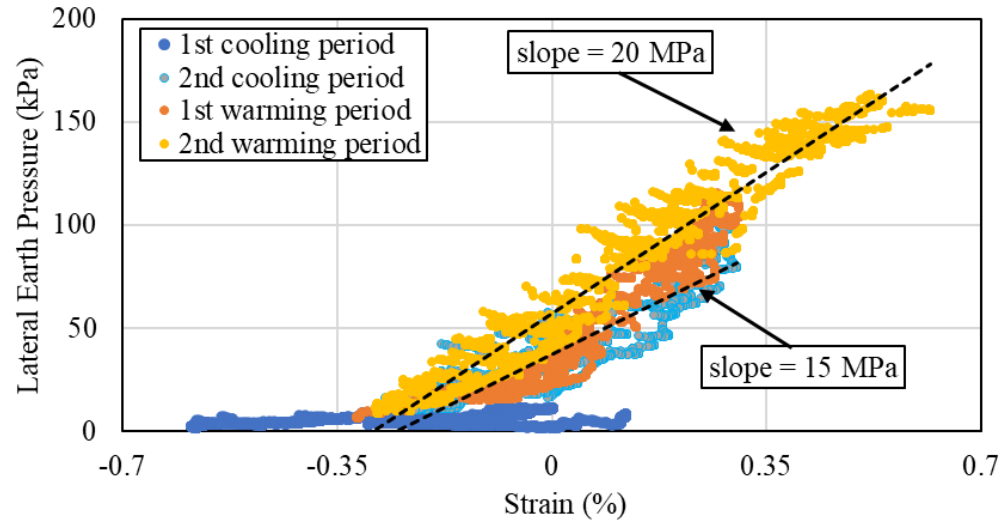

(a)

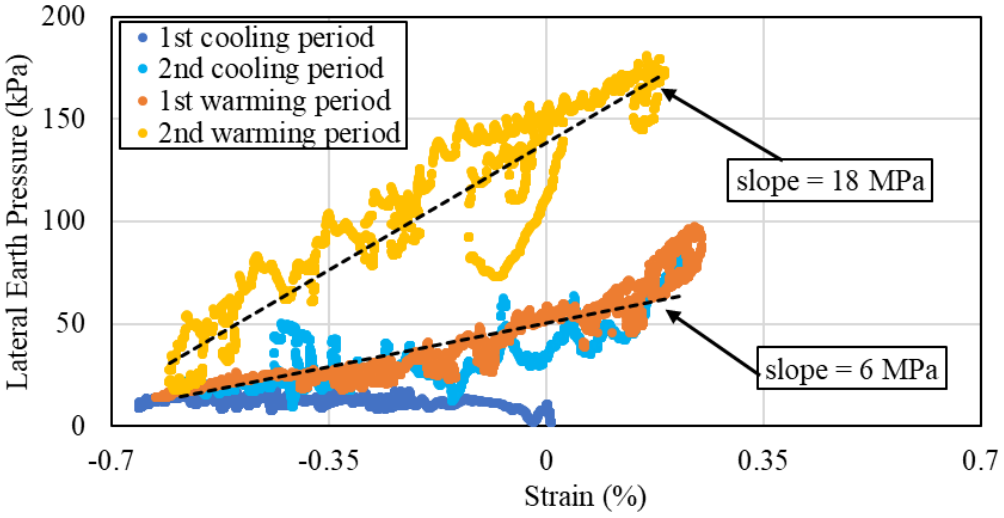

(b)

Figure 4.14: Measured stress – strain behavior for abutment backfills at abutment wall mid-depth: (a) east abutment; and (b) west abutment. (Note: positive strain values indicate backfill compression.)

4.6. ABUTMENT BACKFILL SETTLEMENTS

In addition to the influence of thermal expansion/contraction cycles on increasing backfill lateral earth pressure, it is important to also understand their impact on the settlement of the abutment backfill. This is a relevant topic because backfill settlement may lead to the development of a bump at the end of the bridge when flexible approach pavements are used or lead to a faster rate of fatigue and cracking in rigid approach slabs. The next section presents observations on the settlement of abutment backfills at China Creek Bridge.

In this section, the data collected from the four backfill settlement sensors (see Figures 1 and 2) is evaluated. Figure 4.15 displays the settlement data collected by these sensors. Unlike most other data presented herein, the settlement data was defined in reference to the sensor readings taken at the start of the monitoring period (October 2020) as opposed to the time of sensor installation (June 2020) to facilitate a side-by-side comparison. However, it is worth noting that during the period between June 2020 to October 2020 (not included in Figure 4.15), the west abutment sensors had recorded settlements of 30 and 50 mm, while the settlements recorded by the east abutment sensors were 25 and 35 mm of settlement. The higher on average settlement recorded for the west abutment backfill from June to October 2020 could be attributed to the larger active direction displacement of the west abutment wall compared to the east abutment wall.

Focusing on the backfill settlement data shown in Figure 4.15, it is observed that the four sensors recorded settlements ranging from 3 to 8 mm over the monitoring period. In this dataset, the two highest settlement magnitudes were recorded by the sensors installed closest to the abutment wall (approximately 0.8 m away), while the sensors installed nearly 1.8 m away from the abutment wall recorded smaller settlement magnitudes. The measurement of higher magnitude settlements closer to the abutment wall is consistent with the findings of Walter (2018) based on large-scale experimental testing of integral abutments. It is possible that the partial collapse of the soil near the abutment

wall (within the active wedge) may have led to a higher rate of settlement in the vicinity of the abutment walls in comparison to points farther away.

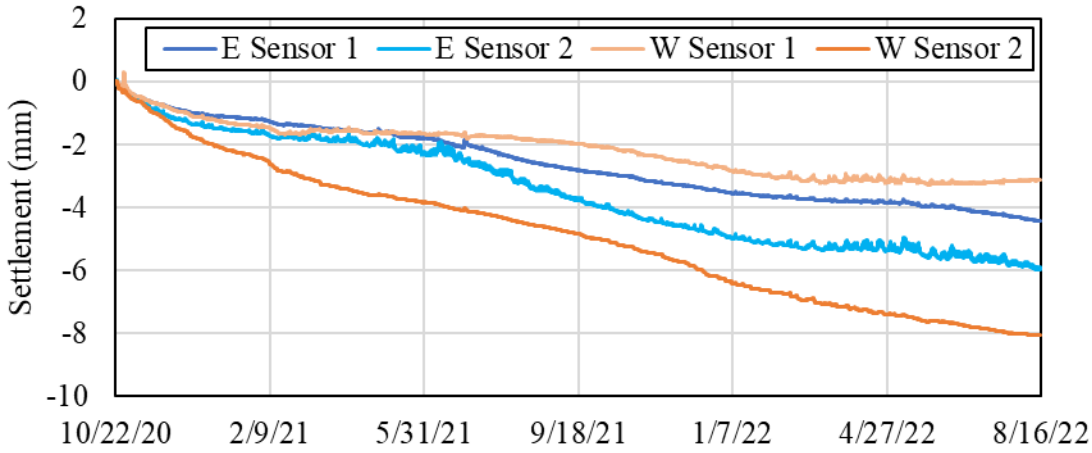

Figure 4.15: Time history of settlement data collected from four backfill settlement sensors. Settlement data presented is calculated relative to start of monitoring (10/22/2020).

While the data collected during the monitoring period indicates that the settlement in both abutments increases with time, on a smaller time-scale some of the backfill settlement was observed to be recovered (i.e., resulting in soil heaving). A close-up of the settlement data measured by one of the east abutment settlement sensors along with the east abutment wall displacement is shown in Figure 4.16. The results in this figure indicate that the abutment wall displacement toward the backfill is accompanied by a decrease in settlement (heaving) such that there is an overall decrease in settlement during the first four days of this data set. However, the overall trend suggests that the lateral wall displacements in the passive direction do not cause as much heaving as abutment wall displacements in the active direction cause backfill settlement. Therefore, the settlement of the abutment fill tends to increase over time.

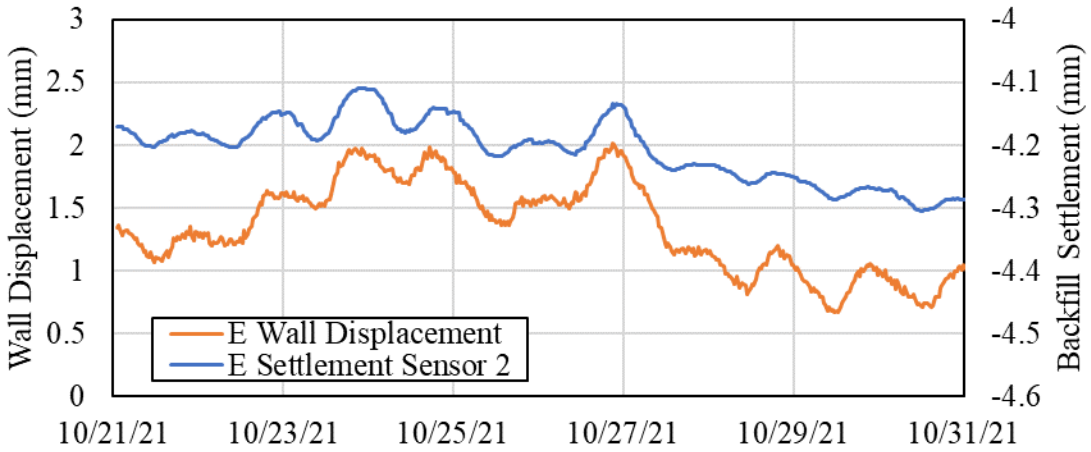

Figure 4.16: East backfill settlement and wall displacement during a 10-day period in October 2021.

While the settlement sensors do not indicate the extent of the backfill area affected by settlement, it is apparent that at least a third of the reinforced concrete approach slabs are no longer resting in direct contact with the abutment backfill soil. This loss of vertical support results in larger shear stresses and bending moments being experienced by the approach slabs, possibly leading to damage and cracking if not properly designed. It is worth noting that despite the increased loading of the approach slabs, no sign of damage has been observed on the approach slabs during the visual inspection of the structure conducted. This is because of the conservative assumption, at the design stage, that no vertical support would be provided by the backfill. However, the settlement observed is undesirable and signifies an area with a large potential for improvement. Such improvements may be achieved by adopting materials and construction techniques that help mitigating backfill settlement, reduce loads on the approach slabs and increase the service life of the structure.

4.7. CONCLUSIONS

This chapter presents the results from nearly 2 years of monitoring a pilot semi-integral bridge in North Texas. Through the comprehensive instrumentation program developed for this study, the thermal expansion and contraction of the bridge superstructure, displacement of the abutment walls and soil-structure interaction within the abutments were successfully captured. These findings facilitate understanding the effect of soil-structure interaction on the performance and behavior of semi-integral bridges with unreinforced granular abutment backfills and can be utilized to improve the design and long-term performance of future semi-integral bridge structures.

The following conclusions were drawn from the analyses of the data collected in this study:

- The abutment wall movements in response to the thermal expansion/contraction of the bridge superstructure can be highly asymmetrical even if the structure is symmetric in geometry. The time history data for the abutment wall positions indicated highly asymmetric displacement of these components. Compared to the east abutment wall, the west abutment wall experienced significantly more displacement away from the abutment backfill due to thermal contraction of the bridge during the winter months. However, more displacement occurred in the east abutment compared to the west abutment during the summer months.
- The position of the neutral thermal expansion point in semi-integral bridges can change seasonally and is rarely in the midpoint of the bridge. Consequently, in China Creek Bridge, it was found that it would be more realistic to use 70% of the total bridge length for estimating the range of movement at the abutment walls due to thermal expansion/contraction of the bridge as opposed to half the bridge length.

- The recommended Coefficient of Thermal Expansion (CTE) by AASHTO (2018) was found to be adequate for predicting the thermal expansion of the instrumented structure. The 27.5 m-long bridge superstructure experienced nearly 12 mm of thermal expansion/contraction over the monitoring period, with a CTE of approximately 9.0×10^{-6}/°C, falling within the expected range for normal weight concrete structures.
- Semi-integral bridge abutment backfills were found to be susceptible to ratcheting caused by the cyclic movement of the abutment walls. In China Creek Bridge, the maximum annual backfill lateral earth pressures were seen to increase by approximately 20% over a year reaching values as high as 300 kPa.
- Lateral earth pressures do not necessarily increase with depth in semi-integral bridge abutment backfills. Through the analysis of China Creek Bridge data, it was concluded that the larger displacement cycle magnitude near the top of the abutment walls compared to the bottom of the walls as well as the larger rigidity of the abutment wall in the top 2/3 of the wall, due to the presence of the girders, can cause the lateral earth pressures to be significantly higher near the top of the wall, compared to the bottom of the wall.
- Ratcheting in semi-integral bridges can also affect the wing walls and abutment caps. The earth pressure data collected from China Creek Bridge indicates that the abutment caps and wing walls also experienced significant lateral earth pressure increase during the summer months. EPCs installed on abutment caps and wing walls indicated that the lateral earth pressure acting on these components changes

seasonally, similar to the abutment walls, and that they are also affected by ratcheting.

- The asymmetric displacement of the abutment walls in semi-integral bridges was attributed to the difference between the stiffness of the abutment elements (e.g., backfill) between the two abutments. In China Creek Bridge, it was observed that the lateral thrust acting on the east and west abutment walls matched very closely during the monitoring period despite the significant difference in the abutment wall movement records between the two abutments.
- The lateral thrust acting on semi-integral bridge abutment walls can exceed Rankine's passive thrust. In China Creek Bridge, the lateral thrust acting on the abutment walls reached approximately 60% of Coulomb's passive thrust estimate by the end of summer 2021. It is possible that the lateral thrust will continue to increase in the coming years as more ratcheting occurs.
- The close match between the two abutments' lateral thrust data and mismatch between the abutment walls' displacement data revealed a discrepancy between the stiffnesses of the abutment backfills. The relatively stiffer west abutment backfill was identified as the cause of the bridge's tendency for eastward expansion during the spring and summer months.
- The stiffness of the semi-integral bridge abutment backfills can significantly over time due to ratcheting. In China Creek bridge, the measured seasonal stress-strain behavior of the abutment backfills indicated that the west abutment backfill was stiffer than the east abutment and both abutment backfill stiffnesses increased each year. The data also indicated that the difference between the abutment backfill

stiffnesses decreased each year and it is therefore possible that the thermal expansion of the bridge will occur more symmetrically in the long-term.

- Unreinforced granular backfills in semi-integral bridges are highly susceptible to settlement due to daily and seasonal cyclic abutment wall displacements. In China Creek Bridge, the settlement of the abutment backfills was measured using four settlement sensors, which recorded 30 to 58 mm of settlement over the monitoring period. Some asymmetry was observed as well, indicating that more settlement occurred within the west abutment backfill. This is likely due to the larger active direction displacement history of the west abutment wall compared to the east abutment wall.
- The settlement records indicated that backfill settlement and heave occur each day as the abutment walls move away and toward the backfill because of the thermal expansion/contraction of the superstructure. The magnitude of heave has typically been smaller than the magnitude of settlement, leading to increased settlement over time. While the observed settlement rate in China Creek Bridge has changed seasonally, no signs of abutment backfill settlement reaching an asymptotic value has been observed during the monitoring period.
- Abutment backfill settlement can lead to a partial loss of vertical support for the approach slabs in semi-integral bridges. In China Creek Bridge, the settlement data indicates that at least a third of the approach slabs are no longer vertically supported by the abutment backfills and the size of the void continues to increase with time. As the void grows larger, the magnitude of stresses acting on the approach slabs due to traffic loads increases as well. Consequently, the loss of vertical support for

the approach slabs may result in a higher rate of fatigue and deterioration, thereby affecting the service life of the structure.

4.8. ACKNOWLEDGEMENTS

The authors thank the Texas Department of Transportation (TxDOT) for funding this research under project 0-6936 through the Center for Transportation Research (CTR) at the University of Texas at Austin.

4.9. REFERENCES

AASHTO. (2020). "AASHTO LRFD bridge design specifications", American Association of State Highway and Transportation Officials

Abendroth, R. E., Greimann, L. F., Lim, K.-H., Sayers, B. H., Kirkpatrick, C. L. and Ng, W. C. (2005). "Field Testing of Integral Abutments." Iowa State University Center for Transportation Research and Education, Ames, IA.

Branco, F. A., and Mendes, P. A. (1993). "Thermal Actions for Concrete Bridge Design." Journal of Structural Engineering, 119 (8): 2313–2331. https://doi.org/10.1061/(ASCE)0733-9445(1993)119:8(2313).

Burke, M. P. (2009). "Integral and Semi-Integral Bridges." Wiley-Blackwell.

Civjan, S. A., Brena, S. F., Butler, D. A., and Crovo, D. S. (2004). "Field Monitoring of Integral Abutment Bridge in Massachusetts." Transportation Research Record, 1892 (1): 160–169. SAGE Publications Inc. https://doi.org/10.3141/1892-17.

Civjan, S. A., Kalayci, E., Quinn, B. H., Brena, S. F., and Allen, C. A. (2013). "Observed integral abutment bridge substructure response." Engineering Structures, 56: 1177–1191. https://doi.org/10.1016/j.engstruct.2013.06.029.

Clayton, C. R. I., Xu, M., and Bloodworth, A. (2006). "A laboratory study of the development of earth pressure behind integral bridge abutments." Géotechnique, 56 (8): 561–571. https://doi.org/10.1680/geot.2006.56.8.561.

Clough, G. W., and Duncan, J. M. (1991). "Earth Pressures." Foundation Engineering Handbook, H.-Y. Fang, ed., 223–235. Boston, MA: Springer US.

Coulomb, C. A. (1776). "Essai sur une application des règles de maximis & minimis à quelques problèmes de statique, relatifs à l'architecture." Paris: De l'Imprimerie Royale.

England, G. L., Tsang, N. C. M., and Bush, D. I. (2000). "Integral bridges: a fundamental approach to the time–temperature loading problem". Thomas Telford Ltd, London.

Frosch, R., and Lovell, M. (2011). "Long-Term Behavior of Integral Abutment Bridges." JTRP Technical Reports. https://doi.org/10.5703/1288284314640.

Huffaker, C. D. (2013). "Behavior and Analysis of an Integral Abutment Bridge." Master's thesis, Utah State University.

Huntley, S. A., and Valsangkar, A. J. (2013). "Field monitoring of earth pressures on integral bridge abutments." Can. Geotech. J., 50 (8): 841–857. https://doi.org/10.1139/cgj-2012-0440.

Mofarraj, B., and Zornberg, J. G. (2022). "Field Monitoring of Soil-Structure Interaction in Semi-Integral Bridges." Geo-Congress 2022, ASCE, Charlotte, NC, 33–42. https://doi.org/10.1061/9780784484067.004.

Oesterle, R., and Tabatabai, H. (2014). "Design Considerations for Integral Abutment/Jointless Bridges in the USA." Civil and Environmental Engineering Faculty Articles. 1. https://dc.uwm.edu/cee_facart/1

ODOT. (2022). “Bridge Design Manual 2020 Edition.” Ohio Department of Transportation, Ohio.

Ooi, P. S. K., Lin, X., and Hamada, H. S. (2010). “Field Behavior of an Integral Abutment Bridge Supported on Drilled Shafts.” J. Bridge Eng., 15 (1), 4–18. https://doi.org/10.1061/(ASCE)BE.1943-5592.0000036.

Purvis, R. L., and Berger, R. H. (1983). “Bridge Joint Maintenance.” Transportation Research Record, 899, 1-10.

Rankine, W. J. M. (1857). “On the stability of loose earth.” Philosophical transactions of the Royal Society of London, 147: 9–27.

Texas Department of Transportation. (1993). “Item 423: Retaining Walls” Texas Department of Transportation.

Walter, J. R. (2018). “Experimental and numerical investigation of integral/semi-integral bridge abutments for Texas conditions.” Master’s Thesis, University of Texas at Austin.

Chapter 5: Long-Term Field Monitoring of Lateral Loads in Semi-Integral Bridge Foundations

ABSTRACT

Jointless bridge designs have become increasingly common over the past several decades, both in the USA and worldwide. The increased utilization of these alternative designs is largely due to the poor long-term performance of expansion joints and often prohibitive cost of joint maintenance. While integral bridges typically require the selection of flexible foundations to accommodate deck thermal movements, most transportation agencies do not require such flexible foundations for the case of semi-integral bridges. This is because, unlike integral bridges, the superstructure of a semi-integral bridge is not directly connected to the abutment wall and therefore is not expected to experience lateral loading. This study presents data collected over two years from the drilled shaft foundations of a semi-integral bridge in Texas. The data indicate that semi-integral bridge foundations may also experience significant, thermally-induced cyclic lateral loading, the magnitude of which changes seasonally. Moreover, the accumulation of plastic strains in the foundation soils due to cyclic loading of the foundations may also result in permanent movement of the abutment caps over the long-term.

5.1. INTRODUCTION

Semi-integral and integral bridge construction is becoming increasingly common, both in the USA and worldwide. The defining characteristic of these bridges is the elimination of expansion joints at the ends of their deck and in between spans. Integral

bridges are continuous single- or multi-span bridges in which the superstructure is constructed integrally with the substructure. Instead, the abutment walls and abutment caps are not integrally connected in semi-integral bridges, a characteristic aimed at allowing the superstructure to move independently from the substructure. Unlike semi-integral bridges.

The increasing utilization of these structures can be attributed to a number of construction and maintenance issues associated with deck expansion joints of conventional bridges. Deck expansion joints are typically used to alleviate stresses in the structure caused by phenomena related to shrinkage, creep, thermal expansion, and contraction, as well as differential settlements of piers and abutments (Burke, 2009). However, several problems are associated with deck expansion joints, including the high rate of wear and tear, exposure of the structure to harmful chemicals and relatively high cost of initial construction and maintenance (Purvis and Berger, 1983). Therefore, many transportation agencies worldwide have opted for alternatives such as semi-integral and integral bridges.

Assessment of the design details of semi-integral and integral bridges across the United States reveals significant differences among the rationales and approaches adopted by different transportation agencies. For example, according to Maruri and Petro (2005), while many states require H-pile foundations oriented toward the weak bending axis to increase flexibility for integral bridges, some states require an orientation toward the strong axis, and some even allow the use of drilled shafts, which are comparatively more rigid than H-piles. Moreover, while lateral loading is considered in the design of integral bridge foundations, such loading is not typically considered in the design of semi-integral bridge foundations. These discrepancies have been reflected in the instrumentation programs that have been implemented to monitor the behavior of integral and semi-integral bridges.

While long-term studies on the behavior of the foundations in integral abutment were identified (Ooi et al, 2010; Lawver et al, 2000; Abendroth et al, 2005), the authors were not able to find studies on lateral loading of the foundations of semi-integral bridges in the technical literature.

While the study of a pilot semi-integral bridge in Texas, described in Mofarraj and Zornberg (2022) did not explicitly focus on possible lateral loading on the bridge foundations, this study found evidence of lateral movements in the abutment caps, though the magnitude of the loads remained unknown. Applying the lessons learned from this study, a more comprehensive bridge monitoring program was developed for a second semi-integral bridge in Texas that included over 70 sensors and a dedicated foundation monitoring system.

The purpose of the study presented in this chapter is to provide an analysis of the data obtained from monitoring lateral deformations of the foundation elements in the semi-integral China Creek Bridge. Specifically, the evaluation focuses on characterizing the deflections and lateral loads acting on the bridge foundations due to thermal expansion and contraction of the superstructure.

5.2. DESCRIPTION OF CHINA CREEK BRIDGE

The semi-integral China Creek Bridge is a state highway bridge built in 2020 outside Wichita Falls, TX. A schematic of this bridge is shown in Figure 5.1. The bridge has two traffic lanes and measures 27.5 m in length. The superstructure includes prestressed concrete I-beam girders, precast concrete panels between the girders, and a cast-in-place reinforced concrete overlay. The abutment walls are integrally connected to the deck and

girders and are 1.25 m deep. The bridge is supported by four 11-m-deep drilled shafts on each side, each of which are 0.9 m in diameter. The deck connects to the approaching roadway via 6-m-long reinforced concrete approach slabs that are structurally connected to the deck and abutment wall on one end and rest on sleeper slabs on the other. The gap between the abutment wall and abutment cap was filled with a 50-mm-thick closed-cell foam, as displayed in Figure 5.1.

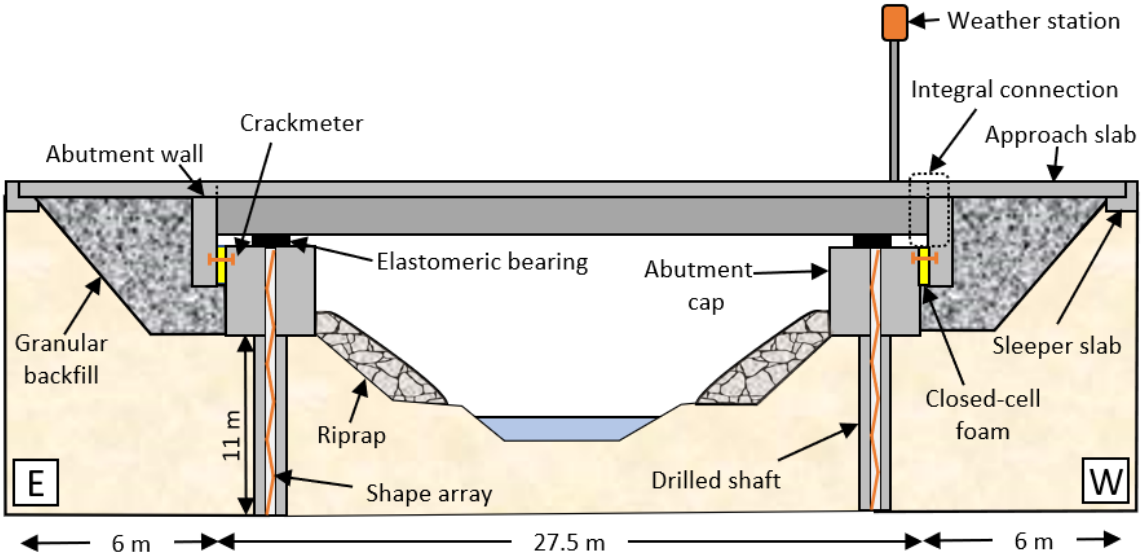

Figure 5.1: Schematic of semi-integral China Creek Bridge, including some of the installed sensors.

While forming the abutment walls, a comparatively stiff closed-cell foam was used on the inner facing of the abutment walls. Although most of this material was removed after construction, the portion of this foam between the abutment cap and abutment wall was left in place (see Figure 5.1). Considering the stiffness of the foam material, it was expected that the deck contraction due to shrinkage and changes in temperature would

contribute to lateral deflection of the drilled shafts, similar to what was previously observed in Mofarraj and Zornberg (2022). Furthermore, as shown in Han et al. (2019), movements at the ends of the bridge deck due to thermal expansion and contraction of the bridge can lead to the development of friction and shear at the base of the elastomeric bearing pads. As a result, semi-integral bridge foundations can experience cyclic lateral loading due to shearing of the elastomeric bearings placed between the abutment cap and the superstructure.

5.3. GEOTECHNICAL CHARACTERIZATION OF THE FOUNDATION SOIL

Prior to bridge construction, 12-m-deep borings were conducted on each side of the bridge for subsurface characterization. Of the materials recovered from these borings, the top 4 m revealed the presence of lean soft clay deposits. The materials recovered from depths of 2.2 to 4 m were described as very soft and saturated. Below 4 m, the recovered materials included mainly stiff and dry lean clay, while the soil below 7 m was very hard and blocky.

In addition to the physical characterization of the in-situ soils, a series of Texas Cone Penetration (TCP) (TEX 132-E, 1999) tests were performed at 1.5-m intervals. A TCP count of 50 (maximum blow count) was reached for depths below 4 m, making it a well-suited bearing stratum for a drilled shaft foundation. However, the top 4 m of the boring logs consisted of soils with TCP counts ranging from 3 to 7, which is associated with soft to medium soils (Touma and Reese, 1972). Considering the characteristics of this top soil layer, a decision was made to protect the drilled shafts from sidewall caving using 4-m-long steel casings.

5.4. INSTRUMENTATION OVERVIEW

During the construction of China Creek Bridge, over 70 sensors were installed to monitor various aspects of the bridge behavior and performance. The installed sensors are shown in Figure 5.1. This chapter focuses on the data collected to monitor the lateral displacements of the drilled shaft elements of this semi-integral bridge.

The lateral displacements of the drilled shafts were obtained using shape arrays (Measurand SAAV) installed within the drilled shafts during bridge construction. The shape arrays consist of a series of rigid segments connected with joints that allow movement in any direction and prevent twisting. Each segment is instrumented with a triaxial Micro-Electro-Mechanical Systems (MEMS) gravity sensor for measuring tilt in two perpendicular directions. The sensor data is used to calculate the relative position of each sensor joint compared to other joints. Therefore, by knowing the absolute position of one of the joints, the position of all others can be calculated. For the purpose of the analyses presented in this chapter, the bottom of the drilled shaft is assumed to be stationary under normal operating conditions. This assumption is used to calculate the absolute position of all other nodes along the length of the installed shape arrays. The potential errors associated with having assumed a stationary bottom of the drilled shaft will be discussed in Section 5. According to the manufacturer, the shape arrays have a precision of ±0.5 mm for a 30-m-array.

Figure 5.2 shows instances of the installation of the drilled shaft rebar cage (fitted with a 70-mm PVC conduit) as well as the placement of the shape arrays in one of the drilled shafts. The shape arrays used in this study consist of 22 segments, each of which measuring 0.5 m in length and providing a 3D deformation profile of the drilled shafts.

While continuous data collection began in October 2020, initial sensor readings were recorded immediately after installation of the shape arrays in June 2020 and before placement of the bridge girders.

(a) (b)

Figure 5.2: Installation of shape arrays in the drilled shaft foundations: (a) Installation of drilled shaft rebar cage fitted with shape array casing; and (b) installation of shape array inside casing after abutment caps were formed.

A ClimaVue50 weather station was deployed at the bridge site to capture changes in ambient air temperature. Additionally, to monitor the thermal expansion/contraction of the bridge, 15 concrete strain gauges (Geokon model 4200 and 4151) were installed on the bridge superstructure to measure deck and girder strains across the length of the bridge.

Lastly, the displacement of the semi-integral abutment walls relative to the abutment caps was measured using a set of Geokon model 4420 crackmeters. These crackmeters essentially measure the change in width of the expansion joint between the abutment caps and abutment walls. As the change in the width of the expansion joints is equivalent to the shear displacement of the elastomeric bearings (see Figure 5.1), the crackmeter data can also provide a measure of the bearing shear and the lateral load applied to the top of the abutment caps due to the movement of the ends of the bridge.

5.5. INSTRUMENTATION DATA

The time-history of the ambient air temperature data collected at the bridge site is presented in Figure 5.3. As can be seen, the ambient air temperature over the monitoring period ranged from -20°C to 45°C. Seasonally, the daily temperature variation recorded during the summer months was 15°C to 20°C, while that recorded during the winter months was 20°C to 30°C. It should be noted that the sharp decrease in ambient air temperature in February 2021 was due to winter storm Uri, an extreme weather event that affected the entire State of Texas and the rest of the country, resulting in nearly a week of subfreezing temperatures and record snowfall events in this area.

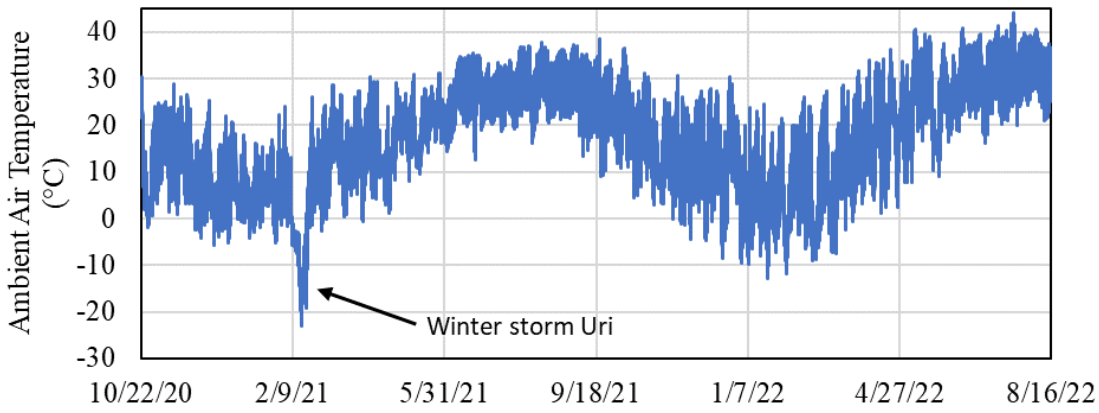

Figure 5.3: Time-history of ambient air temperature data collected by on-site weather station.

Predictably, the daily and seasonal changes in ambient air temperature have resulted in thermal expansion/contraction of the bridge, which was calculated using a series of strain gauges installed on one of the bridge girders. Figure 5.4 displays the time-history of the thermal expansion/contraction of the bridge. Each plot point in the figure indicates how much the bridge length has increased/decreased relative to its initial length in July 2020. For example, relative to its initial length, the bridge length had increased by up to 3.5 mm during the summer 2021 and had decreased by up to 9 mm during the winter 2021.

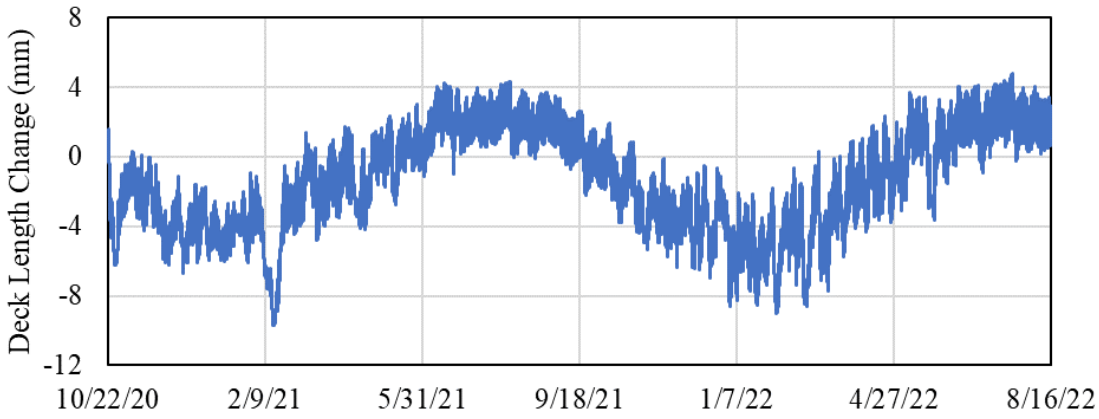

Figure 5.4: Time-history of changes in deck length (deck thermal expansion/contraction).

Because the deck and girders in semi-integral bridges are not rigidly connected to the abutment cap and deep foundation units, thermal expansion/contraction of the bridge is expected to result in opening/closing of the expansion joints between the abutment caps and abutment walls. The changes in the width of these expansion joints were successfully captured using the installed crackmeters. The crackmeter data is presented in Figure 5.5 and shows the change in the width of the expansion joint relative to its initial width. Positive values indicate an increase in the distance between the abutment wall and abutment cap, while negative values indicate the opposite. The crackmeter readings also provide the shear displacement of the elastomeric bearings (see Figure 5.1). In this bridge, the shear stresses that develop at the bearings is transferred to the abutment caps and may conceivably result in lateral loading of the foundation units. Additionally, zero crackmeter readings indicate contact between the abutment wall, expansion joint materials (stiff geofoam) and abutment caps, while negative readings indicate compression of the expansion joint materials.

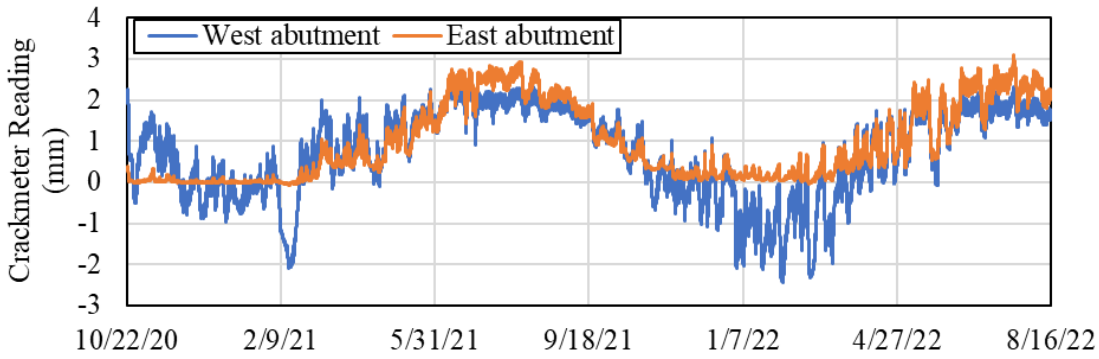

Figure 5.5: Time-history of change in width of expansion joints between abutment caps and abutment walls measured via crackmeters.

As can be seen in Figure 5.5, the change in width of the expansion joints in China Creek Bridge did not develop symmetrically. For example, during the winter months, the east abutment expansion joint width returned to its original width (i.e., zero crackmeter readings), while the negative values recorded by the west abutment crackmeter indicate compression of the geofoam installed at the joint. In both cases, the crackmeter readings indicate that contact had occurred between the abutment cap and abutment walls due to contraction of the bridge in the winter months. Ultimately, this contact can also lead to lateral loading of the foundations.

The time-history of the abutment cap displacement data measured by the shape arrays installed in the drilled shafts is plotted in Figure 5.6. The displacement values indicate changes in position of the abutment caps compared to their initial positions at the time of construction. Positive values in this plot indicate displacement towards the abutment backfill and negative values indicate the opposite.

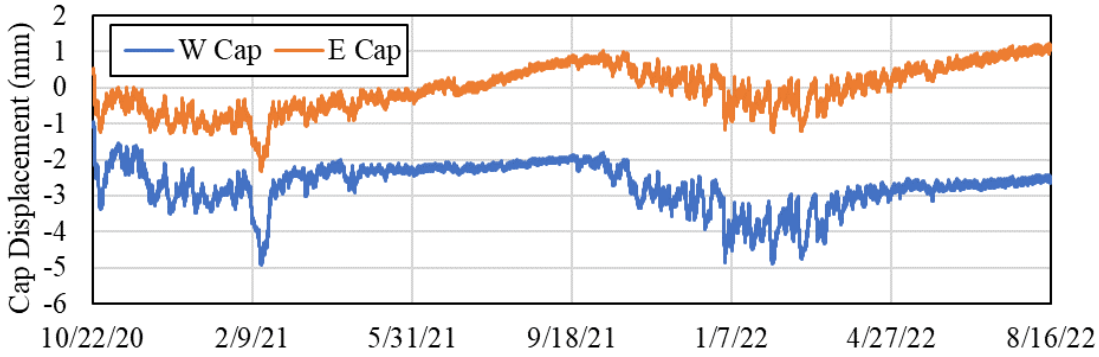

Figure 5.6: Time-history of abutment cap displacement data measured using drilled shaft shape arrays.

While the shape array data indicates that the lateral movement of the abutment caps is correlated with the thermal expansion/contraction of the bridge, additional slope stability analysis was performed to assess the stability of the abutment slopes and ensure there is no additional loads on the foundations due to the instability of the abutment slopes. This analysis was carried out using StablPro software (Ensoft, Inc., 2015). The factor of safety of 2.2 was found for the slope using Bishop's method. Therefore, potential slope failure and foundation movements due to slope failure are not causes of concern at this site.

The shape array data reveals daily movement of the abutment caps in response to the thermal expansion/contraction of the bridge. Even though the overall geometry of the bridge is symmetrical, these abutment cap movements are observed to be highly asymmetrical. For example, during the February 2021 winter storm, the east abutment cap reached displacements (relative to their initial positions at the time of construction) of approximately 2 mm away from the backfill, the displacements recorded for the west abutment cap were as high as 5 mm away from the backfill. Overall, the west abutment cap had moved farther away from its original position compared to the east abutment cap.

Seasonally, the east abutment cap experienced movement toward the backfill during summer 2021 and 2022, while the west abutment cap has maintained a position closer to the center of the bridge compared to its initial position.

Overall, it appears that the drilled shafts of the west abutment have experienced larger displacements compared to the drilled shafts of the east abutment during periods of bridge contraction (i.e., winter months). In contrast, the drilled shafts of the east abutment have experienced larger displacements compared to the drilled shafts of the west abutment during periods of bridge expansion (e.g., summer months).

To better interpret the shape array and crackmeter measurements, Figure 5.7 provides schematics illustrating the relative position of bridge components at the time of construction as well as how this arrangement changes due to abutment wall movements toward or away from the abutment backfill.

Figure 5.7(a) shows the initial position of the illustrated bridge components at the time of construction. As shown in Figure 5.7(b), the expansion joint width increases during periods of bridge expansion (positive crackmeter readings), which implies that shear stresses had developed in the elastomeric bearings, causing lateral deflection of the drilled shafts toward the abutment backfill. Conversely, during periods of bridge contraction, depicted in Figure 5.7(c), the abutment wall may contact the abutment cap and lateral loading may be applied to the abutment caps. In this case, the lateral loading magnitude would either be equal to the contact forces alone or the sum of the contact forces and bearing shear (if the expansion joint material is compressed during contact). It should be clarified that the two cases illustrated in Figure 5.7(b) and Figure 5.7(c) were observed during the monitoring period reported in this chapter. For example, during the February

2021 winter storm, the east abutment cap moved by 1.5 mm while the expansion joint width remained unchanged during this period. This implies that the east abutment cap moved because contact forces developed between the east abutment cap and wall, although no shearing developed in the bearings. On the other hand, during the same period, the west expansion joint width decreased by 2 mm and the abutment cap moved by 2.5 mm due to bridge contraction. This observation implies 2 mm of shear displacement for the west bearings in addition to the contact forces between the west abutment cap and wall.

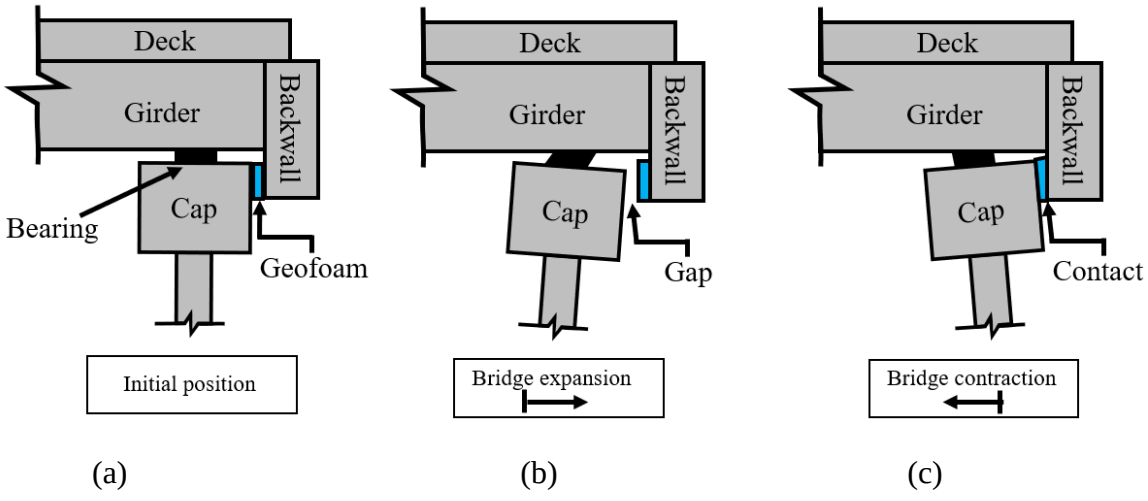

Figure 5.7: Schematics of changes to abutment area in response to thermal expansion/contraction of bridge: (a) initial position; (b) bridge expansion; and (c) bridge contraction.

Notably, the cyclic lateral loading of semi-integral bridge foundations is typically not considered in the design of semi-integral bridges. In fact, no prior reporting of such behavior was identified in the available literature. However, as demonstrated by the shape array data, semi-integral bridge foundations may also experience cyclic lateral loading in response to thermal expansion and contraction of the bridge superstructure. The next

section provides further analysis on the data collected from the shape arrays and crackmeters to expand on the interaction between the superstructure and foundation elements, and the implications of this interaction on the long-term performance of semi-integral bridges.

5.6. ANALYSIS OF THE DRILLED SHAFT BEHAVIOR

As noted earlier, the deflection profile of the drilled shafts was recorded using the installed shape arrays. In turn the deflection profile of the drilled shafts can be used to also estimate the curvature and bending moment profiles. Figure 5.8 displays the deflection, curvature, and moment profiles from two different dates for the drilled shafts of the west abutment. The procedure for the analysis of the deflection profiles was described in detail in **Chapter 3** and therefore, will not be reiterated in this chapter.

The shape of the deflection profiles shown in Figure 5.8 resembles that corresponding to the behavior of short piles (e.g., Broms, 1964), indicating that the foundation units are most likely rotating about a point within the hard clay layer. While determining the position of such point may slightly impact the displacement estimates for the points along the drilled shafts (typically by less than 0.1 mm), this would not affect the prediction of curvature and bending moments, which constitute the primary focus of the evaluation presented herein. To investigate the effect of bridge thermal expansion/contraction on the foundation units, a python code was developed to analyze each recorded deflection profile and calculate the maximum bending moments acting on drilled shafts of the east and west abutments according to the procedure outlined in **Chapter 3**.

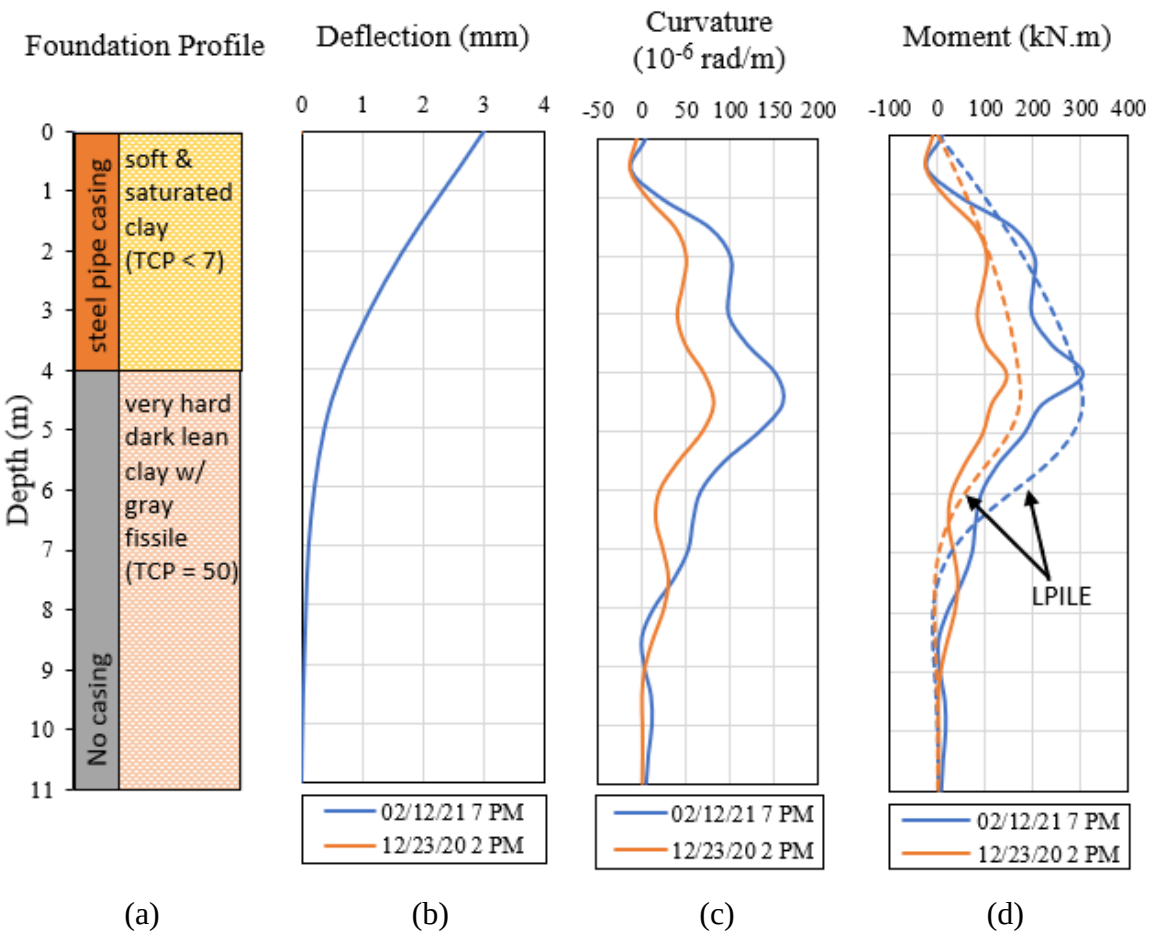

Figure 5.8: Profiles for the west abutment drilled shaft profiles on two different dates: (a) subsurface profile (b) lateral deflection profile (c) curvature profile, and (d) flexural moment profile

In addition to the analysis performed using the shape array data, it was decided to compare these results with p-y analysis performed using LPILE (Wang et al., 2022). For this analysis, the top soft clay layer was idealized by the built-in "Soft Clay (Matlock)" model and the stiff clay layer below that was idealized using the built-in "Stiff Clay w/o

Free Water (Reese)" model. The parameters for these models were selected based on the TCP test results obtained at the site. The bending moment profiles for both cases is shown in Figure 5.8 using dashed lines. As can be seen, the magnitude of maximum moments based on both methods is similar and this maximum moment occurs at nearly the same depth. However, there are also some dissimilarities between the two methods, including the depth of zero bending moment. This is not a surprising outcome considering the limitations of calculating second-order differentials based on discrete data, which was explained in more details in Chapter 3. Moreover, the soil model used in LPILE is an idealized model and does not consider certain factors such as the effect of cyclic loading on the p-y curves. Although only two instances are shown here, similar outcomes were observed for many other cases as well, indicating the closeness of the maximum bending moments predicted using the two methods. Therefore, the shape array data is considered suitable for assessing how the maximum bending moments of the drilled shafts have changed over time.

The time-history of the maximum bending moments acting on the drilled shafts is presented in Figure 5.9. This dataset includes the time-histories of the maximum bending moment in both directions (bending toward and away from the backfill) because the lateral loading changes direction depending on the season. Notably, the maximum bending moment typically occurred near the top of the stiff clay layer. However, the direction of the maximum bending moment changed throughout the year depending on the position of the abutment cap.

As shown in Figure 5.9, the maximum positive bending moment acting on the drilled shafts was typically larger than the negative bending moment when the cap was

pushed toward the center of the bridge (see Figure 5.7(c) sketch). For example, because the drilled shafts of the west abutment were primarily pushed toward the center of the bridge, the positive moments were always larger than the negative moments, and the largest positive bending moments occurred during the winter months when the bridge experienced maximum thermal contraction. On the other hand, the negative bending moments were typically larger than the positive bending moments when the abutment caps were pushed toward the backfill (see Figure 5.7(b) sketch). This case was observed primarily for the drilled shafts of the east abutment during the summer months when the abutment cap was pushed toward the backfill. During both summers, the positive bending moment for the drilled shafts of the east abutment decreased and the magnitude of the negative bending moments increased.

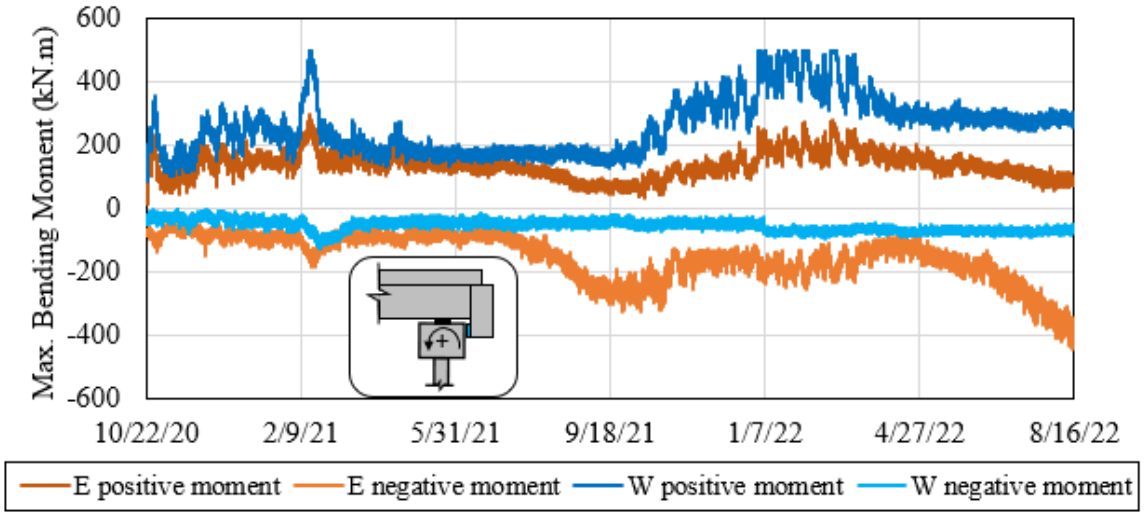

Figure 5.9: Maximum bending moment acting on drilled shafts (positive bending moments indicate bending toward center of bridge as sketched).

Overall, the data presented in Figure 5.9 confirms that semi-integral bridge foundations can experience significant cyclic lateral loads in response to thermal expansion/contraction of the structure. This finding is deemed particularly relevant as it may have important implications in the design of semi-integral bridge foundations. This is because deep foundations in this type of bridge structure are typically designed for axial load bearing capacity only. The results reveal that only a few millimeters of movement at the abutment caps in response to bridge thermal expansion/contraction resulted in the development of very large bending moments. For reference, the estimated cracking moment for the drilled shafts is 490 kN.m, which appears to have been reached on several occasions for the drilled shafts of the west abutment according to the analyses performed for the monitoring period.

There are certain considerations in the analysis that can potentially explain why despite the large calculated bending moments, physical signs of distress in the foundation units have not been found so far. For example, the cracking moment is determined based on the 28-day compressive strength of lab-tested concrete samples, which can potentially differ from the actual strength of the drilled shaft concrete after several months or years of curing in field conditions. Also, the calculation of curvature in this analysis was based on the finite difference analysis of the discrete measurements of the deflection profile by the shape arrays. Considering these potential limitations, the results presented in Figure 5.9 are discussed primarily qualitatively in this chapter.

Considering the monitoring results involving the abutment cap (Figure 5.6) together with the changes in the deck length (Figure 5.5) and crackmeter data (Figure 5.5), slight changes in the response of the drilled shafts to thermal expansion/contraction of the

bridge was observed in the second year of monitoring compared to the first year. For example, the bridge thermal expansion/contraction and abutment cap crackmeter records (Figures 4 and 5) are very similar during the summers of 2021 and 2022. However, it can be seen that the position of the abutment caps when comparing the summer 2021 and summer 2022 data are different. As Figure 5.6 illustrates, in August 2022, the west abutment cap was positioned 0.5 mm east of its position in August 2021. Similarly, in August 2022, the east abutment cap was also positioned 0.25 mm to the east of its recorded position in August 2021. Therefore, the data in Figure 5.6 indicates that both abutment caps have slightly moved toward east from summer 2021 to summer 2022.

The eastward movement of the drilled shafts also resulted in a 50% to 60% increase in the maximum bending moments, from summer 2021 to summer 2022 (see Figure 5.9). This signifies that, much like the soil-structure interaction in integral and semi-integral bridge abutments, the interaction of the superstructure with the foundations is also a long-term phenomenon and the foundation loads in semi-integral bridges can actually increase over time and potentially cause long-term performance issues.

Another observation regarding the foundation behavior is the continued displacement of the east abutment cap toward the abutment backfill in summer and fall 2021, despite the decreasing trend in the expansion joint width, which is proportional to the bearing shear stress. As schematically illustrated in Figure 5.7(b), from August 2021 to October 2021, the lateral load transferred to the abutment caps was through shearing of the elastomeric bearings. Therefore, it is reasonable to expect that the decreasing trend in the expansion joint width from August 2021 to October 2021 would also result in the reduction of lateral loads applied to the east abutment cap during this period. Moreover, smaller

lateral loads are often expected to result in smaller lateral deflections of the drilled shafts. However, the instrumentation data indicates that the abutment cap continued moving in the direction of backfill.

To provide a better overview of the behavior of the drilled shafts of the east abutment to the decreasing trend in the east abutment's expansion joint width, Figure 5.10 presents the time-history of the east abutment cap displacement and crackmeter readings. There are three types of behavior highlighted in Figure 5.10 to help with the discussion of the observed drilled shaft behavior:

1. Behavior type 1, highlighted in orange, shows that the abutment cap moved further toward the backfill during the period with an increasing expansion joint width (increasing bearing shear on average).
2. Behavior type 2, highlighted in blue, indicates that the abutment cap moved away from the abutment backfill during the period with a decreasing expansion joint width (decreasing bearing shear on average).
3. Behavior type 3, highlighted in green, indicates that the abutment cap moved towards the backfill during a period that the expansion joint width remained relatively constant on average (no change in bearing shear on average).

While the behavior types 1 and 2 match expectations, (larger load causes larger displacement and vice versa), behavior type 3 requires additional investigation to understand why the abutment caps continue to move despite there being no change in the applied load. It is believed that the key to understanding this behavior lies in understanding the response of clay deposits to cyclic loading by deep foundations.

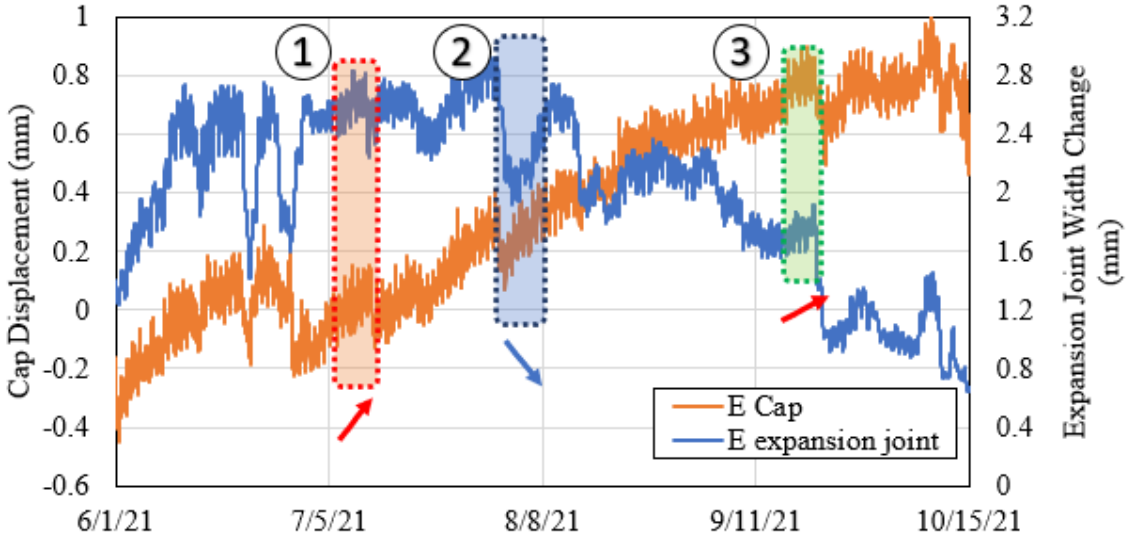

Figure 5.10: Time-history of changes to east abutment cap position and changes to east abutment cap expansion joint width (arrows indicate abutment cap general displacement direction during highlighted periods).

The soil resistance-deflection behavior of clays under static and cyclic loading conditions has been studied extensively (Matlock, 1970; O'Neill and Dunnavant, 1984; Reese and Welch, 1975). A well-established method for analyzing the soil response to lateral loading involves modeling the foundation soils as a series of layers that provide the resistance (P) for a specific level of deflection (y). This method is generally known as the "p-y analysis method." To understand the behavior observed in Figure 5.10, the p-y analysis framework, based on the typical behavior of cyclically loaded clays (e.g., Matlock, 1970), can be used to qualitatively assess the underlying mechanisms.

To aid this discussion, a schematic of the p-y behavior occurring under each of the three behavior types highlighted in Figure 5.10 is given in Figure 5.11. Figure 5.11(a) displays the typical response of foundation soils to a cyclic loading regime that increases in magnitude over time (behavior type 1 in Figure 5.10). In this case, part of the pile

deflection is partly due to the accumulation of plastic strains during daily thermal expansion/contraction and partly due to the increasing soil resistance demand from the lateral load increase, which requires larger soil deflection to provide enough resistance. Figure 5.11(b) shows the effect of load reduction on the lateral deflection of the drilled shafts (behavior type 2). In this period, the lateral deflection of the pile is slightly reduced due to the reduction in the lateral load, although the decrease in lateral deflection and decrease in load would not be proportional. Figure 5.11(c) shows the typical response of a clay deposit experiencing cyclic loads of similar magnitude (behavior type 3 in Figure 5.10). As illustrated in Figure 5.11(c), repeated loading can result in the accumulation of plastic strains in the clay deposit and, as the number of cycles increases, larger deflections are needed to provide the same level of resistance to the applied loads. Therefore, the behavior described above can explain why the east abutment cap continued moving toward the abutment backfill, despite the overall decreasing trend in the bearing shear force during periods such as August to October 2021.

Overall, it can be seen that daily thermal expansion/contraction of the bridge can result in the slow accumulation of plastic strains in the foundations of semi-integral bridges and cause the abutment caps to slowly move over time. As illustrated by the results in Figure 5.9, this behavior can also cause larger stresses in the foundations over time (larger magnitude negative bending moments in the drilled shafts of the east abutment in summer 2022 compared to summer 2021) and negatively affect the overall performance of the foundation elements over time. Therefore, it is important to assess the long-term

performance of semi-integral bridge foundations against the cyclic lateral loads transferred to the abutment caps from thermal expansion/contraction of the bridge superstructure.

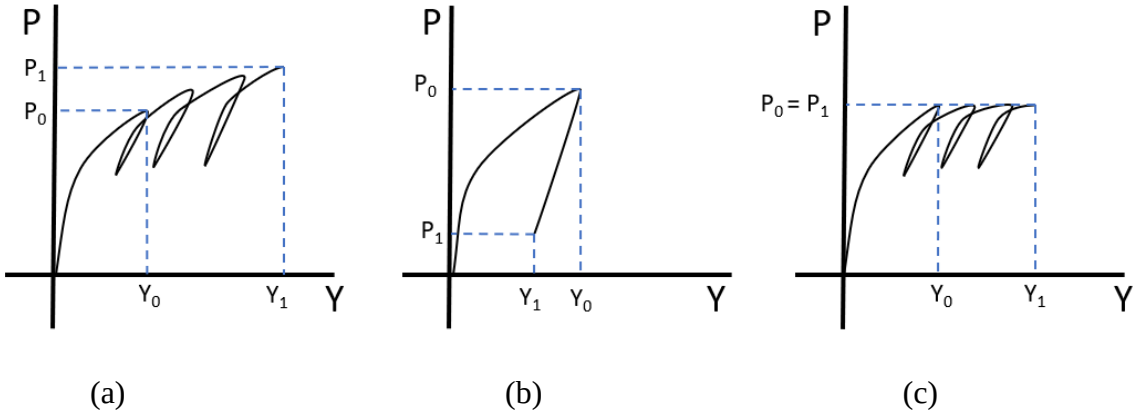

(a) (b) (c)

Figure 5.11: Schematic illustration of cyclic p-y behavior of foundation soil in different conditions: (a) period of increase in average daily temperature; (b) period of decrease in average daily temperature decrease; and (c) period of essentially unchanged average daily temperature.

5.7. CONCLUSIONS

Field monitoring data was evaluated over a period of two years for a semi-integral bridge constructed near Wichita Falls, TX. The evaluation focused on assessing the performance and behavior of deep foundations in semi-integral bridges due to thermal expansion/contraction of the superstructure. In this study, shape arrays were used to collect the deflection profile of the instrumented drilled shafts. The shape array data was evaluated together with bridge thermal expansion/contraction data and abutment cap expansion joint monitoring data to assess short-term and long-term trends in the response of the foundation units.

The following conclusions were drawn from a careful evaluation of the field monitoring data:

- Despite the lack of an integral connection between the superstructure and foundation elements in the semi-integral bridge, its foundation units still experienced cyclic lateral loading and deflection in response to bridge thermal expansion/contraction.
- Extreme weather events can cause significant lateral deflection of semi-integral bridge foundations. In the case of the China Creek Bridge, the collected data indicates that the east and west abutment caps moved 2 and 5 mm toward the center of the bridge, respectively, due to bridge contraction caused by the winter storm Uri in February 2021.
- Despite the symmetrical geometry of the bridge, the response of semi-integral bridge foundations to thermal expansion/contraction of the bridge can be asymmetrical. Moreover, the response of the foundation units to the thermal expansion/contraction of the bridge can change seasonally. For example, in China Creek Bridge, the west abutment cap experienced larger displacements and bending moments compared to the east abutment cap in the winter months, while the east abutment cap experienced larger displacements during the summer months compared to the west abutment cap.
- The instrumentation data also revealed that the cyclic loading of semi-integral bridge foundations installed in clay deposits may lead to accumulation of strains. In the case of the China Creek Bridge, the cyclic loading resulted in a slow increase in lateral displacements of the east and west abutment caps from August to October

2021. As a result, both abutment caps moved slightly eastward from the time of construction to the end of the monitoring period.

- The lateral loads applied to the abutment caps in semi-integral bridges can be due to bearing shear, contact between the abutment cap and abutment wall or the combination of the two modes. In China Creek Bridge, all three types of loading were observed during different periods of the monitoring program. Specifically, the west abutment foundation experienced loading due to the combination of bearing shear and contact between the west abutment cap and abutment wall during most days of the monitoring period. On the other hand, the east abutment cap experienced lateral loading due to bearing shear alone on some occasions and due to contact between the east abutment cap and abutment wall on other occasions.
- While semi-integral bridge foundations are not typically designed for cyclic lateral loading caused by the thermal expansion/contraction of the superstructure, the trends observed indicate that it would be beneficial to assess the long-term performance of semi-integral bridge foundations in response to the daily and seasonal thermal expansion/contraction of the bridge. For example, in China Creek Bridge, it was estimated that bending moments close to the cracking moment of the foundation elements were developed due to thermal expansion/contraction of the bridge deck in less than a year of being in service.

5.8. ACKNOWLEDGEMENTS

The authors would like to thank the Texas Department of Transportation for funding this research under project 0-6936 through the Center for Transportation Research at the University of Texas at Austin.

5.9. REFERENCES

Abendroth, R. E., Greimann, L. F., Lim, K.-H., Sayers, B. H., Kirkpatrick, C. L., Ng, W. C. (2005). "Field Testing of Integral Abutments." Iowa State University Center for Transportation Research and Education, Ames, IA.

Broms, B. B. (1964). "Lateral Resistance of Piles in Cohesive Soils." Journal of the Soil Mechanics and Foundations Division, 90 (2), 27–63. https://doi.org/10.1061/JSFEAQ.0000611.

Burke, M. P. (2009). "Integral and Semi-Integral Bridges." Wiley-Blackwell.

Ensoft, Inc. (2015). "STABLPRO 2015 – User's Manual", Ensoft, Inc., Austin, TX.

Fawaz, G., and Murcia-Delso, J. (2021). "Three-Dimensional Finite Element Modeling of RC Columns Subjected to Cyclic Lateral Loading." Engineering Structures, 239: 112291. https://doi.org/10.1016/j.engstruct.2021.112291.

Han, L., Belivanis, K. V., Helwig, T. A., Tassoulas, J. L., Engelhardt, M. D., and Williamson, E. B. (2019). "Field And Computational Investigation of Elastomeric Bearings in High-Demand Steel Girder Application." Journal of Constructional Steel Research, 162: 105758. https://doi.org/10.1016/j.jcsr.2019.105758.

Karalar, M., and Dicleli, M. (2016). "Effect of Thermal Induced Flexural Strain Cycles on The Low Cycle Fatigue Performance of Integral Bridge Steel H-Piles." Engineering Structures, 124, 388–404. https://doi.org/10.1016/j.engstruct.2016.06.031.

Lawver, A., French, C., and Shield, C. K. (2000). "Field Performance of Integral Abutment Bridge." Transportation Research Record, 1740 (1): 108–117. SAGE Publications Inc. https://doi.org/10.3141/1740-14.

Maruri, R. F., and Petro, S. H. (2005). "Integral Abutments and Jointless Bridges (IAJB) 2004 Survey Summary." Integral Abutments and Jointless Bridges 2005, FHWA, Baltimore, MA, 12-29.

Matlock, H., 1970. "Correlations for Design of Laterally Loaded Piles in Soft Clay," Proceedings, 2nd Offshore Technology Conference, Vol. I, pp. 577-594.

Mofarraj, B., and Zornberg, J. G. (2022). "Field Monitoring of Soil-Structure Interaction in Semi-Integral Bridges." Geo-Congress 2022, ASCE, Charlotte, NC, 33–42. https://doi.org/10.1061/9780784484067.004.

O'Neill, M. W., and Dunnavant, T. W., 1984. "A Study of the Effects of Scale, Velocity, and Cyclic Degradability on Laterally Loaded Single Piles in Overconsolidated Clay," Report No. UHCE 84-7, Department of Civil Engineering, University of Houston-University Park, Houston, 368 p.

Ooi, P. S. K., Lin, X., and Hamada, H. S. (2010). "Field Behavior of an Integral Abutment Bridge Supported on Drilled Shafts." J. Bridge Eng., 15 (1), 4–18. https://doi.org/10.1061/(ASCE)BE.1943-5592.0000036.

Purvis, R. L., and Berger, R. H. (1983). "Bridge Joint Maintenance." Transportation Research Record, 899, 1-10.

Reese, L. C., and Welch, R. C., 1975. "Lateral Loading of Deep Foundations in Stiff Clay," Journal of the Geotechnical Engineering Division, ASCE, Vol. 101, No. GT7, pp. 633-649.

Texas Department of Transportation. (1999). "Tex-132-E: Test Procedure for Texas Cone Penetration." Texas Department of Transportation.

Touma, F. T., and Reese, L. C. (1972). “The Behavior of Axially Loaded Drilled Shafts in Sand.” Center for Highway Research, The University of Texas at Austin.

Wang, S. T., Vasquez, L. G., Arrellaga, J. A., and Isenhower, W. M. (2022). “LPILE v2022 User’s Manual.” Ensoft Inc., Austin, TX.

Chapter 6: Conclusions

6.1. SUMMARY

In this dissertation, the data collected from the long-term monitoring of two pilot single-span semi-integral bridges constructed in the state of Texas were presented. The state-of-the-art instrumentation and monitoring program consisted of utilizing more than 80 sensors to learn more about the factors affecting the behavior of semi-integral bridges. The monitoring system allowed for the determination of thermally-induced strains and stresses developed within various bridge components. It has also been made possible to accurately track the displacement of various bridge components and provide an explanation regarding the factors driving the complex behavior of the semi-integral bridges in response to changes in temperature.

In Chapter 2, important observations were made regarding the behavior of the first pilot semi-integral bridge in Texas using a relatively small monitoring program, compared to the China Creek Bridge's. In addition to the important observations made during this monitoring program, many valuable lessons were learned for the development of the next instrumentation program which resulted in a comprehensive monitoring program involving nearly 80 sensors with remote data collection access. The capabilities and characteristics of this system were discussed in detail in Chapter 3.

Due to the large volume of data collected from China Creek Bridge, the analysis of the data was divided into two chapters. In Chapter 4, the primary focus of the discussion was the soil-structure interaction in the abutment area. And in Chapter 5, the focus was placed on the discussion of the cyclic lateral loading of the foundation due to thermal

expansion/contraction of the bridge, a topic that is found to be primarily overlooked in the design of semi-integral bridge foundations.

Overall, given the observations made in each chapter, the following conclusions were selected because they are considered highly impactful in design and analysis of the future semi-integral bridges:

1. Thermal expansion/contraction of the bridge can be highly asymmetrical even if the structure appears symmetrical on chapter. The causes of this behavior can be traced back to factors such as backfill placement order, unequal backfill compaction, bridge slope, minor differences in foundation soil strength. Since the control of these issues is considered to be infeasible or impossible, it is recommended to design the structure considering the possibility of this behavior. Based on the collected data from China Creek Bridge, it is more realistic to consider 70% of the bridge length (instead of 50%) for estimating the abutment wall displacement and expansion joint demands for each abutment.
2. The lateral earth pressure in the abutment backfills was seen to increase significantly each year due to ratcheting. The field data indicates that ratcheting occurs primarily in the cold season during periods of significant temperature change. The highest annual earth pressures are recorded during the summer when the bridge experiences maximum thermal expansion.
3. The collected data indicates that the total lateral thrust acting on the abutment walls can increase by 25% from one summer to the next. Moreover, the calculated lateral thrust for China Creek Bridge significantly exceeded the

estimates based on Rankine's passive earth pressure theory and have reached 60% of the estimates based on Coulomb's passive earth pressure theory after 2 years of service. Moreover, the earth pressure increase was seen to affect wing walls and abutment caps in a similar manner.

4. Lateral earth pressures do not necessarily increase with depth in semi-integral bridge abutment backfills. Through the analysis of China Creek Bridge data, it was concluded that the larger displacement cycle magnitude near the top of the abutment walls compared to the bottom of the walls as well as the larger rigidity of the abutment wall in the top 2/3 of the wall, due to the presence of the girders, can cause the lateral earth pressures to be significantly higher near the top of the wall, compared to the bottom of the wall.
5. The collected data from both instrumented semi-integral bridges indicate that the bridge foundations experience cyclic lateral loading due to thermal expansion/contraction of the superstructure. The lateral foundation loads are caused by the bearing shear, direct contact between the abutment walls and the abutment caps or the combination of the two. Therefore, it is recommended that the semi-integral bridge foundations be designed for the expected daily and seasonal cyclic lateral loads to improve the long-term performance of these structures.
6. It is recommended that the potential asymmetric response of semi-integral bridges be considered when developing the instrumentation system for future. Some degree of redundancy in measurement of highly important variables can prove to be beneficial in order to increase the reliability of the data and analysis

overall. As climate has a large effect on the behavior of jointless bridges, it is highly recommended to use a reliable on-site weather station instead of relying on local weather station data or datalogger panel thermistor data.

6.2. FUTURE WORK

While a great deal of information was learned from the rigorous monitoring of the two pilot semi-integral bridges in Texas, it is clear that there is still a lot more to be learned to perfect the art of designing and constructing semi-integral bridges. First and foremost, it would be highly valuable to continue the current monitoring program to be able to identify longer-term trends in the behavior of semi-integral bridges. For example, while we've seen significant increase in abutment backfill pressures over the years, we still do not have enough data to determine what the future will look like, whether earth pressures would continue to increase, reach an asymptotic value or even decrease. The same can be said about almost any other variable that has been tracked in this research as well. Majority of the field monitoring studies encountered are limited to 5 years or less of data and so there is a serious lack of long-term performance monitoring data that spans decades for a structure that is typically expected to have a service life of 75 years or longer. It is hoped that with the collection of longer-term field monitoring data which is becoming more and more feasible with the advances in monitoring systems, the current designs can be significantly improved in terms of optimization and long-term reliability.

Moreover, there is very little information about the long-term performance of semi-integral bridges constructed with reinforced backfills. Several transportation agencies currently include standard details for construction of integral and semi-integral bridges

with geosynthetic reinforced backfills. While reinforced backfill is expected to show superior performance compared to the unreinforced granular abutment backfills, not enough studies have been published regarding their long-term performance. It is speculated that geosynthetic reinforcement can significantly improve the backfill performance by supporting the backfill during bridge contraction and therefore minimizing backfill settlement and occurrence of ratcheting. This improved backfill performance can lead to reduction of the lateral loads acting on the abutment walls, wing walls and abutment caps. Moreover, the reduced backfill settlement can result in provision of better vertical support to the approach slabs and improve their service life in general. By collecting long-term data regarding the performance of reinforced abutment backfills, it would be possible to further optimize the bridge design and further improve the cost-saving potential of jointless bridges.

Appendix A: Instrumentation of Mack Creek Bridge

A.1. INTRODUCTION

Instrumentation of Mack Creek Bridge was performed in two separate phases. Phase 1 of the bridge instrumentation involved the installation of earth pressure cells on the abutment walls during the construction of the bridge. The details regarding this installation are provided in Walter (2018). In this segment, the second phase of the instrumentation of Mack Creek Bridge, which occurred in winter 2020, is described. The goal of phase 2 was to collected data regarding the thermal expansion/contraction of the bridge, movements at the abutments, better measurement of temperature and other climate variables to complement the research on the long-term behavior of the bridge. The steps taken to achieve this task are outlined in the following sections.

A.2. ASSEMBLY AND IN-HOUSE TESTING

A new IP68 rated enclosure was purchased in order to house the sensors and loggers for this temporary monitoring project. Once the arrangement of components inside the enclosure was decided, holes were drilled in the steel mounting panel and the components were wired accordingly (Figure A. 1). Once the sensors were placed inside the enclosure, a “peep hole” for the laser distance meter was carved out of the side of the enclosure and covered with plexiglass. This would help protect the sensor from the environment while allowing it to make measurements. It should be noted that before placing the plexiglass, it was verified that plexiglass does not absorb a significant amount of infrared light emitted by the sensor. The finished assembly is shown in Figure A. 2. In addition to the laser

distance meter, it was decided to deploy ClimaVue50, SI-111SS and two crackmeters as well to get more familiar with how these sensors work and test their performances in the field. Most importantly, it was decided to use the cell modem to facilitate data collection and test out the remote data collection capability which would be more important for China Creek SIAB due to the project location's distance from Austin, TX. In order to power this setup, it was decided to use one of the solar panels purchased for monitoring of China Creek.

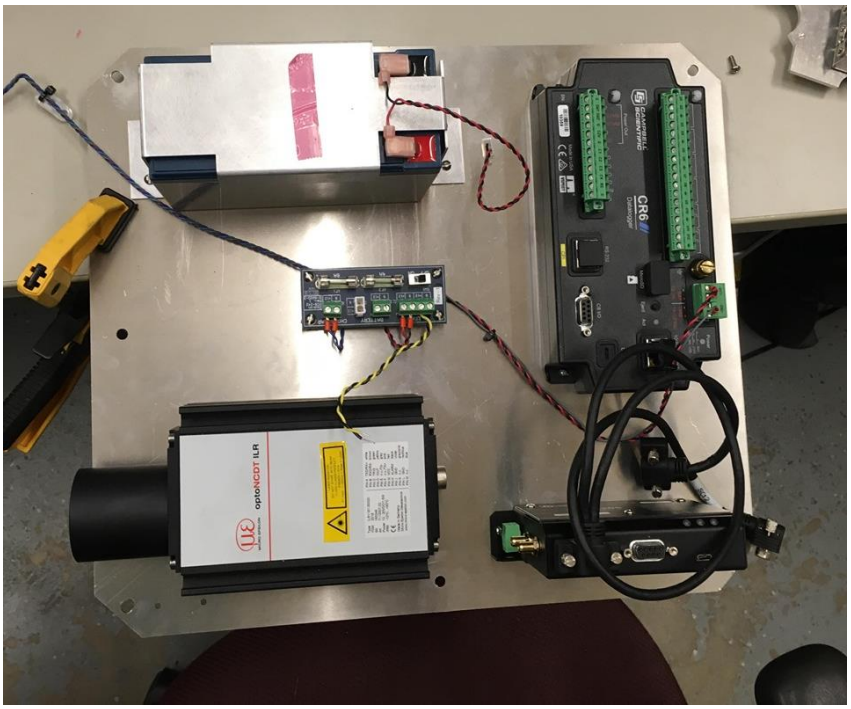

Figure A. 1: Assembly of sensor and logger equipment for temporary additional instrumentation of Mack Creek SIAB

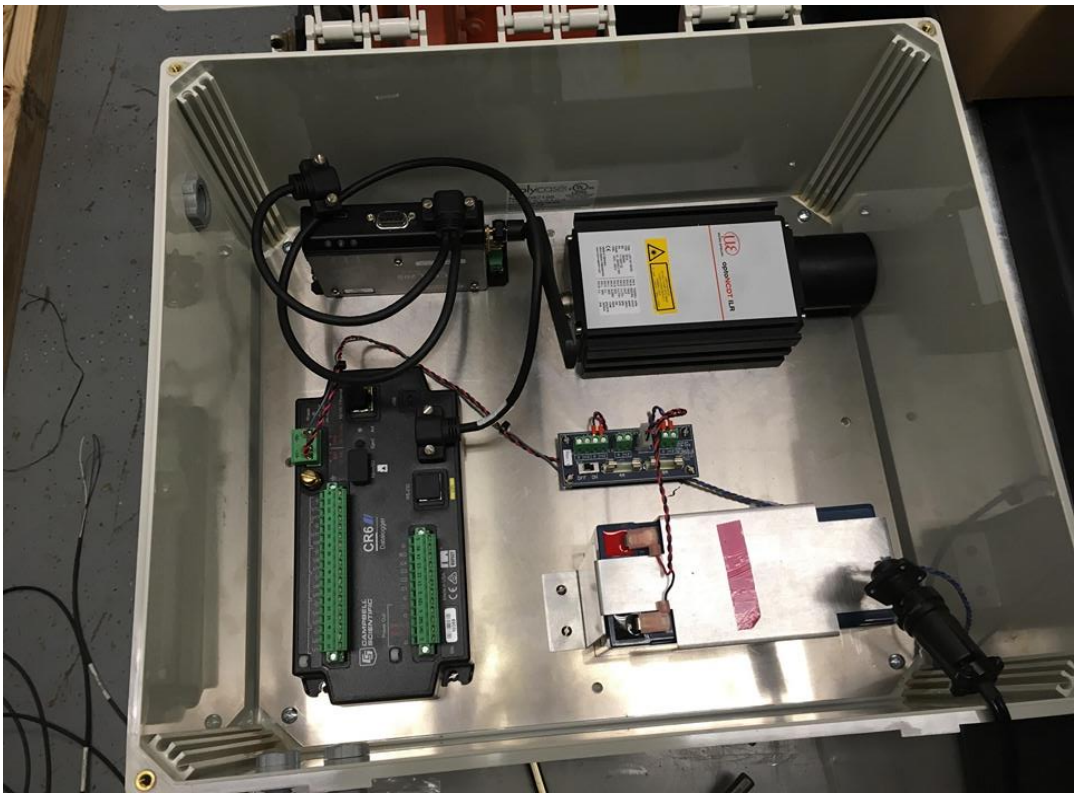

Figure A. 2: Enclosure assembled for additional monitoring of Mack Creek SIAB

As the research team had no prior field experience with this kind of instrumentation setup (wireless data transmission, solar powered, etc.), it was decided to test out the equipment on the rooftop of Civil Engineering department at UT Austin as show in Figure A. 3. In this picture, the enclosure is set next to the wall on the right hand side, while solar panel, ClimaVue50 and SI-111SS are placed on the left.

This initial test led to the discovery that the wireless data transmission block of the code developed was causing power draw more than what the solar panel was able to compensate for. This eventually led to system shutdown and therefore the code was adjusted accordingly.

Over time, the CRBasic code has undergone many revisions in order to optimize the performance of the system and currently it is capable of turning on the modem at a certain time for a certain duration, automatically sending data through email and is also capable of sending text alerts when battery voltage drops below a certain number, threatening shutdown or incorrect measurements. An important advantage of having wireless connection to the logger is that it enables the user to update the program running on the logger without having to be physically present at the location and monitor the performance of the new code while in office.

Figure A. 3: Testing of the equipment on the rooftop of Civil Engineering department at UT Austin

A.3. DATA COLLECTION, PROCESSING AND VISUALIZATION PROGRAM

As mentioned in the previous section, the CRBasic code was developed so that the sensor measurements done each day would be sent via email to a specified email address so that the users would not have to wait for the exact time the cellular modem is turned on in order to download the newly acquired data. For this purpose, a specific email account was created to solely receive emails from the datalogger and an email is sent everyday with data collected over the preceding 24 hours. It should be noted that, it is possible to have the data logger send all the data each time it sends an email but it will not be efficient/economical considering the upload time of the larger files for the logger and data costs.

As this is a long term monitoring program, it is evident that the research team would have to combine many small data files in order to visualize the results which will be very tedious if done manually every time. Therefore, a Python program was developed to help with data collection, processing and visualization. Python is a popular, high-level programming language which is used in a large variety of applications, especially in data sciences and scientific applications.

As the research team deemed it beneficial to be able to execute the code when needed and on any computer device needed, it was decided to develop this code in "Google Colab". Google colab is basically a Jupyter notebook environment which does not require the user to install any software on his/her personal computer in order to write or execute the code. Instead, the code is executed by a virtual machine dedicated to the user's account and so all needed for the code to work is an up-to-date browser and a working internet connection.

The flowchart shown in Figure A. 4, shows the general processes handled by the code developed which will be explained in following subsections.

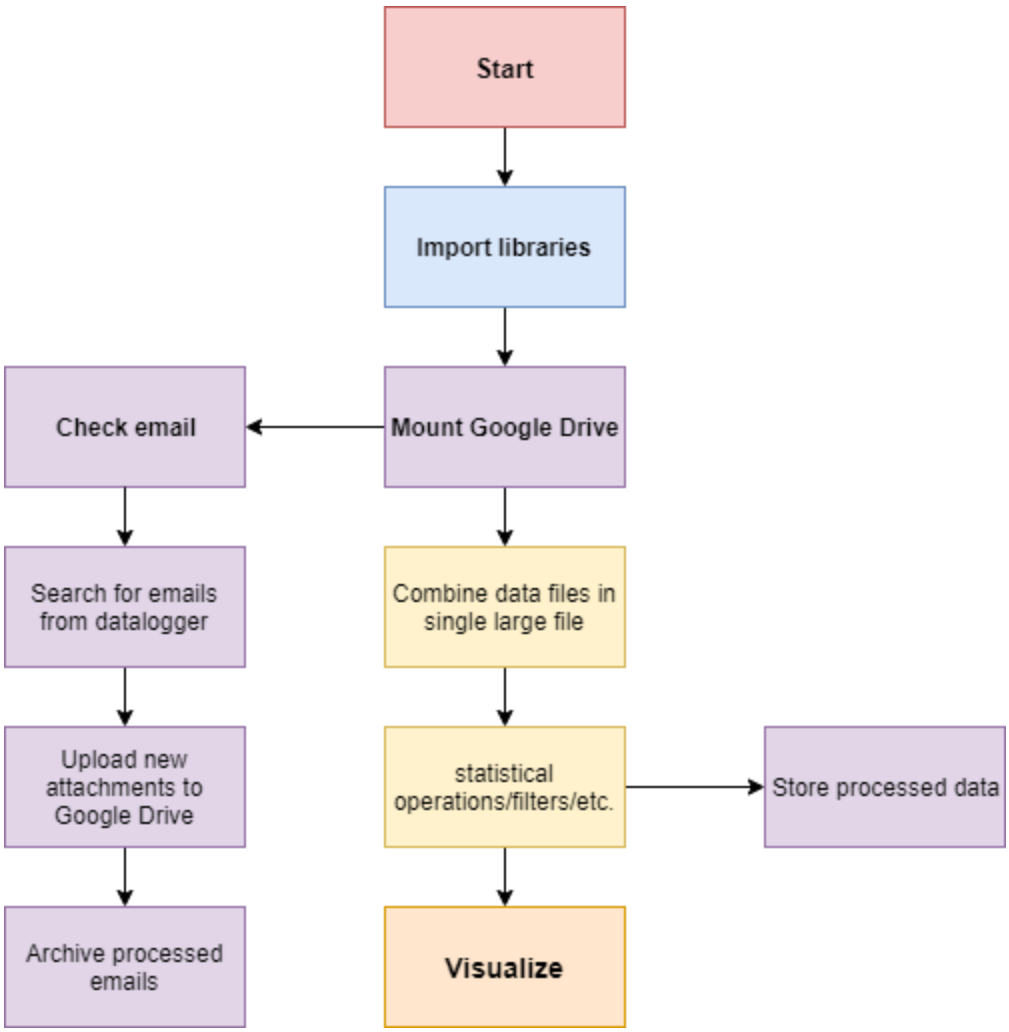

Figure A. 4: Flow chart of the python program developed for data collection, processing and visualization

A.4. PYTHON LIBRARIES

Although python comes with a pre-installed standard library, many functions such as plotting, filtering, advanced mathematical operations, file management, etc. are not readily available. These functionalities are added by finding the appropriate library and importing them in the program to make their instructions available for use. Some of the libraries used for this code are,

- os (file management)
- numpy (mathematics)
- impalib and email (email-related operations)
- pandas (data file processing/reading and writing data files)
- plotly (data visualization)

More details about these libraries can be found on their respective documentation and websites.

A.5. FILE MANAGEMENT

The most important function of this code is to automate the process of checking email for new data sent from the datalogger, download the attachments, upload them to google drive and combine them in one single file with previously downloaded files.

For this purpose, a code was developed that would login to the email address were datalogger messages are received (Figure A. 5). Once logged in, all the relevant emails that match the description of what is expected from datalogger are searched for and their attachments are downloaded. Once downloaded, these messages are archived to avoid processing them again on future executions of the code (Figure A. 6).

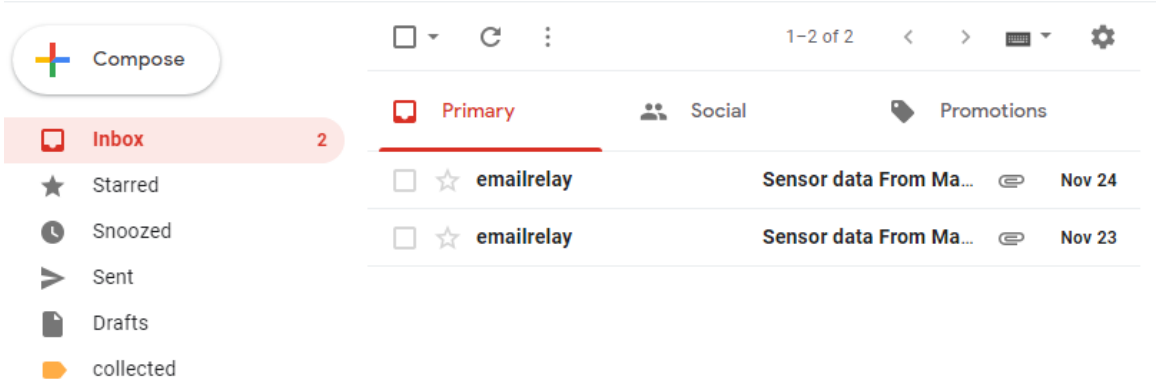

Figure A. 5: New messages received from the datalogger

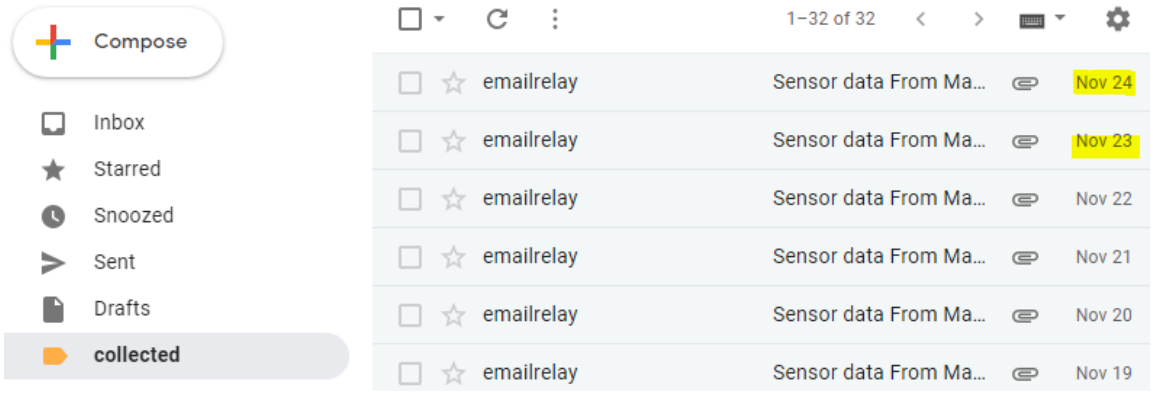

Figure A. 6: Archived messages after they were processed by Python

Next, the downloaded attachments are directly uploaded to a google drive location to enable ease of access and data sharing when needed.

After the email-related operations are executed, a separate algorithm is executed that will look into the contents of the google drive for unprocessed files and would add them to the “master file” which contains all data previously processed or creates a new “master file” if one does not exist yet. An example output of this algorithm is shown in Figure A. 7.

This simple algorithm provides a great time-saving advantage over the manual alternative which is opening multiple CSV files in Excel and copying and pasting data to create a “master file” which is also prone to human errors.

```
Output.csv already exists.
New files found in folder.
Output.csv was updated!
CELL_DIAG30.dat Moved to gdrive/cr6data/Processed
SensorData30.dat Moved to gdrive/cr6data/Processed
CELL_DIAG31.dat Moved to gdrive/cr6data/Processed
SensorData31.dat Moved to gdrive/cr6data/Processed

Here's how Output.csv looks like:
Number of records = 768
```

	TIMESTAMP	RECORD	BatteryV	ChargeIn	ChargeOut	LithiumV	PTemp_C	TT_C_Avg	SBT_C_Avg	SlrFD_kW_Avg
0	TS	RN	Volts	Volts	Volts	Volts	Deg C	Deg C	Deg C	kW/m^2
1	2019-10-23 15:00:00	0	13.81	0	0	3.788	27.9	38.5	28.94	0.837
2	2019-10-23 16:00:00	1	13.8	0	0	3.786	28.71	35.29	29.31	0.677

Figure A. 7: Example output of the file management algorithm developed in Python

An advantage of using Pandas library to interpret datafiles is that it is capable of interpreting timestamp data automatically which would be very handy in calculating statistics such as daily/monthly averages or maxima with a single line of code.

A.6. VISUALIZATION

Perhaps the most complex part of the algorithm developed so far is the part dedicated to visualization of the acquired data as it is perhaps the most significant step in gaining an understanding of data gathered from the field.

As a result, the research team decided to get familiar with the extensive plotting library offered by Plotly to help visualize the collected time series along with helpful

statistics in an interactive manner. The interactivity of this algorithm is deemed a huge advantage over conventional plotting methods using Excel as that process can be extremely cumbersome when dealing with large number of variables. To give an idea, the small number of sensors planned for additional instrumentation of Mack Creek, provide more than 20 independent measurements every hour. Plotting this many variables, especially if new data is to be added everyday would be very hard to manage if done manually using a spreadsheet program such as Excel.

An example output of the plotting algorithm is shown in Figure A. 8. This mini-program would allow the user to load the "master file" and create an interactive time history plot of past measurements, equipped with a handy range slider which would allow the user to focus on a certain portion of data as desired. Moreover, a histogram of daily averages, maxima and minima for the variable in focus are plotted as well to aid in understanding of the data. Most importantly, a dropdown menu (shown in the left hand side of Figure A. 8) has been programmed which allows the user to select the variable to be plotted with a simple click.

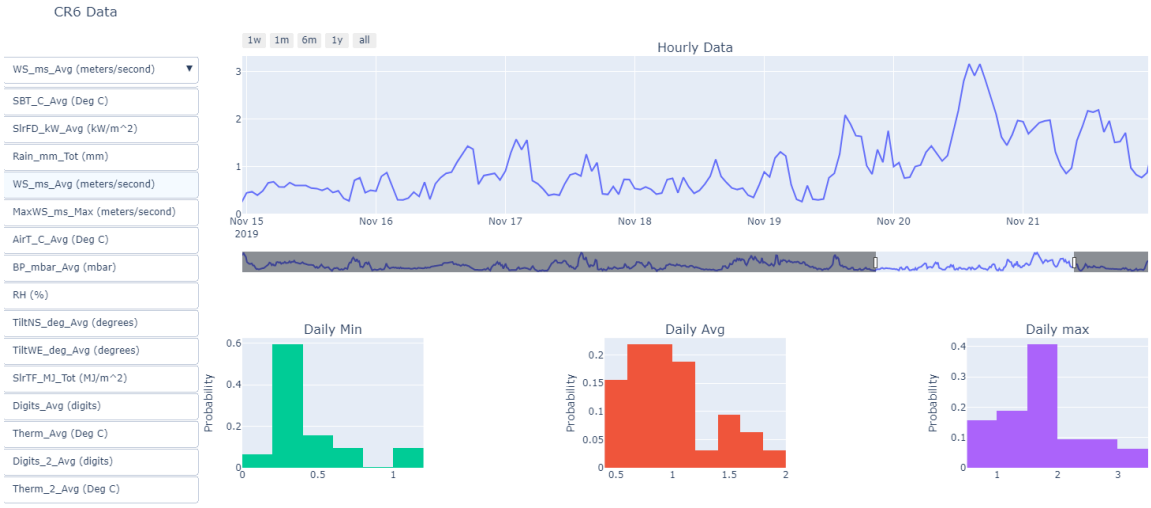

Figure A. 8: Example output of the plotting program developed in Python

As demonstrated, programming tedious and repetitive tasks such as data collection, storage, processing and plotting, will save a large amount of time and removes room for error.

In the future it is expected to add interactive tools that would enable noise filtering capabilities as well.

A.7. FIELD INSTALLATION

Upon conclusion of testing the new equipment on the rooftop of Civil Engineering building and making final revisions on the logger program, the research team planned a field visit to Mack Creek to mount the new set of sensors on Mack Creek in order to begin collecting complementary data previously not collected. As shown in Figure A. 9, the logger equipment, laser source, solar panel, ClimaVue50, SI-111SS and one of the crackmeters were installed on the south abutment and the laser target and a crackmeter were installed on the north abutment. The datalogger was programmed to take

measurements 3 times each hour and store average/maximum values of recordings (depending on parameter). The logger was also programmed to communicate the collected values every day at noon.

In Figure A. 10, equipment installed on the south abutment are shown. Although no flooding/submersion is anticipated in this location, the enclosure and cable glands were tested against prolonged submersion for up to 0.9 m of submersion and therefore this enclosure should keep the equipment safe against surface water and rain for the duration of this project. As can be seen in Figure A. 10 (b), a rain guard was attached to the laser's peep hole to minimize splashback and accumulation of dirt due to rain and reduce the need for maintenance. It should be noted that the enclosure which holds the laser source is installed on top of the backwall while the crackmeter is attached to both backwall and pile cap.

Figure A. 9: Equipment installed on Mack Creek in January 2020

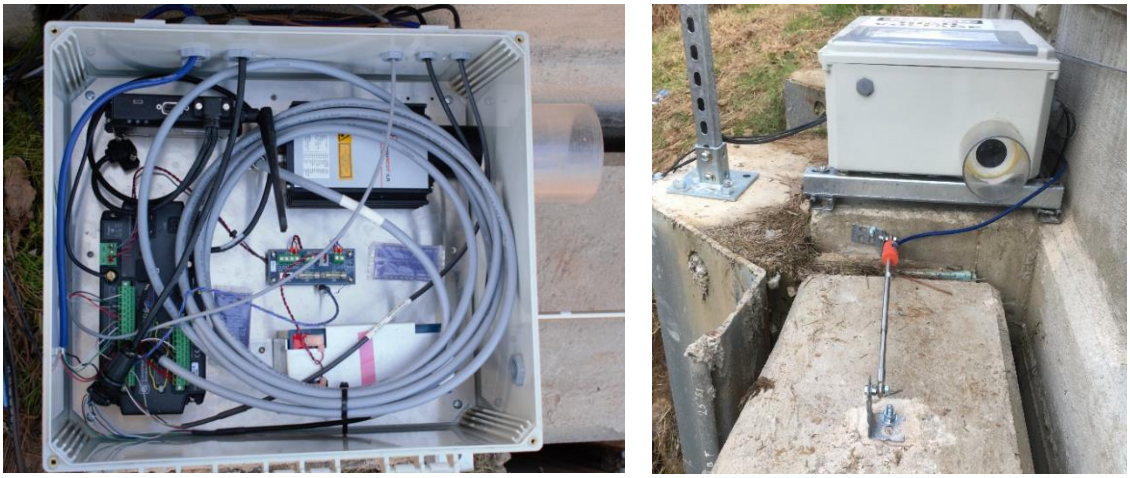

(a) (b)

Figure A. 10: Closeup of equipment installed on the south abutment: (a) Logger equipment and laser distance meter (b) crackmeter installed between backwall and pile cap + loggerbox

A closeup of the components installed on the north abutment is shown in Figure A. 11. It should be noted the laser target is installed on top of the backwall to capture the total expansion/contraction of the deck as deck and backwall are connected in SIAB structures. Similar to the south abutment, the crackmeter is connected to both backwall and pile cap to capture the relative displacement between the two.

(a) (b)

Figure A. 11: Closeup of equipment installed on the north abutment, laser target and crackmeter installed between backwall and pile cap. (a) view from behind (b) top view

Finally, a 3.3 m unistrut section was used as a pole to install solar panel, ClimaVue50, SI-111SS and lightning protection equipment (Figure A. 12). This pole was placed as far from the road as possible on the edge of the wingwall. The solar panel faces south to catch the most sun and ClimaVue50 was equipped with a bird spike kit to prevent issues arising from birds sitting on top of the device. Moreover, SI-111SS which has a 22° half angle field of view was mounted near the top and pointed at the deck in such way that full field of view of the device, covers the deck and not the surroundings. This device is designed to measure the average temperature of the surface it is pointed at, based on the infrared radiations coming from the target surface.

(a) (b)

Figure A. 12: Closeup of pole mounted equipment on the south abutment, which includes solar panel, ClimaVue50, SI-111SS and lightning protection device: (a) installation of SI-111SS for measuring deck surface temperatures (b) Closeup of SI-111SS

A.8. REFERENCES

Walter, J. R. (2018). "Experimental and numerical investigation of integral/semi-integral bridge abutments for Texas conditions." Master's Thesis, University of Texas at Austin.

Appendix B: Construction and Instrumentation of China Creek Bridge

B.1. Introduction

In this appendix, a detailed account regarding the construction process of the China Creek Bridge as well as the installation of sensors is provided. The construction of China Creek Bridge was initially planned to start in summer 2018. The construction plans were delayed to the fall of 2018 due to the discovery of nests belonging to migratory birds. The construction was further delayed due to bad weather conditions including heavy rains and flooding during the coming fall and winter. This construction delay also presented the opportunity to visit the original bridge and evaluate the conditions of the existing bridge before the demolition of the existing structure started.

B.2. Survey of the Original Bridge Structure

A brief visit to the site of China Creek bridge was planned in August 2018 to get familiar with the site and inspect the structure which was to be replaced.

During this visit, the high water levels in the creek (Figure B. 1) made it impossible to inspect the bridge from underneath and look for signs of deterioration. Despite the limitations caused by high water level, the bridge was examined from the distance. It was observed that the existing bents underneath the bridge had experienced corrosion damage (Figure B. 2). Moreover, it was observed that during precipitation events, water would easily find its way through the joints of the bridge which would cause damage to the concrete, as was evident by the looks of the concrete surface close to the joints (Figure B. 3).

Figure B. 1: High water level in China Creek after a precipitation event in August 2018

Figure B. 2: Corroded bents under China Creek bridge to be replaced

Figure B. 3: Seepage of water through the deck joints

In addition, although it appeared that the asphalt pavement had been repaved several times, there were still small cracks near the edges of the road where the approach slab reached the bridge deck (Figure B. 4), which means that backfill settlement is an ongoing issue for this settlement. However, it will be hard to judge the severity of this problem due to lack of monitoring information on this bridge.

Overall, the initial visit to China creek proved to be very beneficial despite the limitations caused by the high water table. It helped the researchers to get familiarized with the location of the project as well as some of the common issues in the existing structure which are hoped to be avoided by the semi-integral bridge technology. For example, one of the main advantages of SIAB technology is the omission of joints which would reduce the amount of seepage on concrete surfaces.

Figure B. 4: Cracked edge of pavement at the end of the approach slab due to backfill settlement

In addition, another purpose for this trip was to assess the possibility of transferring acquired instrumentation data over the internet in order to monitor changes on the bridge more frequently and more closely. Based on the tests conducted in the location of the bridge, it is possible to transmit data via the internet and in real time.

B. 3. CONSTRUCTION OF THE CHINA CREEK BRIDGE

The construction of the China Creek Bridge was planned to be done in 2 phases in order to maintain traffic flow while the construction activities were ongoing. The demolition of the first half of the bridge using heavy machinery is shown in in Figure B. 5. Also, in order to protect the active roadway on the other half of the bridge, a temporary

soil-nail wall was constructed to protect the backfill underneath the open lane. A picture of this temporary support (soil nail wall) is shown in Figure B. 6.

Figure B. 5: Demolition of the first half of the old China Creek Bridge

Figure B. 6: Installation of soil nail wall as temporary support for the active roadway crossing the undemolished half of the bridge (Picture provided by Samuel Groves)

One of the challenges encountered during the first phase of construction was the discovery of a heavy reinforced concrete structure in the planned location for the new bridge foundations. It was determined that the buried obstruction belonged to the bridge structure that was at this location before the bridge that was under replacement. After encountering the buried obstructions in June/July 2019, construction of drilled shafts was delayed until mid-November of 2019. A trip to the China Creek for the day of drilled shaft construction was planned in order to document the construction process.

During the drilling operations, the top 4.5 to 6 m of soil appeared to be a mix of sandy materials mixed with highly plastic clayey soil with no visible layering changes. The material deposited in this depth were once removed in order to remove the buried

obstruction and placed back after removal of the obstruction. Reportedly, sheep foot rollers were used to recompact the soil after placement. Another important observation was encountering signs of groundwater flow at depths of about 6 m as well; the soil removed from this depth was found to be very sticky and wet relative to what was recovered above that depth. After reaching this depth, the rig operator placed a permanent casing in the hole due to presence of collapsible soils at the top (Figure B. 7).

At the depth of about 7.5 m and deeper, the cuttings recovered appeared brittle and flaky (Figure B. 8). The heap of soil removed by the auger is shown in Figure B. 9; in this picture, the broken flakes of gray shale (covered in powdered red dirt) can easily be seen on top while the remolded wet/plastic material can be seen below.

Once the target depth was reached, the rebar cage (Figure B. 10) was gently lowered into the hole while construction workers attached plastic spacers to the rebar on all sides to maintain the minimum cover.

Figure B. 7: Casing used for the top portion of the drilled shafts

Figure B. 8: Gray shale covered with powdery red dirt recovered from 8 m depth

Figure B. 9: Heap of soil excavated from the drilled shaft. Note the broken pieces of shale on top (depths of 7.5 m and lower) and wetter/plastic material removed beforehand

Figure B. 10: Placement of one of the west abutment drilled shafts' rebar cage

By the end of February 2020, the contractor finished forming the phase 1 abutment caps and wing walls and placed the girders and precast panels for the first phase in position. It is worth noting that because the precast/prestressed girders were stored in a remote location for more than a year, they had experienced a significant creep resulting in excessive camber when initially brought to the site. To reduce the camber, the contractor delayed the deck construction of the deck slab by a few days to allow for some of the camber to dissipate under the weight off the precast concrete panels placed on top of the girders.

As work on forming the abutment walls began (Figure B. 11), the research team visited the site during the first week of March 2020, in order to place the first set of

instrumentation, earth pressure cells (GK-4810) on both abutment walls to be cast in concrete.

Figure B. 11: Forming of abutment walls after placement of girders and precast panels, March 2020 (East abutment)

Unlike the procedure followed in the Mack Creek Bridge, it was decided to mount the pressure cells on the inside of the wooden forms, nailed to the forms. This way, once the forms are removed, the surface of the pressure cell would be flush with the concrete and potentially eliminate any errors due to the arching effect. As experienced during laboratory calibration of these sensors, due to the difference in stiffness of the EPC steel plate and the soil, if the sensor is mounted on the surface of the concrete (as opposed to being flush with it), some arching effects would occur resulting in higher magnitudes of stress being recorded by the cell. Another improvement over the procedure followed in the Mack Creek Bridge is elimination of the need to place a sand cushion around the sensor to

prevent point-loading effects. These cells were designed with thicker steel in order to give correct reading when in contact with granular media.

In Figure B. 12, the earth pressure cell installed on the west abutment is shown. As can be seen, once the concrete is placed, this sensor will be integrated with the abutment wall and its exposed face will be directly in contact with the granular backfill. The cables for these sensors were routed through the polystyrene to the inside of the bridge and coiled up above the abutment cap, awaiting the installation of dataloggers. Baseline measurements of the installed cells were taken upon installation using GK-404 handheld logger.

Figure B. 12: Top view of the earth pressure cell (GK-4810) installed on the inside of the form on the west abutment wall, photographer standing on one of the precast panels placed on the deck, March 2020

The concrete was placed the day after installation and a subsequent visit was made during the form removal process in order to examine the finished surface. As expected, the finished surface looks great and the concrete placement did not cause the pressure cell to

move away from the form (Figure B. 13). Upon form removal and before placement of the backfill, another set of measurements were made using the handheld GK-404 logger.

Figure B. 13: Finished surface of the east abutment wall with the pressure cell (GK-4810) installed between the two girders on the left, March 2020

For instrumentation of the deck, a total of 11 concrete strain gauges were brought to the site. 10 of these strain gauges were model GK-4200 which were placed in evenly spaced pairs (top and bottom of the deck profile) along the longitudinal axis of the deck. The other one was a GK-4200L which was placed perpendicular to the longitudinal axis of the bridge (Figure B. 14) close to first pair of GK-4200s near the west abutment. The difference between the two types is that GK-4200L has lower stiffness and to capture early shrinkage deformations of the concrete as well, while the other ones do not deform until the concrete sets and reaches higher stiffness.

Figure B. 14: GK-4200L as installed on the deck, perpendicular to the direction of the bridge, March 2020

A pair of GK-4200 installed on the deck are shown in Figure B. 15. As can be seen, one is attached to the bottom of the top rebar using zipties and blocks of Styrofoam as a spacer and the other is installed near the bottom (top of the girder). As there are no rebars at the bottom, a set of zipties were wrapped between two “U” shaped hooks of the girder and the strain gauges were tied to those as shown in Figure B. 16.

Figure B. 15: A pair of GK-4200 strain gauges installed on the deck during phase 1 of the construction

Figure B. 16: Identification of strain gauges using colored tapes as binary ID code

Unlike other Geokon sensors, the sensor body of the GK-4200 is manufactured separate from the cable and transducer and needs to be assembled in the field. Therefore,

each sensor/cable does not carry a unique serial number tag. In order to keep track of the cables and position of the sensors attached to them, a binary codebook was designed to help with this task. An example of the binary code applied is shown in Figure B. 16 where yellow/green tape represent ones and gray tape represents zeros. The same code is applied to the other end of the cable which is routed through a small gap to the top of the abutment cap (Figure B. 17) which helped identify which cable belongs to which sensor. In the end, these cables were coiled and routed through a block of wood (Figure B. 18) with pre-drilled holes in a specific order, in case the tape is removed due to weathering or a possible flood event. In the end, baseline values for each strain gauge were recorded using the handheld GK-404 logger.

(a) (b)

Figure B. 17: Installation of strain gauges: (a) cables of the strain gauges were routed through a small gap between the foam boards to underneath the bridge, and (b) coiled up wires coming from the strain gauges (red) and earth pressure cell (blue).

Figure B. 18: Predrilled block of wood used to help keep track of the cables coming from embedded strain gauges

In late March 2020, the research team was notified that deck concrete was successfully placed and the sensors appear to have stayed in place (Figure B. 19 to Figure B. 21). Due to the issued guidelines by the University of Texas at Austin regarding travel authorization considering COVID-19 pandemic, the research team was not able to make subsequent visit in order to oversee this task and record the sensor outputs after the concrete placement, or while the concrete sets. As a result, the time-rate of deformations and early shrinkage rate was not captured during this time.

Figure B. 19: Concrete placement on the deck, Phase 1, March 2020

Figure B. 20: Finished surface of the deck, Phase 1, March 2020

Figure B. 21: Covered deck surface after concrete was placed, Phase 1, March 2020

The work on Phase 2 of the bridge proceeded rather quickly, compared with Phase 1 of the bridge construction. This required the research team to make frequent visits to the site in order to install the planned sensors for different parts of the bridge over spring and summer 2020.

The first set of instrumentation for phase 2 began after conclusion of the demolition activities and by the start of excavation activities for the drilled shafts. As the construction crew began with the drilled shaft construction activities, the research team prepared Sch. 40 PVC conduits to be installed inside the drilled shaft's rebar cage for the center drilled shafts on both sides of the bridge. The purpose of the PVC conduits was to serve as housing

for the Measurand Shape Array (SAAV) sensors that were intended to capture potential lateral deformations in the drilled shafts.

To alleviate the transportation of PVC conduits, the pipe sections were cut into shorter sections that could be easily carried by a car from Austin to Wichita Falls (Figure B. 22). The day before the excavation, these pipe sections were assembled at the location using PVC cement and various types of couplers to ensure the finished conduit does not collapse during the installation phase (Figure B. 23). Because the rebar cage was to be lifted only from one end by the crane prior to installation in the hole, a significant amount of bending was expected to occur in the cage and the conduit attached to it. Therefore, several methods of reinforcement were used to ensure the joints were just as strong as the uncut portions of the conduit by using heavy duty PVC cement and hose clamps as shown in Figure B. 24.

Figure B. 22: 1.5 m PVC conduits transported to China Creek Bridge to house SAAV sensors in the drilled shafts. In this picture, 1.5 m conduits are already assembled into 3 m sections using PVC cement and couplers

Figure B. 23: PVC conduits assembled into 11 m sections using additional couplers and joint reinforcement.

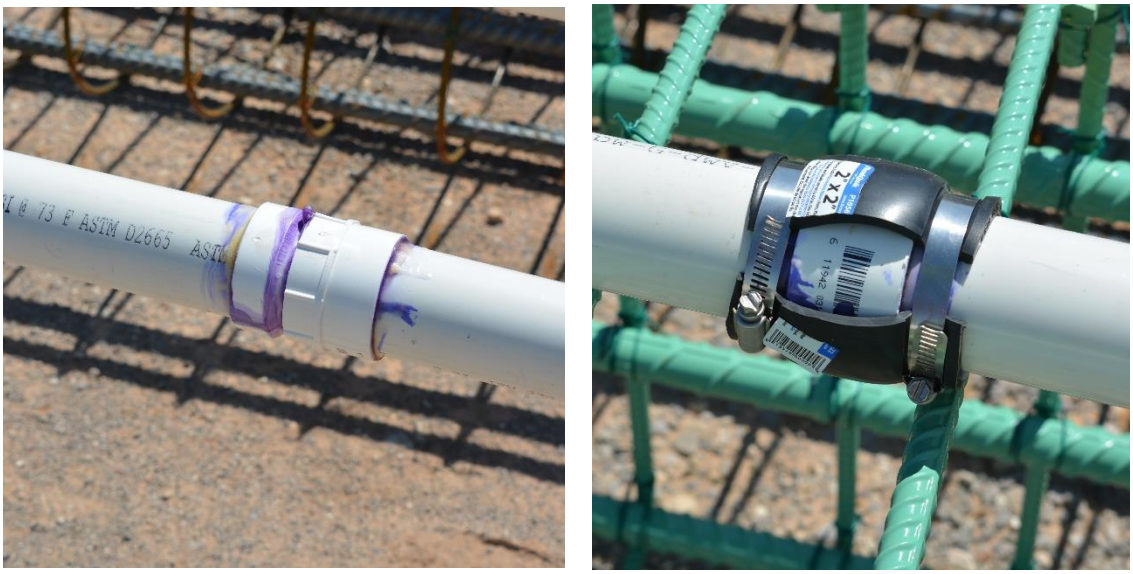

(a) (b)

Figure B. 24: Reinforcement of PVC conduit joints: (a) Threaded couplers + Heavy Duty PVC cement (b) Compression couplers + Flexible couplers + Hose clamps

Furthermore, in order to reduce stresses on the pipe and joints, heavy duty zipties and hose clamps were used at roughly every meter to secure the PVC conduit against the spiral rebars of the drilled shaft in the order shown in Figure B. 25. The final result of attaching the assembled PVC conduit to the rebar cage can be seen in Figure B. 26, where the conduit runs in the space between two vertical rebars from top to bottom of the cage. It should be noted that while all of the different types of reinforcements used for the assembly of this conduit may not have been necessary, the cost of adding these layers of reinforcement outweighs the cost of potential damages to the conduit during construction; a failure of the PVC during construction is equal to the loss of opportunity for the installation of a very expensive and important sensor as there will be no chance to repair or replace.

(a) (b)

Figure B. 25: Attachment of the PVC conduit to the rebar cage: (a) Heavy duty zipties used on either side of the joints (b) combination of steel hose clamps and heavy duty zipties used at the middle of each section.

As it appears in Figure B. 26, the conduit is slightly longer than the drilled shaft. This extra length was to account for the height of the abutment cap, after the construction of which, the SAAV sensors were to be installed.

Figure B. 26: Assembled PVC conduits attached to drilled shafts to serve as SAAV housing

In addition to planned instrumentation of drilled shafts with SAAV, 3 pairs of strain gauges were attached to the East-Center drilled shaft at 1.5 m distances from the top. The goal for the installation of these sensors was to gain better understanding of vertical and horizontal loads applied to the drilled shafts and even get an estimate of skin friction for the top 3 m.

A close-up view of the instrumented rebar cage which was used for the center drilled shaft on the east abutment is shown in Figure B. 27 and Figure B. 28. The strain

gauges were installed in pairs according to the expected direction of bending in order to decouple compression from bending strains.

Figure B. 27: Strain gauges attached to the long. rebars of drilled shafts

Figure B. 28: Instrumented rebar cage intended for Center-East drilled shaft (Phase 2) of China Creek bridge

After the completion of instrumentation tasks intended for rebar cages, the construction crew proceeded to carefully lift the rebar cages using cranes and front loaders and put them in place (Figure B. 29).

(a)

(b)

Figure B. 29: Installation of east abutment instrumented drilled shaft: (a) lift and transportation of the rebar cage using a front loader to the drilled shaft location (b) lifting of the rebar cage from the top using a crane (note the bending of the rebar cage and PVC conduit)

Once the drilled shafts were placed and excavation machinery were removed from the location, concrete was pumped into the drilled shafts and the final adjustments on the

rebar cage were made to ensure the orientation of sensors were correct for the expected direction of movement (Figure B. 30).

One week after the construction of drilled shafts, the construction crew began forming the abutment caps (Figure B. 31). For this stage, the research team intended to install earth pressure cells on the side facing the backfill to record earth pressure acting on the abutment caps and any potential changes in them.

As can be seen in Figure B. 32, earth pressure cells were mounted on the inside of the form at the mid-height of the abutment cap and near the location of the center drilled shafts. Upon completion of formwork, installation of abutment cap sensors and routing the sensor wires to a suitable location, the abutment cap concrete was poured using a concrete tremie (Figure B. 33). Also, it can be seen in Figure B. 33 (a) that once the abutment cap was poured, the SAAV conduit stuck out of the top by roughly 0.3 m, leaving enough room to lower the SAAV into the conduit and clamp it at the top, per installation requirements.

Immediately after pouring the abutment caps, the construction crew began the formwork on the wing walls which were cast integrally with the abutment cap but in a separate pour. Before the forms were installed, the research team took the opportunity to mount an earth pressure cell on each side in order to measure changes in earth pressure on the wing walls due to movements in the abutment walls. The earth pressure cells were mounted at a location which would be close to the face of the abutment wall and the forms were clearly marked using spray paint to ensure the cells were installed at the correct location (Figure B. 34).

(a)

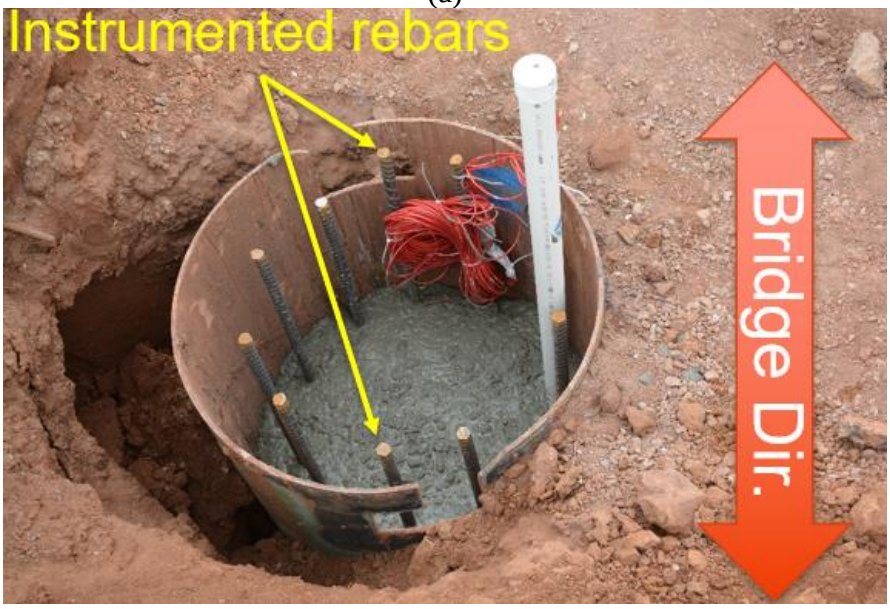

(b)

Figure B. 30: Construction of the instrumented east abutment drilled shaft: (a) concrete being pumped into the drilled shaft (b) Final orientation of the instrumented shaft and sensors

Figure B. 31: Formwork for construction of abutment caps and wing walls

Upon the completion of abutment cap and wing wall construction, another visit was made to the site in order to install the SAAV sensors before the girders were placed. As can be seen in Figure B. 35, the SAAV was shipped on a reel which required to be carefully unloaded by rotating the reel as the sensor was fed into the conduit. This installation is best done with at least two people in order to ensure SAAV segments do not bend too much to avoid getting damaged during installation, as the joints are vulnerable to snapping if bent too much. Once the SAAV was fully lowered into the conduit, the extension fiber glass tube was attached to the top, and the whole sensor was lifted several times and rammed into the conduit (pumping motion) to ensure that the sensor had fully settled into the conduit and all joints were compressed against the walls. This step was very important because if the sensor is not fully settled into the conduit, SAAV may slowly settle over the

first few weeks after the installation causing errors in the readings. Once the sensor was settled, the extension piece was cut using a hacksaw and clamped to the top of the conduit using the compression clamp provided by the manufacturer. This compression clamp ensures there is a specific amount of vertical compressive force acting on the SAAV segments to prevent them from moving out of place and generating bad readings. Once the compression clamp was assembled, the installation verification tool provided by the manufacturer was used to ensure the amount of tilt recorded at each SAAV segment is within the expected range given the internal diameter of the conduit chosen (Figure B. 36). By analyzing the sensor readings from all segments of the SAAV, and given the internal diameter of the casing, the installation verification tool calculates amount of compression on the system, total compression required, tilt angle of each segment and whether these angles exceed the minimum tilt angle expected for the casing chosen. If the tilt angle of the majority of segments pass the angle calculated by the software, a green light is given and the installation is considered successful.

Once the installation was completed, SAAV conduits were capped using 10 cm diameter PVC conduits to prevent water and debris from entering the conduits and interfering with the performance of the system (Figure B. 37). This is very important because if water enters the conduits and freezes over the cold season, the pressure due to expansion of water can cause serious harm to the sensors.

(a)

(b)

Figure B. 32: Instrumentation of the abutment caps: (a) west abutment cap pressure cell (before formwork is completed) (b) east abutment pressure cell (after formwork is completed)

(a)

(b)

Figure B. 33: Construction of the west abutment cap: (a) Pouring concrete for abutment cap using a concrete tremie (west abutment) (b) finishing the surface of the abutment cap, notice SAAV conduit sticking out between the two girder pedestals

(a)

(b)

Figure B. 34: Installation of EPCs on wing wall forms to measure backfill pressure acting on the wing walls: (a) EPCs mounted on the wing wall forms (b) west abutment wing wall after form removal

Figure B. 35: Installation of SAAV in the east abutment center drilled shaft

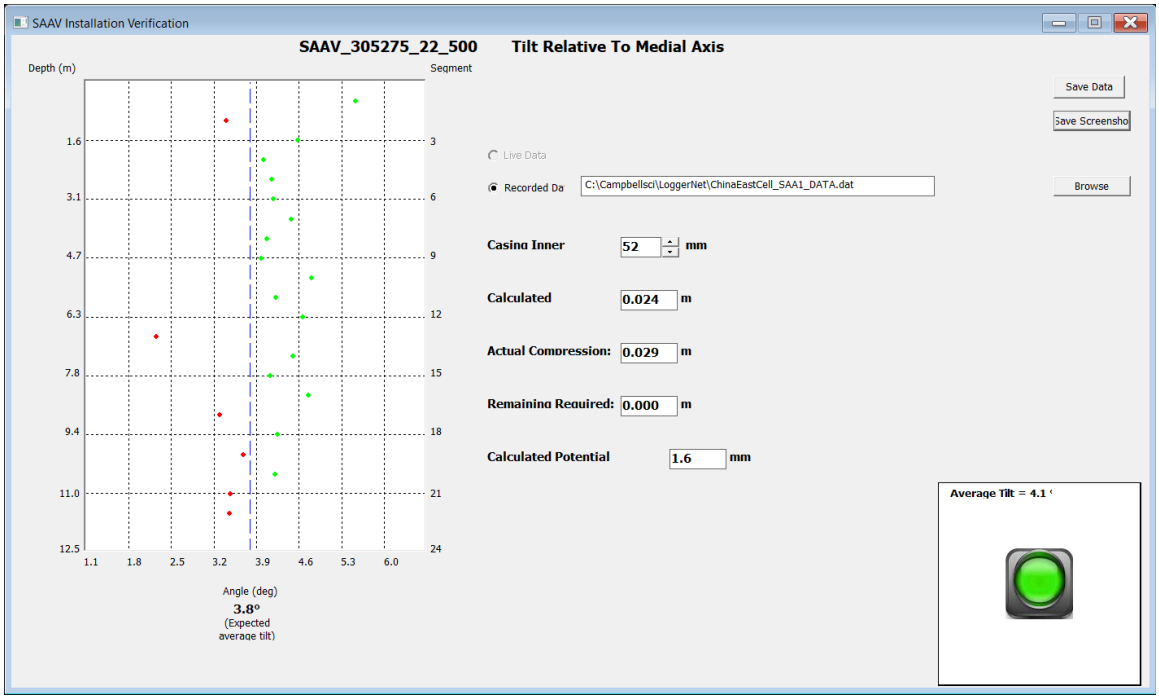

Figure B. 36: SAAV verification tool screen (green light indicates successful installation)

Figure B. 37: Capped SAAV conduit on east abutment

After the girders were placed, a set of 5 VW miniature strain gauges were mounted on the bottom flange of the middle girder of the bridge with the spacing of 4.5 m. For the installation of these sensors, a drilling guide (Figure B. 38) was used to make shallow holes in the bottom flange of the girder that were the same distance as the pegs on the strain gauges. For drilling, extra care was taken to not drill holes deeper than necessary in order to minimize the risk of damaging prestressed reinforcement in the girders. Next, these holes were cleaned using canned air and filled with quick-setting epoxy before setting the strain gauges. The strain gauges were held in place using a piece of duct tape until the epoxy set (Figure B. 39). In the end, a metallic cover was epoxied on top of these gauges to protect them from potential flood debris. The finished installation can be seen in Figure B. 40.

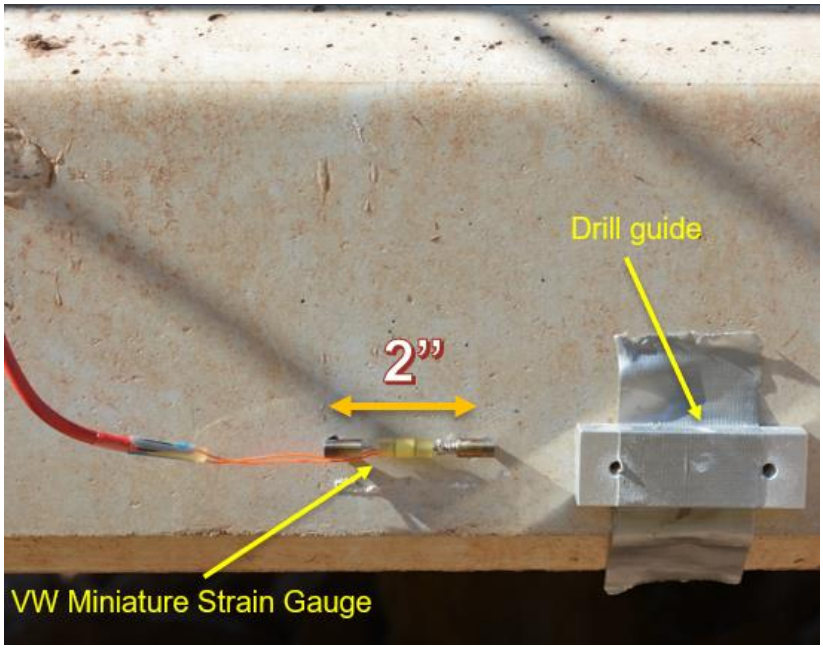

Figure B. 38: Miniature strain gauge next to the drill guide used for installation on the side of the bottom flange of the bridge girder

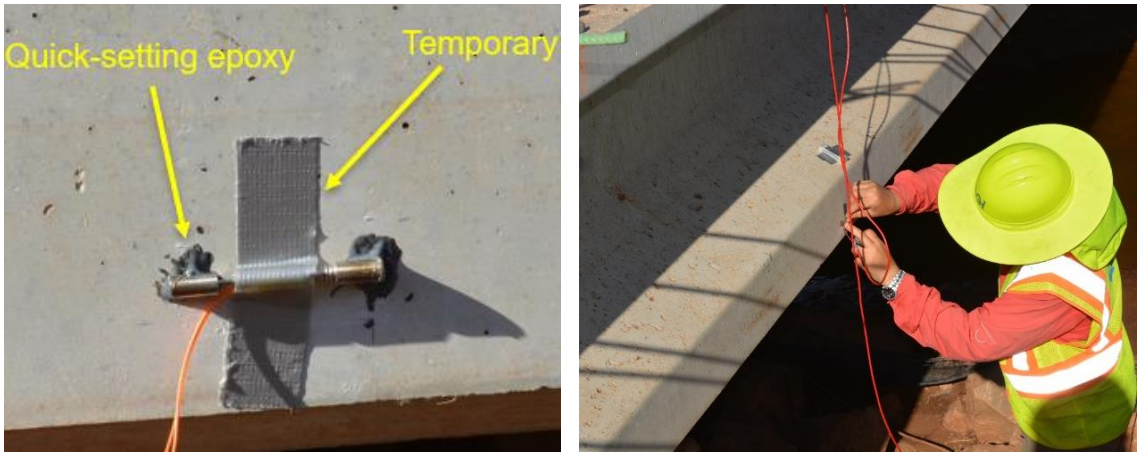

(a) (b)

Figure B. 39: Installation of miniature strain gauges on the bridge girder: (a) epoxied strain gauge (b) strain gauge installation, cables are routed along the top flange

Figure B. 40: Mounted miniature strain gauges on the bottom flange of the middle girder

As the abutment walls were formed, it was decided to attach 3 pairs of strain gauges to the rebars in different locations and orientations in order to record strains in the abutment wall due to changes in backfill pressure as well as have a measure of heat flow in the abutment wall using the thermistors of these sensors (Figure B. 41). In addition to the strain gauges, two pairs of earth pressure cells were also mounted to the back of the forms intended for each abutment wall to complement the measurements made by the EPCs mounted during the phase 1 of the construction (Figure B. 42).

Once the abutment walls were formed, precast concrete panels were placed in between the girders using a crane as shown in Figure B. 43. Upon completion of this task, the rebar for the deck was placed and the concrete for the deck and abutment walls was placed on the same day (Figure B. 44).

Figure B. 41: Location of the 3 pairs of concrete embedded strain gauges on the east abutment wall

Figure B. 42: A pair of earth pressure cells mounted on the back of the form intended for the west abutment wall

Figure B. 43: Placement of precast concrete panels on the deck

Figure B. 44: Phase 2 deck concrete placement

As the concrete for the deck was delivered, the research team prepared two instrumented fresh concrete sample cylinders using low modulus VW strain gauges (Figure

B. 45). The goal of this task was to monitor thermal and shrinkage strains occurring in the deck concrete without the influence of other live or dead loads as well as structural constraints. One of these cylinders was intended to be placed on a wing wall to be exposed to direct sunlight and the other was placed under the bridge to be only influenced by the ambient temperature changes. It was hoped that the data collected from these two instrumented cylinders would help the researchers better define the coefficient of thermal expansion as well as shrinkage of the concrete used in this bridge.

Figure B. 45: Instrumented concrete sample cylinders

After the completion of the bridge deck, the research team began work on the installation of backfill sensors which include backfill settlement sensors and soil extensometers which are both made of VW displacement transducers housed in a Sch. 40 PVC conduit and measure the distance between their flanges. The installation of the settlement sensor was one of the trickiest installations in this project as it required several

feet of excavation below the backfill. For this purpose, a two-man gas-powered auger was used to excavate a hole deep enough. Next, the settlement sensor was placed into the hole and set in place by adding quick-mix concrete, mixed onsite using a drill equipped with a paddle mixer attachment. This point below the backfill served as the reference point for backfill settlement measurements (Figure B. 46)

To better understand how settlement in the backfill occurs, it was decided to spread the settlement sensors in different directions on each side. As a result, the settlement sensors were placed at different distances from the abutment wall and centerline of the bridge (Figure B. 47).

In order to monitor horizontal movements and horizontal extension/compression in the backfill due to expansion/contraction of the bridge deck, two daisy-chained extensometers were installed in each backfill as well. Each of these extensometers was attached to a pre-machined angle iron flange which would extend or compress the displacement transducer due to interaction with the surrounding backfill soil.

Once the backfill placement was completed, a large and heavy stainless steel plate was attached to the top flange of the settlement sensors to ensure the top flange follows the motion of the backfill soil at the surface (Figure B. 49). These plates were tested prior to installation to ensure they are heavy enough to compress the displacement transducer under their own weights considering the sliding resistance provided by the set screws and tapes on the body of the sensor.

(a)

(b)

Figure B. 46: Installation of VW displacement transducers to be used as backfill settlement sensors: (a) excavation of the hole using auger (b) vertical placement of the sensor in the hole

(a)

(b)

Figure B. 47: Settlement sensor installation locations: (a) west abutment (b) east abutment

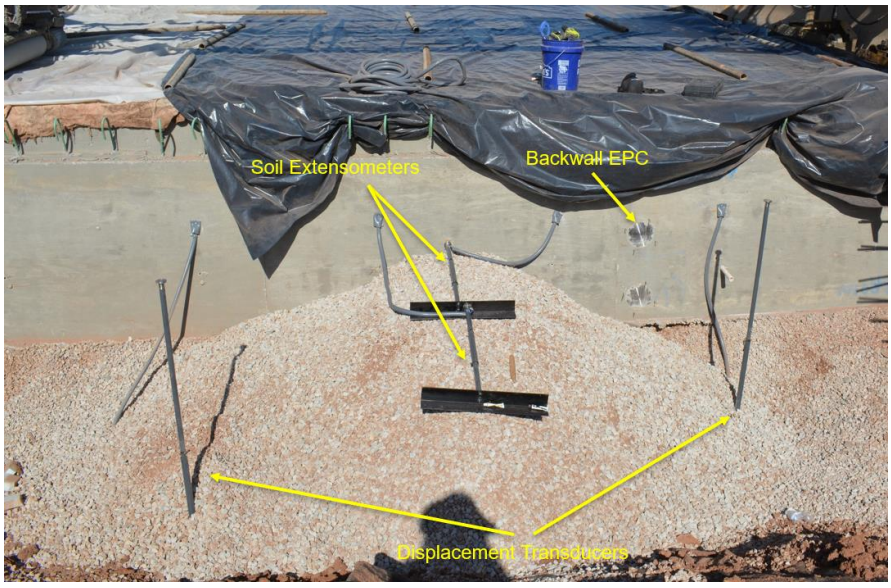

(a)

(b)

Figure B. 48: Installation of soil extensometers in the backfill: (a) west abutment (b) east abutment

Figure B. 49: Stainless steel plates attached to the top flange of the settlement sensors

After the construction crew finished the placement of backfill material, work on forming the sleeper slab and approach slab began. No sensors were planned for this phase of the construction.

After the completion of the approach slabs, three VW crackmeters were placed on each side to monitor relative displacement between the sleeper slab & approach slab (Figure B. 50), approach slab & wing wall (Figure B. 51) and abutment cap and abutment wall (Figure B. 52) on each side of the bridge. A tiltmeter was also installed on each side to measure any potential tilt in the abutment walls due to thermal cycles of the bridge.

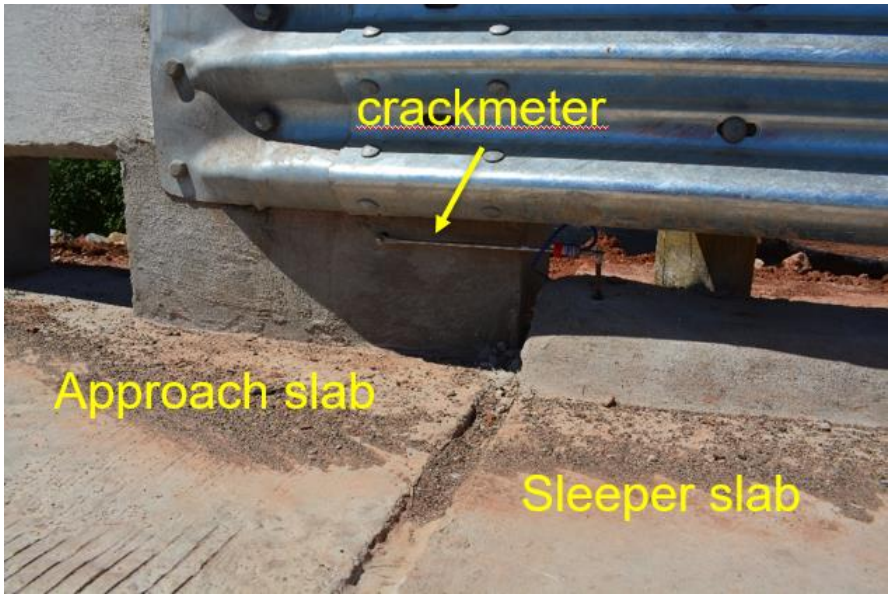

Figure B. 50: Crackmeter installed for measuring relative displacement between approach slab and sleeper slab

Figure B. 51: Crackmeter installed for measuring relative displacement between approach slab and wing wall

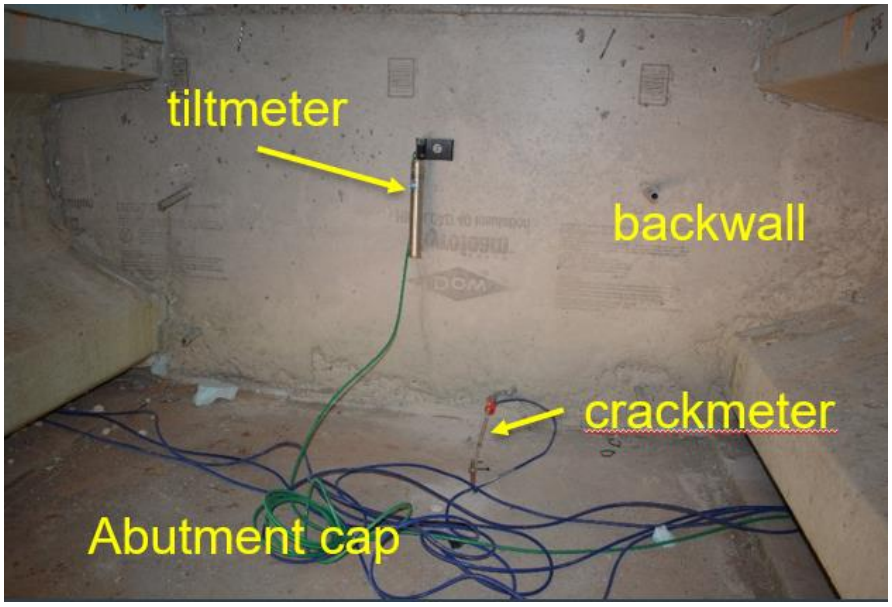

Figure B. 52: Crackmeter installed for measuring relative displacement between abutment cap and abutment wall + tiltmeter installed on the abutment wall

The purpose of these crackmeters was to see if there is any relative motion occurring between these structural components as they are not constructed integrally and it is possible to see relative movement between these components due to a variety of reasons including pressures generated in the backfill and thermal expansion of concrete.

Due to the frequent flooding of China Creek which passes below the bridge, it was decided to instrument the structure with 2 piezometers as well to track significant flood events and see if there are any changes in the other parameters associated with the floods. To this end, one piezometer was installed inside the abutment wall with the tip of the piezometer in contact with the backfill soil (Figure B. 53). The other piezometer was installed vertically on the abutment cap's side facing the creek to help track how high the water in the creek rises (Figure B. 54).

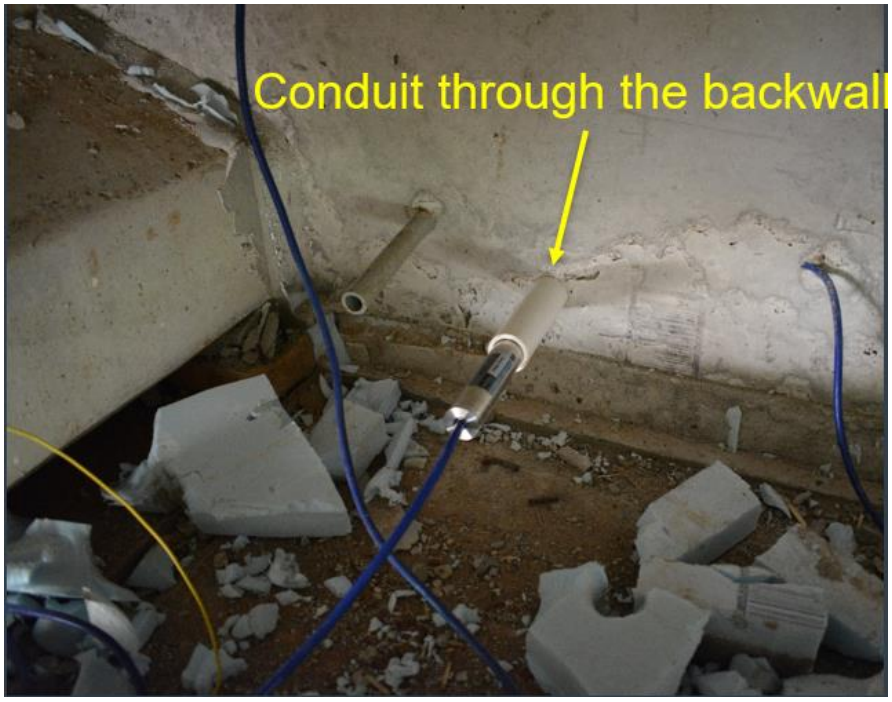

Figure B. 53: Piezometer measuring water pressure in the backfill (prior to installation). The sensor is fully inserted and sealed on the back to prevent water infiltration from the creek side in case of flooding

Figure B. 54: Creekside piezometer installed on the abutment cap

The last set of sensors intended for China Creek bridge were mounted on a 3-m-long superstrut mounted on the southwestern wing wall of the bridge. These sensors can measure weather-related parameter (ClimaVue50) and deck surface temperature (SI-111SS infrared radiometer). In addition, a powerful cell antenna was mounted to help establish a remote connection with the datalogger using a cell modem.

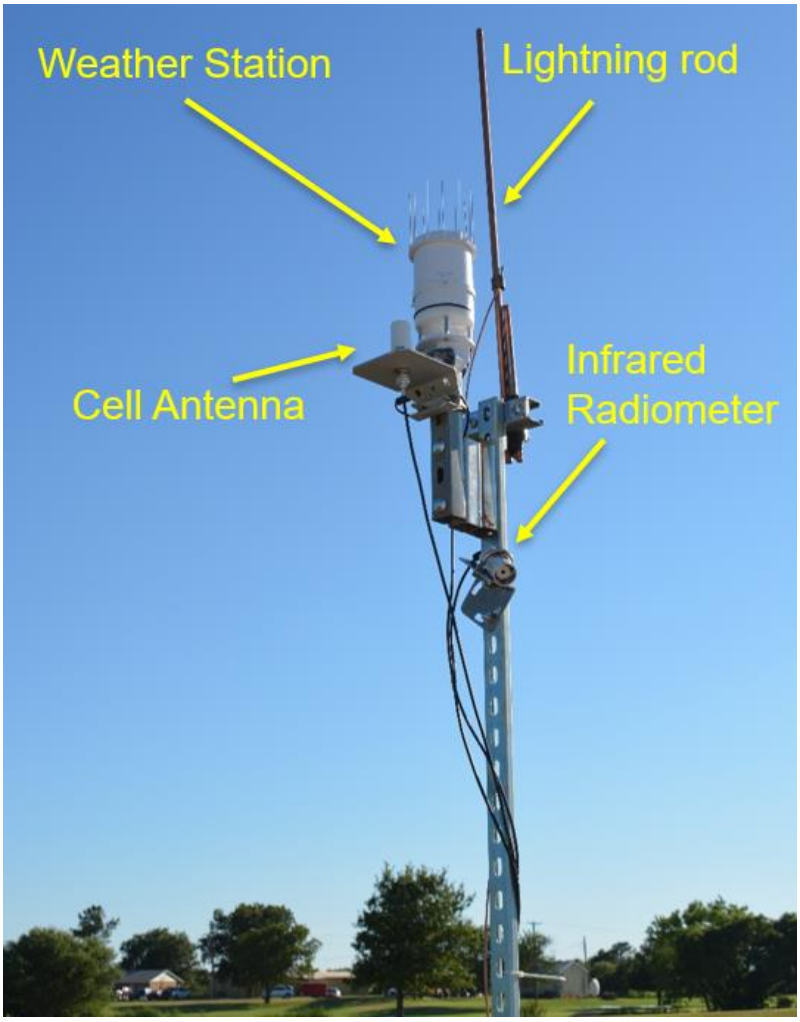

Figure B. 55: The superstrut mounted on southwest wing wall. Infrared radiometer is pointed towards the deck surface to measure surface temperature.

To power the datalogger system, two 40W solar panels equipped with 12V charge controllers were installed on the south railing of the bridge, with one on each end (Figure B. 56). Installing these solar panels on the south side enabled them to produce maximum amount of electricity and ensure continuous operation of the dataloggers with the help of sealed lead acid batteries placed inside the datalogger enclosures.

Figure B. 56: Solar panel mounted on the south railing of the east end of china creek bridge

After the completion of construction (Figure B. 57), pre-assembled datalogger enclosures were brought to the site and were mounted upside-down under the deck between two adjacent girders. The datalogger enclosures were mounted underneath the bridge and at the request of TxDOT to minimize the potential for tampering by hiding them from plain sight. However, due to the history of flooding under the bridge (recent instances of flood

reaching the deck height), extra measures had to be taken to protect the system from water damage as none of these components were waterproof.

Figure B. 57: China Creek bridge construction completed and opened to traffic on July 31, 2020

The first measure taken in waterproofing the enclosures was to switch the original enclosures provided by the manufacturer with IP68 rated enclosures fitted with IP68-rated cord grips. To test the performance of these enclosures under continuous submersion, they were filled with heavy metallic pieces and placed inside a large drum filled with water for 2 days to see if there is any water ingression. On the first try, it was found that a considerable amount of water ingression had happened which was found to be due to a faulty cord grip. A second try was made after the faulty cord grip was replaced. No signs of water intrusion was found at the conclusion of the second try. Therefore, it was decided

that even though the equipment is rated as IP68, there is a good chance for at least one of the pieces to be faulty and this could undermine the integrity of the whole system. Consequently, in addition to the IP68-rated cord grips and enclosures, several additional measures were taken to ensure there can be no water ingression in case of heavy flood events:

1. The enclosures wre mounted at the highest point possible below the deck, which is directly under the precast concrete deck panels
2. Enclosures were mounted upside down with cord grips as close to the lid as possible. This arrangement leads to the creation of an air pocket inside the enclosure which would keep the water out even if there are faulty cord grips in place (Figure B. 58). The working principle is that if there is no place for the air molecules to escape from, water pressure from the outside would only lead to compression of the air pocket, not its drainage; therefore, the air pressure developed in the air pocket will be equal to the water pressure from outside and no flow can occur. This mechanism is based on the same principle used in the design of shallow water diving helmets.

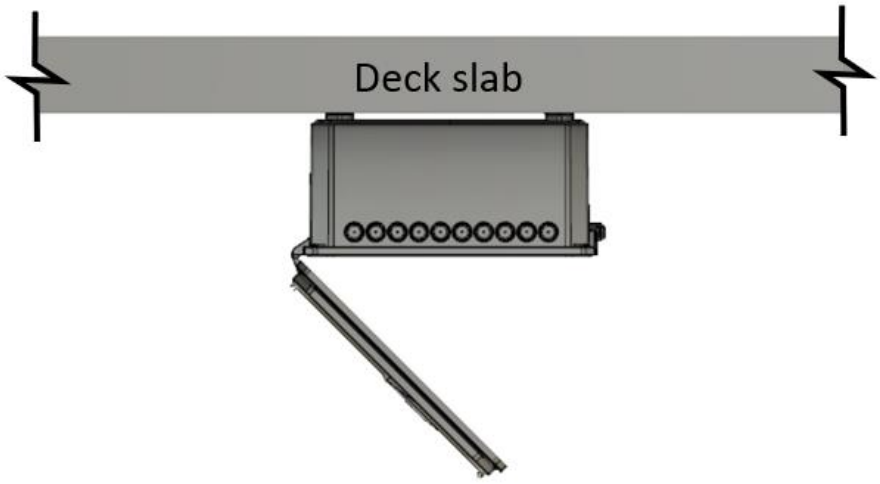

Figure B. 58: Upside-down installation of the logger enclosures below the deck. Enclosure is mounted to the bottom of the deck. To keep water from damaging the equipment housed inside, all cord grip holes need to be as close to the lid as possible.

3. It was expected that an even larger air pocket can form in the space between adjacent girders since girders were cast into the abutment wall at the end and the precast concrete panels and deck concrete seal the top. With no place for the air to escape from, water is not expected to rise much in between the girders even if it reaches the deck height on the outside.

Therefore, there were 4 layers of protection devised to keep the enclosures from getting flooded given the steep cost of the loss of equipment.

The major downside to the installation method explained earlier is that accessing the logger equipment for wiring or troubleshooting becomes significantly challenging as all work has to be done in a cramped space and over the head (Figure B. 59). To put things in perspective, there were roughly 75 sensors installed, with each having at least 5 wires which amounts to more than 350 wire connections to be made on an over the head terminal

while balancing on ripraps in a cramped space in late-July heat. Given the volume of the work, it took nearly 2 weeks to route the cables on the abutment caps and connect them to the pre-assigned terminals on the dataloggers and multiplexers.

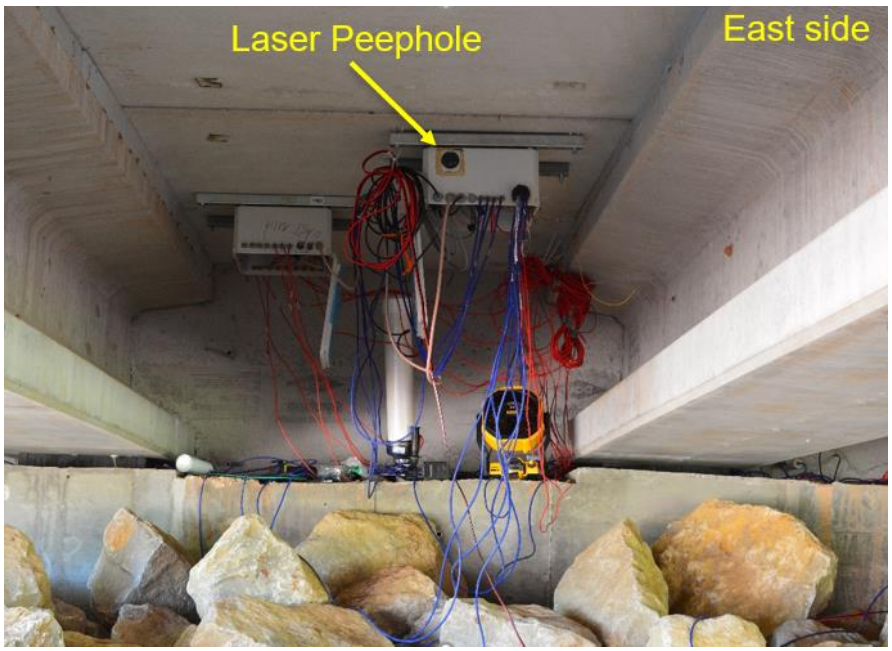

Figure B. 59: Wiring of the east side datalogger station which is equipped with a laser distance meter as well. Fun fact: This battery-operated fan was our best defense against the late-July heat and the large number of mosquitoes and wasps living around the creek area while wiring the loggers

In October 2020, a trip was made to the bridge site. The purpose of this trip was to troubleshoot remote connectivity issues and replace a faulty multiplexer. During this trip, it was discovered that rodents were attempting to build nests on top of the abutment cap in the space between the abutment wall and bearing pads under the girders. These rats also appeared to have been very attracted to the sensor cables routed on top of the abutment caps and had extensively damaged some of these cables in a short period. As a result,

several cables had lost connectivity and one had completely disappeared! The disconnected cables were spliced quickly and reconnected to the dataloggers. After the discovery of rodents under the bridge, it was decided to protect the cables by adding flexible PVC conduits around the cables as an added layer of protection. Since the wires were already attached to the dataloggers, the PVC conduit was cut open lengthwise using a utility knife and fitted around the cables. This was a temporarily measure to keep the rodents away from the cables until a more permanent solution can be applied in a subsequent visit.

After talking with other professionals experienced with outdoor wiring, it was decided to use a harder material to protect the cables from rodents as there has been instances of rodents chewing through flexible conduits and even aluminum. For this purpose, Sch. 40 PVC pipes were cut in half lengthwise using a bandsaw and carried to the bridge site. The two halves of the PVC pipe were then placed around the cables and clamped together using hose clamps (Figure B. 60). The majority of cables were covered using this method, except for the locations of cable entry or behind the bearing pads which were protected by adding a thick layer of expandable foam. It is worth noting that no sign of damage to the sensor cables has been observed after 2 years of operation and therefore the modifications were considered successful.

Figure B. 60: PVC pipes used for protection of cables routed on top of abutment caps

Vita

Behdad Mofarraj Kouchaki was born and raised in Tehran, Iran. Growing up in a family of engineers, Behdad was also determined t3.7o pursue engineering as he was growing up. At the end of high school, Behdad took the national university entrance exam and got ranked 314 among +400,000 participants that year and got accepted to the Civil Engineering program at the Sharif University of Technology, the most prestigious engineering school in Iran. Behdad finished his Bachelor's with a thesis on the design of shallow foundations on layered clays which resulted in his first journal publication as well. Being highly interested in research and academia, Behdad joined the University of Arkansas at Fayetteville in 2015 for his Master's studies. In Arkansas, Behdad worked on developing a rapid non-destructive testing framework for the assessment of levees using geophysical testing methods. In 2017, Behdad joined the PhD program at the University of Texas at Austin and worked on developing design details for several different novel bridge systems involving semi-integral bridges, GRS bridge abutments and seamless bridges. Post-graduation, Behdad is excited to join the industry and grow as a professional geotechnical engineer.

Email address: mofarraj@utexas.edu

This dissertation was typed by Behdad Mofarraj Kouchaki.